



Deactivation of emission control catalysts for heavy-duty vehicles – Impact of biofuel and lube oil-derived contaminants

Sandra Dahlin

Doctoral Thesis in Chemical Engineering
KTH Royal Institute of Technology
Department of Chemical Engineering
Stockholm, Sweden 2020

Deactivation of diesel emission control catalysts
– Impact of biofuel- and lube oil-derived contaminants

Sandra Dahlin

TRITA-CBH-FOU-2020:10

ISBN: 978-91-7873-437-5

@ Sandra Dahlin, Stockholm 2020

Tryck: US-AB, Stockholm 2020

Akademisk avhandling som med tillstånd av Kungliga Tekniska Högskolan i Stockholm framlägges till offentlig granskning för avläggande av teknologie doktorsexamen den 28 februari 2020, kl 10.00 i Kollegiesalen, Brinellvägen 8, Stockholm. Fakultetsopponent är Professor Isabella Nova, Politecnico di Milano.

Abstract

Catalytic emission control is used to reduce the negative impact of pollutants from diesel exhausts on our health and on the environment. For a heavy-duty truck, such a system consists of a diesel oxidation catalyst (DOC), a diesel particulate filter (DPF), a selective catalytic reduction (SCR) catalyst, and an ammonia slip catalyst (ASC). Due to greenhouse-gas induced global warming, it is necessary to decrease the emissions of such gases. Two strategies for this reduction are: 1) to produce engines that are more fuel efficient, 2) to use sustainably produced renewable fuels such as biodiesel and HVO. However, both these strategies may pose additional challenges for the emission control system: a colder exhaust due to the higher fuel-efficiency requires the use of highly active catalysts; catalyst deactivation related to impurities in biofuels, which requires very robust catalysts.

The objective of this thesis was to study the impact of biofuel as well as lubrication oil-related contaminants on the performance of emission control catalysts (DOC and SCR catalysts) for heavy-duty diesel engines. The main focus has been on the low-temperature performance of $V_2O_5-WO_3/TiO_2$ (VWTi) and Cu-SSZ-13 SCR catalysts.

Results from the project have shown that both Cu-SSZ-13 and VWTi catalysts capture and can be deactivated by phosphorus (P), while only the Cu-SSZ-13 is deactivated by sulfur (S). The degree of the P-related deactivation depends on the concentration in the catalyst, which depends on content of P in the exhaust and the exposure time, as well as the type of catalyst. S-deactivation of Cu-SSZ-13 is observed at low temperatures, where un-poisoned Cu-SSZ-13 are significantly more active than VWTi catalysts. As a contrast, the VWTi-performance can even be improved by sulfur; but alkali metals are severe poisons to VWTi catalysts. Partial performance-recovery of S-poisoned Cu-SSZ-13 can be obtained by exposing it to sulfur-free exhausts at elevated temperatures. The use of an upstream DOC, providing fast SCR conditions to the SCR catalyst, considerably improves the low-temperature performance of the VWTi, as well as sulfur-poisoned Cu-SSZ-13 catalysts. An upstream DOC also protects the SCR catalysts from phosphorus deactivation, as it can trap large amounts of P. However, if too much phosphorus is captured by the DOC, severe deactivation of this catalyst results, which lowers the overall performance of the exhaust treatment system.

Insights from this project will guide the development of robust exhaust treatment systems for various applications. Additionally, it could aid in developing more durable emission control catalysts.

Keywords: NH_3 -SCR, Cu-SSZ-13, $V_2O_5-WO_3/TiO_2$, catalyst deactivation, diesel oxidation catalyst, sulfur, phosphorus, biodiesel, heavy-duty, emission control, regeneration, alkali metals

Sammanfattning

Katalytisk avgasrening används för att minska de negativa hälso- och miljöeffekterna av dieselavgaser. För tunga lastbilar består detta avgasreningssystem av flera komponenter, dieseloxidationskatalysator (DOC), partikelfilter, SCR-katalysator och ammoniaköverskottskatalysator. I och med de klimatnegativa effekterna av växthusgaser, inkl. koldioxid, måste även emissionerna av dessa från tunga fordon minska. Två sätt att uppnå detta är att 1) producera mer bränsleeffektiva motorer, 2) använda förnybara bränslen såsom biodiesel och hydrerad växtolja (HVO). Båda dessa strategier kan dock medföra tuffa utmaningar för efterbehandlingssystemet – kallare avgaser respektive katalysatordeaktivering relaterad till kontamineringsämnen i biobränslena. Detta kräver att katalysatorerna är både aktiva och tåliga.

Syftet med detta doktorandprojekt har varit att studera effekten av biobränsle- och motoroljerelaterade kontamineringsämnens påverkan på avgasreningskatalysatorer för tunga dieselmotorer. Huvudfokus har varit påverkan på lågtemperaturregenskaperna hos två olika typer av SCR-katalysatorer, $V_2O_5-WO_3/TiO_2$ (VWTi) och Cu-SSZ.

Resultat från projektet har visat att fosfor kan ackumuleras i både VWTi och Cu-SSZ-13 och deaktivera dessa, medan svavel endast deaktiverar Cu-SSZ-13. Denna deaktivering syns vid låga temperaturer där Cu-SSZ-13 annars har en betydligt bättre prestanda än VWTi. Prestandan för svavelförgiftad Cu-zeolit kan delvis fås tillbaka genom att öka temperaturen i avgaserna i svavelfri miljö. Närvaro av ammoniak i avgasen underlättar regenereringen. VWTi-katalysatorn är däremot inte känslig för svavel utan får snarare en något förbättrad prestanda. Däremot är alkalimetaller ett starkt gift för VWTi.

En uppströms DOC kan väsentligt förbättra lågtemperaturprestandan för VWTi och för svavelförgiftad Cu-SSZ-13 genom att förse dessa med NO_2 så att snabb SCR kan uppnås. DOCn kan också skydda SCR-katalysatorer från fosforförgiftning genom att själv fånga upp fosfor. För mycket fosfor på DOCn resulterar dock i förgiftning även av denna, vilket påverkar resten av avgasbehandlingssystemet negativt.

Resultaten från detta projekt kan användas för att utveckla robusta avgasbehandlingssystem för olika typer av tillämpningar, och kan bidra till utvecklandet av mer tåliga katalysatorer.

Nyckelord: NH_3 -SCR, Cu-SSZ-13, $V_2O_5-WO_3/TiO_2$, katalysatordeaktivering, dieseloxidationskatalysator, svavel, fosfor, biodiesel, tunga dieselmotorer, avgasrening, regenerering, alkalimetaller

List of Appended Papers

This doctoral thesis is based on the following appended articles and manuscripts, which are referred to in the text of the thesis by their Roman numerals (I–VI). All articles and manuscripts are found in the appendix.

Paper I

Multivariate analysis of the effect of biodiesel-derived contaminants on V_2O_5 - WO_3 /TiO₂ SCR catalysts, Sandra Dahlin, Marita Nilsson, Daniel Bäckström, Susanna Liljegren Bergman, Emelie Bengtsson, Steven L. Bernasek, Lars J. Pettersson, *Applied Catalysis B: Environmental* 183 (2016) 377-385

Paper II

Catalytic aftertreatment systems for trucks fueled by biofuels – aspects on the impact of fuel quality on catalyst deactivation, Jonas Granstrand*, Sandra Dahlin*, Oliver Immele, Leonhard Schmalhorst, Cornelia Lantto, Marita Nilsson, Rodrigo Suarez Paris, Francesco Regali, Lars J. Pettersson, *RSC Catalysis* 30 (2018) 64-145

Paper III

Chemical aging of Cu-SSZ-13 SCR catalysts for heavy-duty vehicles – Influence of sulfur dioxide, Sandra Dahlin, Cornelia Lantto, Johanna Englund, Björn Westerberg, Francesco Regali, Magnus Skoglundh, Lars J. Pettersson, *Catalysis Today* 320 (2019) 72-83

Paper IV

In-situ studies of oxidation/reduction of copper in Cu-CHA SCR catalysts: comparison of fresh and SO₂-poisoned catalysts, Susanna L. Bergman*, Sandra Dahlin*, Vitaly V. Mesilov, Yang Xiao, Johanna Englund, Shibo Xi, Chunhua Tang, Magnus Skoglundh, Lars J. Pettersson, Steven L. Bernasek, *Submitted to Applied Catalysis B: Environmental* (2019)

Paper V

Effect of biofuel- and lube oil-originated sulfur and phosphorus on the performance of Cu-SSZ-13 and V_2O_5 - WO_3 /TiO₂ SCR catalysts, Sandra Dahlin, Johanna Englund, Henrik Malm, Matthias Feigel, Björn Westerberg, Francesco Regali, Magnus Skoglundh, Lars J. Pettersson, *Submitted to Catalysis Today* (2019)

Paper VI

Impact on the oxidation catalyst in a heavy-duty vehicle from the use of biogas, Johanna Englund, Kunpeng Xie, Sandra Dahlin, Dazheng Jing, Soran Shwan, Lennart Andersson, Lars J. Pettersson, Magnus Skoglundh, *Catalysts* 9 (2019) 1014

*These authors shared primary authorship

My Contributions to the Publications

Paper I: I participated in the planning of the experiment and performed some of the experimental work. I processed data and interpreted results together with my co-authors, and was the main author of the manuscript, which was written together with my co-authors.

Paper II: I and Jonas Granestrand wrote the major parts of the paper, which included also planning of the paper and going through relevant literature. We are both main authors.

Paper III: I participated in the planning of the experiments and was supervisor for master thesis student Cornelia Lantto, who performed most of the experiments. I performed some of the experiments. I processed and interpreted data together with Cornelia. I am the main author of the paper, and wrote the first draft of the manuscript, which was then finalized together with my co-authors.

Paper IV: I had a leading role in the planning of the experiments, prepared catalyst samples, and performed some of the experiments. I processed parts of the data, interpreted results and wrote the manuscript together with my co-authors. I am the main author of this paper, together with Susanna L. Bergman.

Paper V: I was the main responsible for the planning of the experiments, and performed the major part of the experiments, including all the SCR performance tests. Me and Johanna Englund prepared the aging experiments at Umicore Denmark ApS together. I processed the data, interpreted the results and wrote the first draft of the manuscript, which was then finalized together with my co-authors.

Paper VI: I did the XRF measurements and contributed to the data interpretation and the finalized manuscript.

Conference contributions

Conference contributions related to this thesis. The presenting author is marked with bold font.

Oral presentations

The effect of biodiesel-derived contaminants on Automotive SCR catalysts, **S. Dahlin**, M. Nilsson, D. Bäckström, S. Liljegren Bergman, E. Bengtsson, S.L. Bernasek, L.J. Pettersson, 9th International Conference on Environmental Catalysis (ICEC), Newcastle, Australia, 10-13 July, 2016

Chemical aging of V₂O₅-WO₃/TiO₂ and Cu/SSZ-13 SCR catalysts for heavy-duty trucks – The influence of sulfur and phosphorus, **S. Dahlin**, L. Schmalhorst, F. Regali and L. J. Pettersson, 25th North American Catalysis Society Meeting (NAM), Denver, USA, 4-9 June, 2017

Deactivation of exhaust aftertreatment catalysts for heavy-duty vehicles – influence of sulfur on the activity and selectivity of Cu-SSZ-13 SCR catalysts, **S. Dahlin**, J. Englund, C. Lantto, B. Westerberg, F. Regali, M. Skoglundh, L. J Pettersson, 8th Tokyo Conference on Advanced Catalytic Science and Technology (TOCAT), Yokohama, Japan, 5-10 August, 2018

Deactivating effect of biofuel and lube-oil components on Cu-SSZ-13 and V₂O₅-WO₃/TiO₂ SCR catalysts, **S. Dahlin**, J. Englund, Matthias Feigel, H. Malm, B. Westerberg, F. Regali, M. Skoglundh, L. J. Pettersson, 26th NAM, Chicago, USA, 23-28 June, 2019

Selective catalytic reduction of NO_x – The effect of biofuel and lube oil components, **S. Dahlin**, J. Englund, H. Malm, B. Westerberg, F. Regali, M. Skoglundh, L. J. Pettersson, 14th European Congress on Catalysis (Europacat), Aachen, Germany, 18-23 August, 2019

Impact of Aging on the Oxidation Catalyst And SCR Catalyst Using Biogas in A Heavy-Duty Gas-Engine Application, J. Englund, **K. Xie**, S. Dahlin et al. SAE 2019 Powertrains, Fuels & Lubricants Meeting, San Antonio, Texas, USA 22-24th January 2019

Poster presentations

Investigating the effect of biodiesel-derived contaminants on vanadia-based NH₃-SCR catalysts in heavy-duty exhaust aftertreatment, **S. Dahlin**, M. Nilsson, D. Bäckström, S. Liljegren Bergman, E. Bengtsson, S.L. Bernasek, L.J. Pettersson, 17th Nordic Symposium on Catalysis (NSC), Lund, 2016, 14-16 June, 2016

Influence of sulfur and phosphorus on automotive V₂O₅-WO₃/TiO₂ and Cu/SSZ-13 SCR catalysts, **S. Dahlin**, L. Schmalhorst, F. Regali and L. J. Pettersson, 13th

Europacat, Firenze, Italy, 28 August – 1 September, 2017. Received the Best Poster Award.

The effect of biofuel and lube oil-derived contaminants on the durability of Cu-SSZ-13 and V_2O_5 - WO_3 /TiO₂ SCR catalysts for heavy-duty vehicles, **S. Dahlin**, J. Englund, F. Regali, M. Skoglundh, L. J Pettersson, 18th NSC, Copenhagen, Denmark, 26-28 August, 2018

Investigation of fuel and lube oil contaminants on Cu-SSZ-13 and V_2O_5 - WO_3 /TiO₂ SCR catalysts: **S. Dahlin**, J. Englund, F. Regali, M. Skoglundh, L. J. Pettersson, 10th ICEC, China, September 22-26, 2018

Effect of SO₂ and Engine-Aging on the Activity and Selectivity of Cu-SSZ-13 NH₃-SCR Catalysts for Heavy-duty Vehicles, **S. Dahlin**, J. Englund, C. Lantto, B. Westerberg, F. Regali, M. Skoglundh, L. J Pettersson, 11th International Congress on Catalysis and Automotive Pollution Control (CAPoC) Brussels, Belgium, October 29-31, 2018

Deactivating effect of a Pd/Pt oxidation catalyst, **J. Englund**, K. Xie, S. Dahlin, S. Shwan, L. Andersson, M. Skoglund, 26th NAM, Chicago, USA, 23-28 June, 2019

The effect of using a biogas powered Euro VI engine on the Pd/Pt oxidation catalyst and the V_2O_5 - WO_3 /TiO₂ SCR catalyst, **J. Englund**, S. Dahlin et al., 14th European Congress on Catalysis (EUROPACAT 2019) Aachen, Germany 18-23rd August 2019

In situ characterization of fresh and sulfur contaminated Cu-zeolite SCR catalysts using XAFS. **S. Liljegren Bergman**, S. Dahlin, Y. Du, S. Xi, L.J. Pettersson, S. Bernasek. 14th European Congress on Catalysis – EuropaCat-XIII, Aachen, Germany, 18-23 August, 2019

Other contributions

Other contributions, not included in this thesis. Bold font indicates the presenting author.

Samspelseffekter vid deaktivering av efter-behandlingskatalysatorer för biobränsledrift, **S. Dahlin**, F. Regali, L. J. Pettersson, FFI-konferens, October 2014, Gothenburg

The role of alkali in heterogeneous catalysis for gas cleaning in stationary and mobile applications, **P.H. Moud**, J. Granstrand, S. Dahlin, M. Nilsson, K. J. Andersson, L.J. Pettersson, K. Engvall, 249th American Chemical Society National Meeting, Denver, Colorado, 22-27 March, 2015 (*Invited lecture*)

The Use of Biofuels in Heavy-Duty Trucks – Fuel Production and Exhaust Treatment. **L.J. Pettersson**, J. Granstrand and S. Dahlin, 10th International Conference on Environmental Catalysis, Tianjin, China, September 22-26, 2018 (*Invited keynote lecture*)

Contents

Abstract	I
Sammanfattning	II
List of Appended Papers	III
My Contributions to the Publications	IV
Conference contributions	V
Oral presentations	V
Poster presentations	V
Other contributions	VI
List of abbreviations	X
Part I: Introduction	1
1.1 Setting the scene	1
1.2 Objective of the thesis	6
1.3 Scope of the thesis	6
1.4 Background	8
1.4.1 Emission legislation	8
1.4.2 Diesel and renewable fuels used for heavy-duty applications	10
1.4.2.1 Petroleum-derived (conventional) diesel	10
1.4.2.2 Biodiesel	11
1.4.2.3 Hydrotreated Vegetable Oil, HVO	12
1.4.2.4 Ethanol/ED95	13
1.4.2.5 Biogas	14
1.4.2.6 Summary of possible contaminants in fuels for heavy-duty vehicles	15
1.5 Catalytic exhaust treatment in diesel trucks	15
1.5.1 Diesel and methane oxidation catalyst (DOC and MOC)	16
1.5.2 Diesel Particulate Filter, DPF	17
1.5.3 Selective Catalytic Reduction, SCR	18
1.5.4 Ammonia Slip Catalyst, ASC	20
1.6 SCR catalysts: Cu-SSZ-13 and V₂O₅-WO₃/TiO₂	21
1.6.1 V₂O₅-WO₃/TiO₂	21
1.6.2 Cu-SSZ-13	23
1.7 Catalyst deactivation	26
1.7.1 Deactivation by various fuel- and lube oil-derived components	27
1.7.2 Hydrothermal aging	32

Part II: Experimental	35
2.1 Catalyst samples	35
2.2 Evaluation of catalytic performance using laboratory flow reactors	36
2.2.1 Test protocol for SCR catalyst samples.....	36
2.2.2 Test protocol for DOC samples	38
2.3 Aging experiments and construction of an aging rig	39
2.3.1 Screening of the poisoning effect of biodiesel-related contaminants by wet impregnation using a DoE (Paper I).....	39
2.3.2 Construction of an aging rig.....	40
2.3.3 SO ₂ -exposure and regeneration in lab-reactor (Paper III-IV).....	43
2.3.4 Exposure of DOC and SCR catalysts to FAME-exhausts with phosphorus and/or sulfur using a diesel burner rig (Paper V).....	43
2.3.5 Aging of a Pd-Pt/Al ₂ O ₃ oxidation catalyst in an engine operated on biogas (Paper VI)	45
2. 4 Catalyst characterization	45
2.4.1 Copper oxidation state and coordination by in-situ Synchrotron X-ray absorption spectroscopy (XAS).....	45
2.4.2 Bulk elemental analyses by XRF and ICP	47
2.4.3 Surface species by XPS	48
2.4.4 Electron microscopy to study the morphology of DOC and SCR catalyst samples	48
2.4.5 Determination of sulfur content by TGA-MS or using a LECO sulfur analyzer	50
2.4.6 Acidity by NH ₃ -TPD.....	50
2.4.7 Reducibility and copper speciation by H ₂ -TPR.....	51
2.4.8 Surface area measurements by N ₂ physisorption	52
2.4.9 Powder X-ray diffraction (XRD).....	52
2.5 Calculations/Theory	53
2.5.1 Evaluation of the screening design using Multiple Linear Regression (Paper I).....	53
2.5 2 Evaluation of aging using a relative rate constant	53
2.5.3 MCR-ALS for analysis of in-situ temperature dependent XAS spectra and DFT-assisted theoretical XANES	55
Part III: Results and Discussion	57
3.1 Performance of fresh SCR catalysts	57
3.1.1 V ₂ O ₅ -WO ₃ /TiO ₂	57
3.1.2 Cu-SSZ-13	59

3.1.3 Summary of NO ₂ /NO _x ratio effect on the SCR performance: NO _x conversion and N ₂ O selectivity/production.....	62
3.2 The effect of biodiesel-derived contaminants on V ₂ O ₅ -WO ₃ /TiO ₂ SCR catalysts – a screening study (Paper I)	65
3.3 The effect of SO ₂ and engine-aging on the performance of Cu-SSZ-13 SCR catalyst (Paper III)	70
3.3.1 Effect of lab-scale SO ₂ -exposure	70
3.3.2 Effect of engine-aging.....	77
3.4 Copper sites and oxidation and reduction behavior of fresh and SO ₂ -poisoned Cu-SSZ-13 catalyst by in-situ synchrotron XAS (Paper IV)	81
3.5 The effect of phosphorus and sulfur in biodiesel exhaust on Cu-SSZ-13 and V ₂ O ₅ -WO ₃ /TiO ₂ SCR catalysts (Paper V)	87
3.5.1 Aging effects on the V ₂ O ₅ -WO ₃ /TiO ₂ catalyst.....	87
3.5.2 Aging effects on the Cu-SSZ-13 catalyst	89
3.5.3 Effect of sulfur desorption during SCR test – partial regeneration of Cu-SSZ-13	90
3.5.4 Capture of phosphorus and sulfur in the SCR catalysts.....	92
3.5.5 SCR performance in relation to captured contaminants	95
3.5.6 Effect of phosphorus on the DOC.....	97
3.6 The effect of biogas operation on a Pd-Pt oxidation catalyst (Paper VI).....	99
Part IV: Concluding Remarks and Outlook	103
Conclusions.....	103
Suggestions for further work.....	105
Acknowledgements	107
References	111

List of abbreviations

ASC: ammonia slip catalyst

a.u: arbitrary unit

B100: 100% biodiesel (FAME)

BET: Brunauer-Emmett-Teller, model for calculating specific surface area using N₂ physisorption

CARB: California Air Resources Board

CEM: controlled evaporation and mixing

CHA: chabazite framework structure

CI: compression-ignited (engine)

CO: carbon monoxide

CO₂: carbon dioxide

cpsi: cells per square inch (a measure of cell density in catalyst substrates)

deSOx: desulfurization, same as sulfur regeneration, removal of sulfur from the catalyst

DFT: density functional theory

DOC: diesel oxidation catalyst

DoE: design of experiment

DOT: Department of Transportation

DPDS: dipropyl disulfide

DPF: diesel particulate filter

E85: ethanol-fuel with 85% ethanol and 15% gasoline

ED95: ethanol-fuel with 95% ethanol and additives

EDX: energy dispersive X-ray spectroscopy

EPA: Environmental Protection Agency (US)

EXAFS: extended x-ray absorption fine structure

FAME: fatty acid methyl ester

FTP: federal test procedure

FUL: full useful life

GHG: greenhouse gas(es)

HC: hydrocarbons

HD: heavy-duty

hp: horse-power

HVO: hydrotreated vegetable oil

ICP-OES: inductively coupled plasma – optical emission spectroscopy

LCF: linear combination fit

LD: light-duty

MCR-ALS: multivariate curve resolution alternating least square

MLR: multiple linear regression

MS: mass spectrometry

NHTSA: National Highway Traffic Safety Administration

n.a: not analyzed

N₂O: nitrous oxide/laughing gas (strong greenhouse gas)

NO_x: nitrogen oxides (x=1: nitric oxide; x=2: nitrogen dioxide)

RED: renewable energy directive

RMC-SET: ramped-mode cycles supplemental emissions test

RME: Rape methyl ester (a type of FAME)

RT: room temperature

SCR: selective catalytic reduction

SEM: Scanning Electron Microscopy

SI: spark-ignited (engine)

STEM: scanning transmission electron microscopy

TEM: transmission electron microscopy

HAADF: high-angle annular dark field

TGA: thermogravimetric analysis

TPD: temperature programmed desorption

TPP: triphenyl phosphate

TPR: temperature programmed reduction

TWC: three-way catalyst

ULSD: ultra-low sulfur diesel (<15 ppm)

VWTi: V₂O₅-WO₃/TiO₂ SCR catalyst

WHSC: world harmonized stationary cycle

WHTC: world harmonized transient cycle

XANES: X-ray absorption near-edge spectroscopy

XAS: X-ray absorption spectroscopy

XES: X-ray emission Spectroscopy

XPS: x-ray photoelectron spectroscopy

XRD: X-ray powder diffraction

XRF: X-ray fluorescence spectroscopy

Z₂Cu: Cu²⁺ sites in the SSZ-13 with 2 aluminum atoms (Al)

ZCuOH: Cu²⁺ sites in the SSZ-13 with 1 Al

SSZ-13: small-pore zeolite with CHA framework

Part I: Introduction

1.1 Setting the scene

Transportation is the bloodstream of our modern society

Our society relies on efficient transportation of both goods and humans. As the population grows, and more people are living in densely populated areas, the need for goods transportation is increasing. In Europe, the road freight transportation increased by more than 11% in the years 2013-2017 for most distances (see **Figure 1**), and is expected to continue to grow [1]. The same applies in, for example, the US: the tons of freight moving on roads are expected to grow by 40% in the coming three decades [2]. A common and efficient way of doing this transportation is by trucks powered by internal combustion engines, usually diesel engines. Trucks are flexible and can handle a large volume and weight of goods. In comparison to spark-ignited (SI) Otto engines, which commonly use gasoline or gas for propulsion, compression-ignited (CI) diesel engines are durable and fuel efficient. However, a drawback of diesel engines is the emissions related to the combustion of the fuel, and many parts of the world are heavily polluted due to this. Nevertheless, not only diesel exhausts contribute to this pollution but all types of combustion, whether it is used for propulsion of vehicles or for heat and electricity production in powerplants.

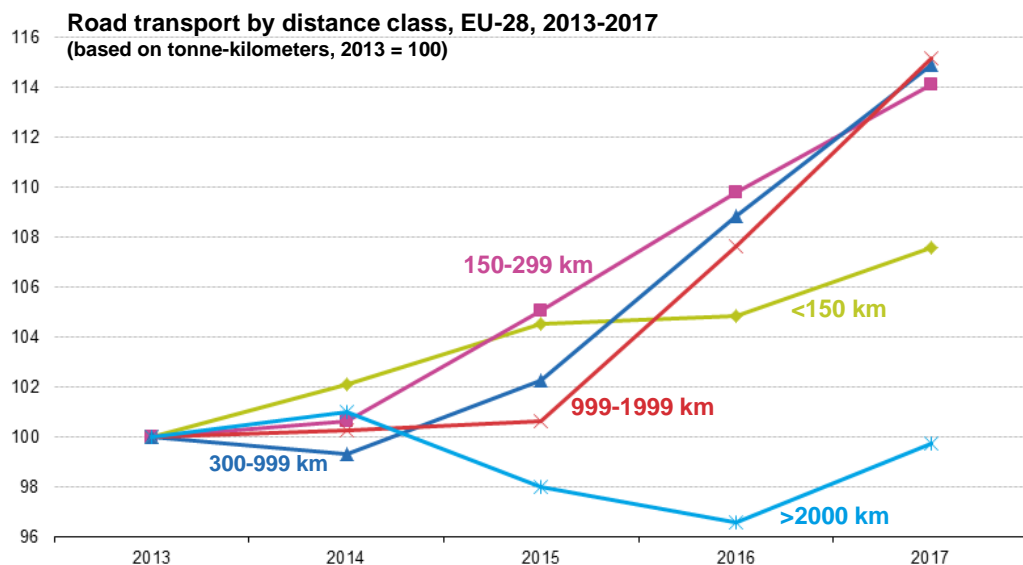


Figure 1: Road freight transportation in the European Union (EU, Malta excluded) from 2013 to 2017 for different distances. A steady increase in road transportation is observed for all distances except the longest distances (>2000 km). The graph normalizes the year 2013 to a value of 100 [3].

The products from combustion of any fuel containing hydrocarbons are carbon dioxide (CO_2) and water (H_2O). Carbon dioxide is a greenhouse gas (GHG), which negatively influences our environment as it contributes to climate changes through global warming of the planet [4]. In addition to CO_2 and H_2O that are the main products from the combustion, pollutants such as carbon monoxide (CO), unburnt hydrocarbons (HC), particulate matter (PM), nitrogen oxides (NO_x , $x=1, 2$), as well as sulfur oxides (SO_x , $x = 2$ or 3) are also formed. CO, HC, and PM in the form of soot is related to incomplete combustion, and PM also forms from incombustible material in the fuel or lubrication oil. NO_x is mainly formed from reaction between nitrogen and oxygen in the air at high combustion temperatures, but could additionally form from nitrogen-containing compounds in the fuel; SO_x originate from sulfur-containing compounds in the fuel. All of these pollutants are harmful for our health and/or the environment. The amount of these pollutants in the exhaust depends on the type of combustion and the fuel. In a combustion with excess oxygen, such as in the diesel engine, the combustion is normally very efficient, and only small amounts of HC and CO are formed. The main pollutants in diesel exhausts are instead nitrogen oxides and PM. [5] A typical composition of diesel exhausts is shown in **Figure 2**, together with a photo showing significant air pollution.

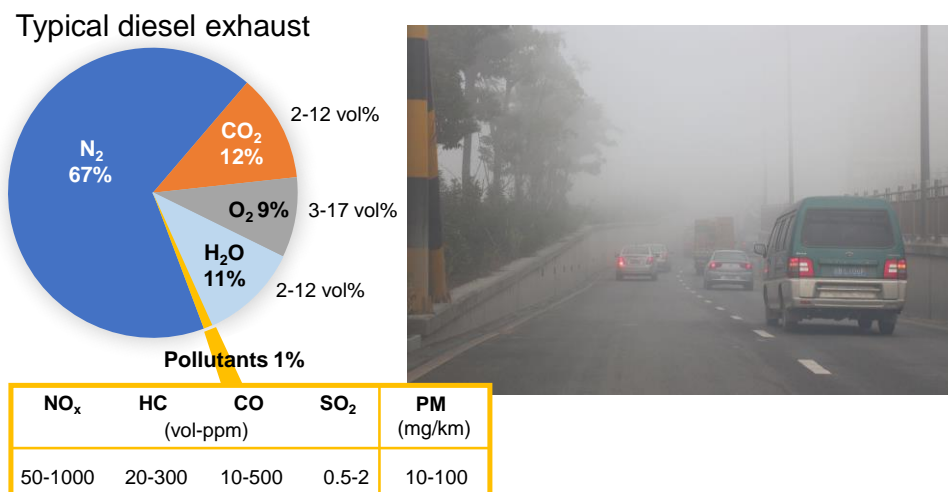


Figure 2: Typical composition of diesel exhausts including realistic concentration ranges of exhaust and pollutants concentrations, and air pollution in Ningbo (left). Figure based on data from [6], [7], combined with the photo by [8] (CC BY-SA 2.0).

Catalytic exhaust treatment is used to minimize emissions of pollutants

To reduce the negative impact of engine exhausts on our health and on the environment, emission legislations were first introduced in the US in 1975. Since then, the emission standards have become gradually more stringent. Today, strict emission legislation applies in many parts of the developed world, and is progressively being introduced in less developed countries as well [9, 10]. This is a

part of reaching the United Nations (UN) Sustainable Development Goal number 3, Good Health and Well-Being. The solution to fulfill the current emission standards, in for example Europe and the US, is to use catalytic aftertreatment of the exhausts. In this, the pollutants are converted over catalysts into less harmful or harmless compounds. The task of the catalysts is to increase the reaction rate of these conversions, such that the reactions occur at the temperatures practical in the exhaust system. In addition to increase the reaction rate, it is important that the catalyst is selective. This means that the reaction should yield the products that are wanted, and not form any undesirable by-products.

In an engine operating at stoichiometric fuel-oxygen conditions, such as a gasoline engine, a three-way catalyst (TWC) is used to simultaneously oxidize HC and CO and reduce NO_x (see **Figure 3**). However, diesel engines operate at conditions with excess of oxygen, also called lean combustion that means that it is fuel-lean and oxygen-rich. Whereas the oxidation of hydrocarbons and carbon monoxide is easy in this atmosphere, the reduction of NO_x is difficult, as displayed in **Figure 3**. Consequently, another strategy is needed for this NO_x reduction. In diesel trucks, the method applied for reducing NO_x is selective catalytic reduction (SCR), using NH_3 as a reductant.

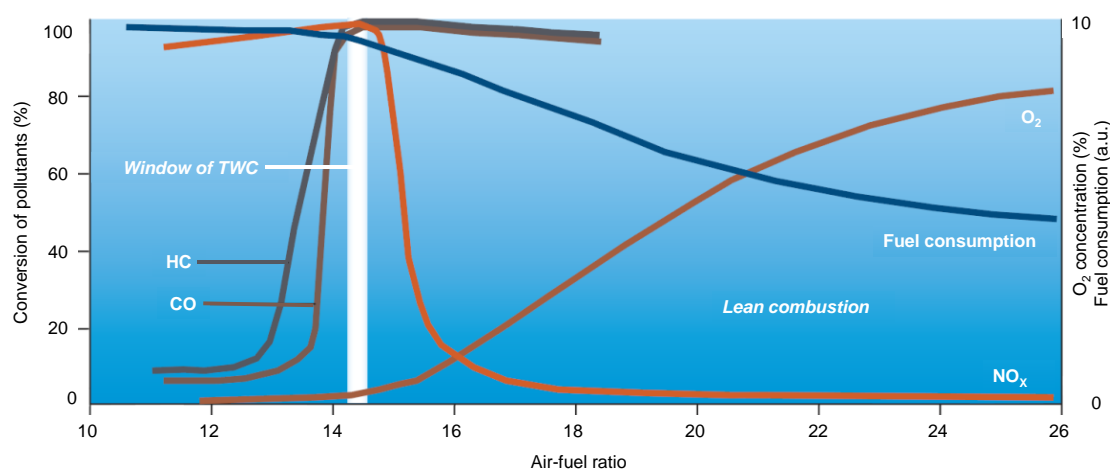


Figure 3: Effect of air-fuel ratio on conversion of HC, CO and NO_x over a 3-way (left axis) and on oxygen concentration and fuel consumption (right axis). Adapted from and used with permission from S. Shwan [11].

Reducing greenhouse gas emissions from diesel vehicles required

In the European Union, trucks and buses are responsible for around a quarter of the total CO_2 emissions from road transport [12]. Emissions of GHGs, such as CO_2 , is a major concern for our environment. Increasing levels of GHGs in the atmosphere, which may lead to global warming of the planet resulting in severe climate changes. Recently, the Intergovernmental Panel on Climate Change (IPCC) therefore announced that a global warming limit of 1.5°C above pre-industrial levels should be targeted [4], rather than the previously stated 2°C limit [13].

Consequently, one important task is to reduce the anthropogenic GHG emissions from trucks, as a part of reaching the UN Sustainable Development Goal number 13, Climate Action. Two strategies of reducing GHG emissions from diesel vehicles are: 1) to produce engines and vehicles that are more fuel efficient and thus consume less fuel; 2) to use sustainably produced renewable fuels/biofuels, such as biodiesel and hydrogenated vegetable oil (HVO). Biofuels in themselves do not emit less CO₂ when combusted; however, the CO₂ that is emitted during the combustion of biofuel was captured during the growing of the plant in a quite near time perspective and will furthermore be captured when a new plant is growing. Thus, there is no extra CO₂ added to the atmosphere from this combustion. The CO₂ that originates from combustion of fossil fuels on the other hand, was captured during a long period of time, millions of years; thus, the release of this CO₂ in a short period of time, with no corresponding uptake during this time, results in a significant amount of net CO₂ to the atmosphere. Both the US [14] and EU (renewable energy directive [15]) have programs or standards related to the use of renewable fuels, although the focus of using biofuels appear to be larger in Europe.

Challenges for catalytic diesel exhaust emission control: low temperature and durability

Although more efficient engines are beneficial from both an environmental and economical perspective, there is a challenge with this in relation to the emission control catalysts. This challenge originates from the colder exhausts that are produced from more efficient engines, as more fuel is converted into useful work while less is wasted as heat. However, lower temperatures in the exhausts results in a slower conversion of the pollutants in the exhaust, and thus more active catalysts are required to increase the rate of conversion.

The use of biofuels, such as biodiesel, also poses a challenge for the catalytic components, as impurities from the biodiesel, e.g. phosphorus, sulfur, and sodium could deactivate the catalysts, making them less active.

Both challenges above are illustrated in **Figure 4**, which shows the conversion of NO_x into mainly water and nitrogen as a function of temperature for a vanadium-based SCR catalyst. In this figure, 100% conversion means that all NO_x that is introduced to the catalyst is converted, i.e. there will be no NO_x in the effluent gas from the catalyst. At temperatures of around 300 °C and above, the NO conversion is good. However, at low temperatures (e.g. <250 °C) the conversion level of NO is rather low. This low-temperature part will become increasingly important as the fuel-efficiency improves. Furthermore, a significant deactivation is observed after use in a truck operated on biodiesel for around 120,000 km, as displayed by the red curve in **Figure 4**. An improved low-temperature performance can be obtained by the use of small-pore metal exchanged Cu-zeolites, such as Cu-SSZ-13. However, a drawback with this kind of catalyst is its sensitivity to sulfur oxides in the exhaust.

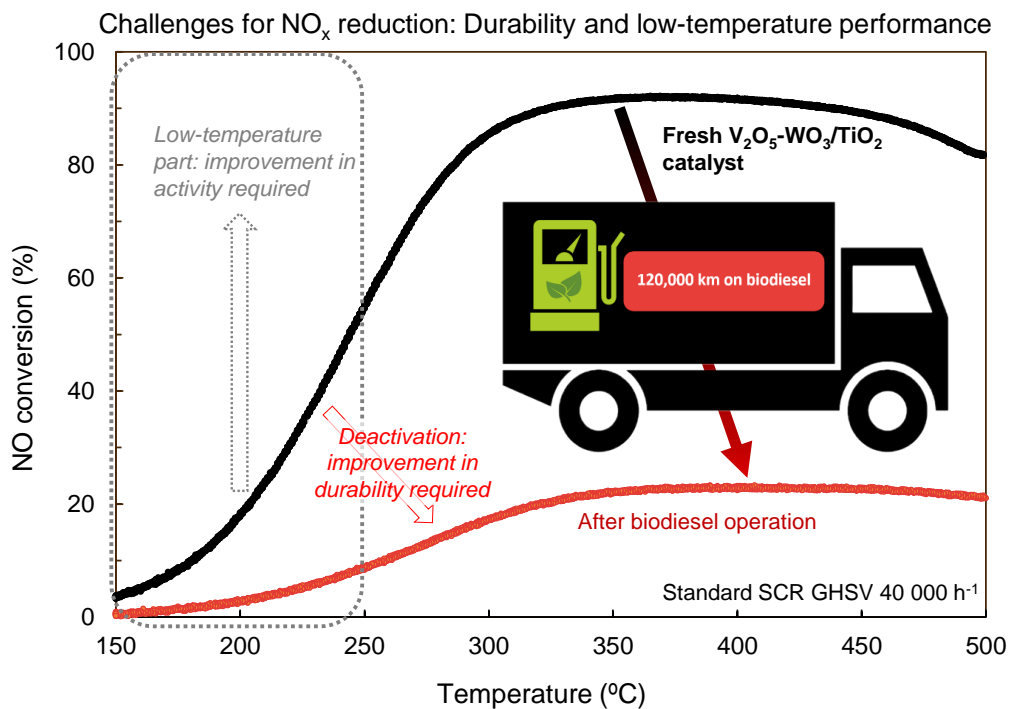


Figure 4: Challenges for NO_x reduction in heavy-duty vehicles displayed by NO conversion profile of a fresh and aged vanadium-based SCR catalyst. The aged catalyst had been operated approximately 120,000 h on biodiesel in a truck with a Euro V emission control system. Figure adapted and printed with permission from J. Englund [16].

Exposure to SO_x leads to a considerable decrease in the low-temperature NO_x reduction performance of this type of catalyst.

Coming emission standards will be even more stringent than today. Specifically, the importance of a fuel efficiency and/or greenhouse gas reduction will grow. Fuel efficiency or greenhouse gas standards for heavy-duty trucks have been adopted both in the EU (Regulation EU 2019/1242) [17] and in the US [17, 18], and these standards will progressively become more stringent. At the same time, the emission standards related to pollutants, such as NO_x and PM, must be fulfilled. These emission standards will be at least as stringent as today, and most likely even more stringent. For example, the California Air Resources Board (CARB) suggested NO_x standards to decrease from the current 0.2 to 0.05-0.08 g/bhp-hr for the years 2024-2026 [19]. Additionally, for the emission standard tests, a stronger emphasis will be put on the cold-start parts, and on on-road compliance tests that ensure the emissions are kept low also in real-world, during the whole lifetime of the truck.

In conclusion, highly active, selective, and durable catalysts are essential to comply with future emission standards and reduce the negative impact of diesel exhausts on our health and on the environment.

1.2 Objective of the thesis

Impact of biofuel and lube-oil related components on emission control catalysts

The objective of this thesis was to study the impact of biofuel and lubrication oil-related contaminants on the performance of emission control catalysts for lean-burn heavy-duty engines. An increased understanding about deactivating effects of different contaminants on the different types catalysts will aid in designing robust exhaust treatment system for various applications. Furthermore, it can aid in the development of more durable catalysts. To understand deactivation phenomena, an understanding of reaction mechanisms and active sites of fresh catalysts are also essential. This in turn, might result in an extended knowledge that additionally could aid in the development of more active and selective catalysts.

1.3 Scope of the thesis

The main focus has been on SCR catalysts, but oxidation catalysts have also been included in some studies. Two different types of SCR catalysts were investigated, vanadium-based ($\text{V}_2\text{O}_5\text{-WO}_3/\text{TiO}_2$ also denoted VWTi) and Cu-zeolite based, namely, copper-exchanged small-pore zeolite (Cu-SSZ-13) catalysts. An overview of the general experimental procedure is shown in **Figure 5**.

The first paper used a multivariate experimental design approach to study the effect of six different biodiesel-related contaminants on the performance of the $\text{V}_2\text{O}_5\text{-WO}_3/\text{TiO}_2$ catalyst using a wet-impregnation method for contaminant exposure. The aim was to establish which of these contaminants that have a significant influence on the catalytic NO_x reduction performance, and elucidate if there are any important interaction effects between various contaminants.

The second paper is a review that investigates what kind of contaminants could be present in different types of biofuels and the subsequent effect they could have on the different types of exhaust treatment catalysts. The main focus is on diesel oxidation catalysts (DOC) and SCR catalysts, but particulates filters are also included. The aim of the paper was to identify relevant contaminants for biofuel-operated vehicles, establish what is known about their deactivating effect on different catalyst materials, as well as to identify knowledge gaps.

The third paper investigated the effect of SO_2 on Cu-SSZ-13 SCR catalysts. SO_2 gas-phase poisoning of two different Cu-SSZ-13 was performed to understand its impact on the low-temperature SCR performance and regeneration possibilities. In addition, an engine-aged catalyst was evaluated. Furthermore, the effect of SO_2 on a third Cu-SSZ-13 and the VWTi catalyst was investigated (not included in Paper III, but in this thesis).

The forth paper went deeper into the copper species in fresh and SO₂-poisoned Cu-SSZ-13 catalysts, and investigated the responses of fresh and poisoned catalysts to oxidizing and reducing gas atmospheres. The aim was to identify possible sulfur-copper species and understand the interaction of S/SO₂ with the copper sites in various conditions.

The fifth paper is an aging study in which exhausts from pure and doped (P, S, and P+S) biodiesels were used to evaluate effects on both a V₂O₅-WO₃/TiO₂ and Cu-SSZ-13 SCR catalysts. In this study, a DOC was also included in the aging experiments. The aging conditions in this work were closer to real-world aging than the lab-aging in the previous studies.

In the sixth paper a Pd-Pt/Al₂O₃ oxidation catalyst was evaluated. This catalyst had been used in an engine operated on biogas and aging effects related to the biogas operation were investigated.

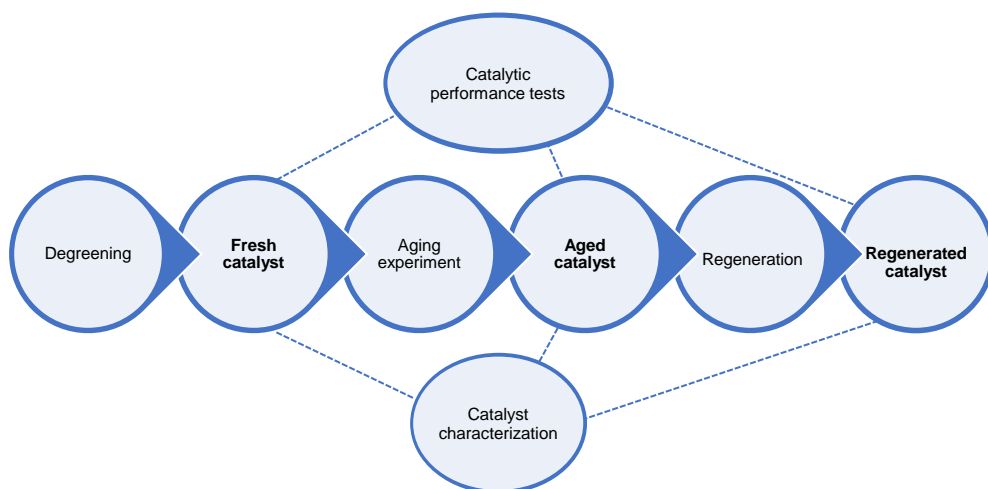


Figure 5: Overview of the general experimental procedure used in most papers.

1.4 Background

1.4.1 Emission legislation

Emission legislations were first introduced in the 1970's in the United States, by the Clean Air Act (CAA), as a response to the heavy air pollution caused by the road traffic. In this act, the federal government established regulations for passenger cars regarding several key pollutants, as well as air quality standards including the following seven outdoor pollutants: CO, NO_x, SO_x, PM, VOC, ozone (O₃), and lead (Pb).[10] In Sweden it became mandatory for gasoline passenger cars to use catalytic converters in 1989 [20].

For heavy-duty vehicles, emission regulations were generally introduced later: in the US, EPA set regulations for NO_x and PM from heavy-duty engines in 1985 [10], whereas the Europe Union introduced the first standards in 1992, for both heavy-duty (Euro I) and light-duty (Euro 1) vehicles [21, 22]. Since then, increasingly stringent emission standards have been introduced [9], and in more and more parts of the world, as can be seen in **Figure 6**. This figure shows how the NO_x and PM limits for heavy-duty trucks in different parts of the world have evolved over time

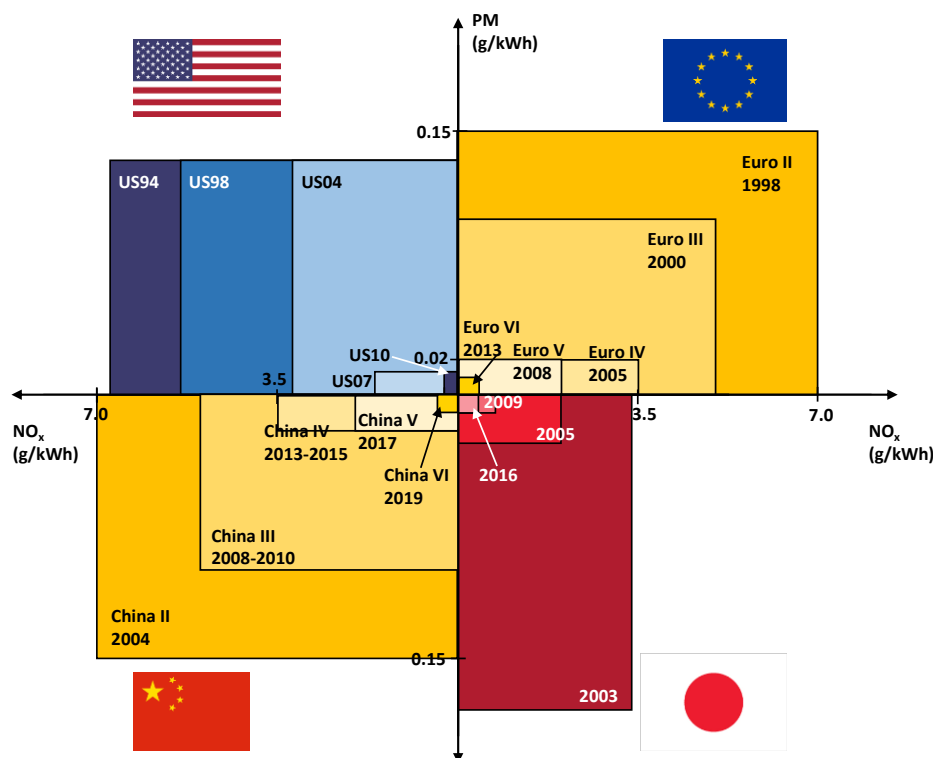


Figure 6: Evolution of heavy-duty diesel on-road NO_x and PM regulations with time in different parts of the world. The years noted are when it started to apply for all vehicles included in the standard, not only type approvals (which commonly is one year earlier) [9]. Note that the very first emission standards are not included in the figure.

In the beginning, mainly engine control methods, which reduce the production of NO_x and/or PM during the combustion, were used. One such method is exhaust gas recirculation (EGR). This method lowers the combustion temperature by diluting the burning mixture with recirculated exhaust gases. A lower combustion temperature, leads in turn to less NO_x produced. The normal procedure by the original equipment manufacturers (OEM) was to control one of the PM or NO_x by engine-means, and add an aftertreatment component to abate the other. [23] In 2003, SCR catalysts were introduced commercially in Europe, and the use of these was continuously growing as the limits for NO_x tightened from Euro IV in 2005 to Euro V in 2008. [24] Today, the Euro VI emission standard applies in Europe, with substantially more stringent limits for NO_x and PM. However, not only NO_x and PM are regulated, also HC, CO, and ammonia are tightly regulated in this standard (see **Table 1**). To comply with this standard, a combination of different catalysts, as well as a particulate filter, are needed, which is described in **Section 1.5**.

Table 1: Current emission standards in Europe – Euro VI^d for heavy-duty (HD) trucks¹, and Euro 6d-TEMP for light-duty (LD) vehicles. For light-duty vehicles, the limits are in g/km while for heavy-duty the limits are in g/kWh. Note that limits for particulate numbers also are included in the standards, although not shown in this table. [25]

	NO _x	PM	HC	CO	NH ₃ (ppm)
HD diesel (g/kWh)	0.46	0.01	0.16	4.0	10
LD diesel (g/km)	0.08	0.005	0.17 ³	0.5	-
LD gasoline	0.06	0.005	0.1	1.0	-

¹ in the world-harmonized transient cycle (WHTC); ² on the New European Driving Cycle (NEDC).

³ (HC+NO_x)

Recently, regulations regarding GHGs, e.g. CO₂, and/or fuel consumption for heavy-duty vehicles have been introduced in parts of the world. For example, EPA and National Highway Traffic Safety Administration (NHTSA) established standards for GHGs (including N₂O) and fuel consumption, which became effective in December 27, 2016 [18]. In March 2019, Japan updated their fuel efficiency standard for trucks and buses, with efficiency improvements of 13.4-14.3% setting 2015 as a base and 2025 as target [26]. In 2019 the European Union also adopted the first EU-wide CO₂ emission standard for heavy-duty trucks and buses. This standard sets targets for reducing CO₂ emissions from new vehicles for the years 2025 and 2030. [12]

In coming emission standards, even stricter demands on NO_x and PM are expected, but the major focus will probably be on fuel efficiency and greenhouse gas emissions. Furthermore, it is likely to be more emphasis on colder parts of the test cycles, as well as on-road compliance tests on vehicles in service through portable emission measurement systems (PEMS). Using PEMS, real-world emissions from the vehicles can be measured. In addition, the durability demand is also expected to increase from today's 700,000 km to 1,000,000 km [27].

1.4.2 Diesel and renewable fuels used for heavy-duty applications

The following section contains a description of some common fuels and impurities that could be found in these fuels. A more thorough description about biodiesel, HVO, and ethanol fuels can be found in **Paper II**.

1.4.2.1 Petroleum-derived (conventional) diesel

Diesel fuel is a mixture of hydrocarbons (boiling point 200-350 °C, at atmospheric pressure) obtained from crude oil via distillation and subsequent treatment. This typically results in a mixture of hydrocarbon chains that contain between 9 and 25 carbon molecules [28]. It mainly consists of paraffinic (saturated) hydrocarbons, but can also contain some aromatic and olefinic (unsaturated) hydrocarbons. The content of these non-paraffinic hydrocarbons depends on the fuel quality. [29]

Diesel fuels also contain impurities such as sulfur. To enable the use of highly efficient exhaust treatment systems, the sulfur content in diesel fuels has been gradually decreased the past decades. For example, in the EU, the allowed sulfur concentration decreased from 0.2% in 1993 (Euro I) to 0.001%, i.e. 10 ppm, in 2009 (Euro V). Today, the use of ultra-low-sulfur-diesel (ULSD) is required in parts of the world, for example the EU and the US, where the sulfur content is regulated to 10 [30] and 15 ppm [31], respectively. However, lower quality diesel fuels are still used in many parts of the world, for example in Brazil. These diesel fuels can contain considerably higher concentrations of sulfur, 50-2000 ppm [32]. Another application in which the sulfur concentration in the fuel can be high is in marine applications, where it is common with an S content of more than 1000 ppm [31].

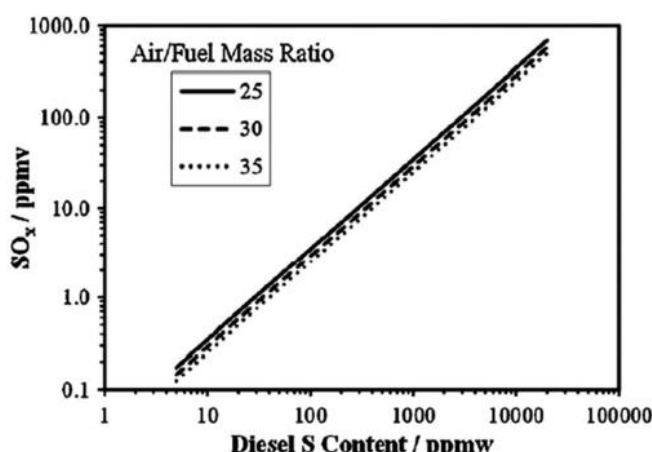


Figure 7: Correlation between fuel sulfur content and corresponding concentration of SO_x in the engine-out exhausts for three typical air/fuel mass ratios. For the calculation of the SO_x concentration, the diesel fuel was assumed to be fully oxidized into CO₂, H₂O, and SO_x during the combustion. Reprinted from Appl. Catal. B 160–161, Y. Xi et al. [33] with permission from Elsevier.

From January 2020, the maximum sulfur content in marine fuels, outside emission-control areas, was regulated to 5000 ppm, or 0.5 wt%. If the concentration of sulfur is higher than this, a scrubber must be used on the ship.[34]

The sulfur concentration in the exhaust, as a function of the sulfur concentration in the fuel, for three different air/fuel mass ratios is shown in **Figure 7**.

1.4.2.2 Biodiesel

Biodiesel is a biodegradable and non-toxic diesel-like fuel made of renewable resources, such as vegetable oil and animal fats. Biodiesel is commonly produced through a catalyzed transesterification reaction. In this reaction, vegetable oils react with an alcohol, usually methanol, to produce biodiesel and glycerol, see **Figure 8**. According to the European biodiesel standard, EN14214, biodiesel is defined as fatty acid methyl esters (FAME), which means that methanol must be the alcohol used for the production. An ester means that the biodiesel molecule contains oxygen, as opposed to petroleum-derived diesel that consists of paraffinic hydrocarbons (**Figure 9**).

Biodiesel is a biodegradable and non-toxic diesel-like fuel made of renewable resources, such as vegetable oil and animal fats. Biodiesel is commonly produced through a catalyzed transesterification reaction. In this reaction, vegetable oils react with an alcohol, usually methanol, to produce biodiesel and glycerol, see **Figure 8**. According to the European biodiesel standard, EN14214, biodiesel is defined as fatty acid methyl esters (FAME), which means that methanol must be the alcohol used for the production. Being an ester means that the biodiesel molecule contains oxygen, as opposed to petroleum-derived diesel that consists of paraffinic hydrocarbons (**Figure 9**). In the US (ASTM D6751) the definition of biodiesel is less strict; it is defined as mono-alkyl esters of long chain fatty acids derived from animal fats and vegetable oils, which means that other alcohols than methanol are allowed to be used for the production of the biodiesel. Another difference between conventional diesel and biodiesel is that the hydrocarbon chains in biodiesel can contain unsaturations (double bonds), depending on the feedstock that it is produced from. These unsaturations lower the oxidation stability of the biodiesel. Biodiesel can be used pure or in blends with petroleum-derived diesel. For blends with a low content of biodiesel, no modifications need to be done to the engine and fuel system. However, when higher blends or pure biodiesel is used, slight modifications are needed.

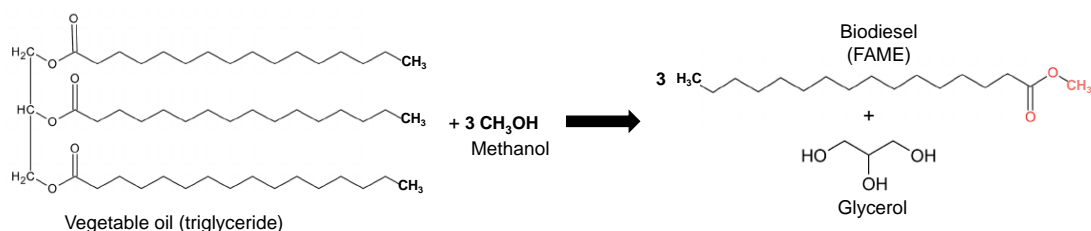


Figure 8: Transesterification reaction scheme for biodiesel production

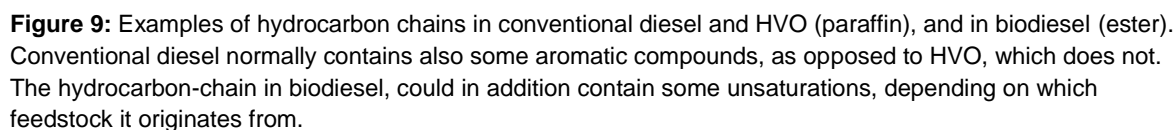
Biodiesel blends are usually called BX, where the X is the percentage of biodiesel in the blend, e.g. B7, B20, B100. The conventional petroleum-derived diesel (EN590) is currently allowed to contain up to 7% biodiesel in Europe.

In biodiesel, impurities related to the raw material and to the production process could exist. These impurities can be phosphorus (P), sulfur (S), sodium (Na), potassium (K), calcium (Ca), and magnesium (Mg). Phosphorus and sulfur mainly originate from impurities in the feedstock/raw material, while the alkali and alkaline earth metals mainly originate from the commonly used base-catalyzed transesterification process (Na or K) or subsequent separation/cleaning steps (Mg and/or Ca). These contaminants could negatively influence exhaust treatment components. As a result, the biodiesel standards (e.g. EN 14214) state the maximum allowable concentration of these elements in the biodiesel (see **Table 2**). Another potential impurity is zinc (Zn), which could originate from another production route that uses a heterogeneous Zn-Al catalyst for the transesterification (Esterfip-H process, used by Perstorp, for example). However, a heterogeneous catalyst is easier to separate from the product than a homogeneous one; consequently, Zn is likely to be present at lower concentrations than those of Na and K from the homogeneous catalytic process. No limit for Zn is included in the biodiesel standards. The biodiesel standard mentioned above states the maximum allowable limits of contaminants; however, it appears as the concentration of impurities in commercial biodiesel often are lower than these values [35].

In **Paper I** and **V**, catalyst exposed to biodiesel exhausts have been evaluated.

1.4.2.3 Hydrotreated Vegetable Oil, HVO

Hydrotreated, or hydrogenated, vegetable oil is a renewable diesel fuel that is produced from treating vegetable oils or animal fats with hydrogen to remove oxygen and double bonds from the hydrocarbon chains. In this process, paraffinic, non-aromatic hydrocarbons are produced, which are very similar to the components in conventional diesel (see **Figure 9**). However, HVO is cleaner than diesel as it contains no aromatics. In addition, this fuel contains low levels of sulfur



Another benefit of HVO compared to FAME is that it has exceptional stability and storage properties. [36]

A difference from conventional diesel is that the density of HVO is slightly lower. Therefore, this fuel does not fulfill the EN590 standard. However, a new standard for paraffinic diesel fuel was introduced in 2016, EN15940, which HVO complies to [38].

Ethanol ($\text{CH}_3\text{CH}_2\text{OH}$) is a clear, colorless, flammable, and volatile liquid that can be produced through fermentation of biomass such as sugar cane and beet, corn, and lignocellulosic material [35]. Ethanol fuels are normally considered mainly for SI engines. However, there are also interests in use for CI engines. One example of such application is the ED95 fuel, which is an ethanol-based fuel for heavy-duty trucks and buses with modified diesel engines. Scania is currently the only supplier of such engines [39]. ED95 consists of around 93-95 vol% ethanol and 5 vol% ignition improvers and corrosion inhibitors (polyethylene glycol derivative, MTBE, and isobutyl alcohol) [40]. Up to 90% CO_2 reduction [41], but more commonly around 68% [40], can be achieved by running on ED95 compared to conventional diesel.

Both ED95 and E85 (85% ethanol, 15% gasoline), which is used for modified gasoline (SI) engines, is allowed to contain maximum 10 ppm S, but the typical value is less than 3 ppm [42]. The presence of other contaminants in bioethanol appears to be low, less than 1.5 ppm and usually well below 1 ppm [35].

1.4.2.5 Biogas

Biogas is a product of anaerobic digestion of biomass, for example sludge from waste water treatment and food wastes. It consists of around 50-70% methane (CH_4) and CO_2 (raw biogas). Biomethane is biogas that has been upgraded to natural gas quality. This gas has a high CH_4 content, at least 90% but usually 96-99%, and low contents of impurities [43].

Trucks operated on biomethane are often equipped with an Otto engine (spark-ignited) and work under stoichiometric conditions such that a TWC can be used for abating emissions. However, to improve the fuel efficiency a lean-burn dual-fuel diesel engine could be used instead. In this engine, diesel is used as an igniter and thereafter biogas is used for operation. In this case, a TWC cannot be used for NO_x reduction; instead an aftertreatment system similar to that for conventional diesel engines must be used. The main difference in biogas operation, compared to gasoline or diesel, lies in the oxidation part of the catalyst, which in addition to oxidizing CO, normal hydrocarbons, and NO (in the case of lean conditions), it must also oxidize any slipped methane (CH_4) efficiently. However, this is a rather difficult task as methane is a very stable hydrocarbon. Palladium (Pd) is currently considered to be the best exhaust gas catalyst for CH_4 oxidation [44].

Contaminants that can be found in biogas include sulfur, siloxanes, and ammonia. According to the Swedish standard for biomethane, the sulfur and ammonia content in the gas is limited to maximum 23 mg/ Nm^3 (1 atm, 0 °C) and 20 mg/ Nm^3 , respectively. Biogas can furthermore contain siloxanes, and the concentration of such compounds must be low when the gas is used for engine applications [45]. Concentrations of siloxanes up to 50 mg/ Nm^3 have been reported [46], but it appears as concentrations lower than this are more common. In a study in which the concentration of seven fuel-grade biogas samples were analyzed, the concentrations of siloxanes were low, only around 0.1 mg/ Nm^3 [47].

In this thesis, the effect of biogas operation on a Pd-Pt/ Al_2O_3 oxidation catalyst has been studied in **Paper VI**.

1.4.2.6 Summary of possible contaminants in fuels for heavy-duty vehicles

A summary of the possible contaminants in different biofuels is provided in **Table 2**.

Table 2: Summary of possible contaminants, density and lower heating value (LHV) of different fuels for heavy-duty vehicles.

	Diesel EN590 [48]	Biodiesel EN14214 [48]	HVO EN15940 [36]	ED95 ¹ (SS 155437:2015)	Biogas ²
S (ppm)	<10	<10	<5	<10	≤23 mg/Nm ³
Ash (wt%)	<0.01	<0.02	<0.001	<3 ppm (sulfate)	-
P (ppm)	-	<4	-	<0.20 mg/dm ³	-
Na+K (ppm)	-	<5	-	-	-
Mg+Ca (ppm)	-	<5	-	-	-
Siloxanes	-	-	-	-	50 ³ mg/Nm ³
Density at 15 °C (kg/m ³)	820-845	860-900	770-790	807-815	0.68 ⁴
LHV (MJ/kg)	42.9	37.2	44.1	25.7	35.8 ⁴

¹ For ED95, limits for the following elements are also included in the standard SS 155437:2015: inorganic Cl <1.0 ppm; Cu < 0.1 ppm

² N indicates NTP, 0 °C, 1 atm; 1 Nm³ biogas is approximately equivalent to 1 dm³ diesel. Values for contaminants taken from the review in Paper II [35].

³ Values up to this concentration reported

⁴ Assuming 100% CH₄, 1 atm. For the LHV the unit is MJ/Nm³

1.5 Catalytic exhaust treatment in diesel trucks

To fulfill current emission legislations (e.g. Euro VI and US10), several different components are required for the emission control, as can be seen in **Figure 10**. This figure shows a schematic of a Scania Euro VI engine with exhaust treatment system, which is typical for a heavy-duty truck complying with Euro VI and equivalent emission standards. It includes a diesel oxidation catalyst (DOC), a diesel particulate filter (DPF), injection of an aqueous urea solution (AdBlue), selective catalytic reduction (SCR) catalysts, and ammonia slip catalysts (ASC).

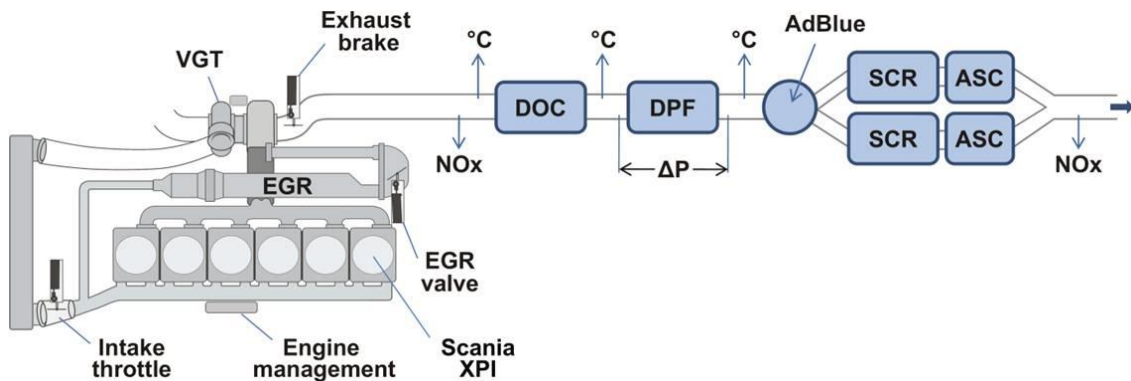


Figure 10: Scania Euro VI engine with extra high-pressure injection (XPI), variable geometry turbocharger (VGT), and EGR. Exhaust treatment system including DOC, DPF, urea solution injection, SCR catalysts and ammonia slip catalysts. ΔP – Pressure Drop. Published by kind permission of Scania CV AB.

To fulfill coming emission standards, some different exhaust treatment systems configurations have been suggested. One example is shown in **Figure 11**. In this an extra SCR catalyst, including an extra urea injection, is added close to the engine, to be able to comply with stringer NO_x limits. Another option is to use a passive NO_x adsorber (PNA), which adsorbs NO_x at low temperatures, before the SCR catalyst is active. It then releases NO_x at higher temperatures where the SCR catalyst is active. [27]

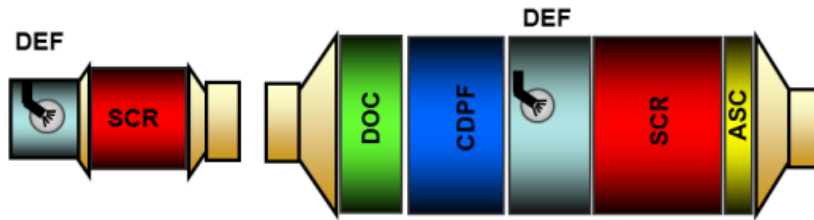


Figure 11: Possible exhaust treatment system configuration to fulfill upcoming emission standards. An additional SCR is placed in a closed-couple position. Another option is to add a passive NO_x adsorber (PNA) that adsorbs NO_x during cold temperature events and then releases it at higher temperatures where the SCR catalyst is active. DEF – diesel exhaust fluid, the aqueous urea solution that in Europe is called AdBlue. [27]

1.5.1 Diesel and methane oxidation catalyst (DOC and MOC)

The role of the DOC is to oxidize hydrocarbons (HC), CO, and NO into CO₂, H₂O, and NO₂ (see **Figure 12**). The NO₂ is desired to facilitate regeneration of the DPF and for improving the performance of the SCR catalysts by achieving fast SCR conditions [49], as will be described later.

The most common material for commercial oxidation catalysts is platinum (Pt) and palladium (Pd) supported on γ-aluminum oxide (Al₂O₃), Pt-Pd/Al₂O₃. However, other types of materials, such as CeO₂, SiO₂, ZrO₂, and zeolites, are sometimes also mixed into the support material. [50]

Pt has a higher oxidation activity for NO and non-methane hydrocarbons, but is easily poisoned by CO. Pd has a better activity for CO oxidation and CH₄ oxidation, but almost no activity for NO oxidation. A combination of Pt and Pd results in an increased stability of the catalyst, to atmospheres containing water and SO_x. The presence of Pd stabilizes the catalyst against sintering. [50]

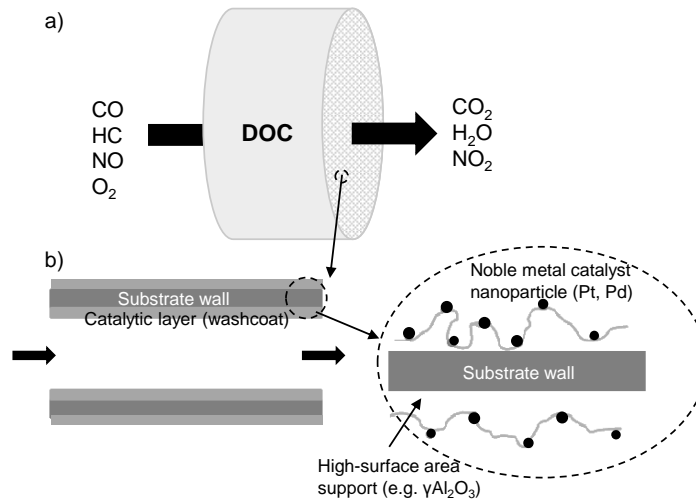


Figure 12: Schematic of a) the functions of the DOC, and b) a simplified structure of the DOC indicating the substrate wall and the catalytic layer on the wall, i.e. the washcoat that contains a high-surface area support on which noble metal particles are dispersed.

1.5.2 Diesel Particulate Filter, DPF

Particulate matter from the exhaust is a health hazard that can cause severe problems, including cardiovascular diseases [51]. To remove, or the decrease, the amount of this PM, a diesel particulate filter is needed. This filter traps the particulates in the exhaust. The DPF is commonly a flow-through filter (see **Figure 13**), which has alternately open and plugged ends [52]. This design forces the exhaust with particulates to flow through the porous wall, which acts as a filter. The PM consists of soot, ash, and condensed hydrocarbons as well as sulfuric acid. A typical PM composition is shown in **Figure 14**; however, it varies significantly with engine design, calibration, and operational conditions. [53] With time, the accumulation of PM in the filter results in an increasing pressure drop over the filter, and the available filter volume decreases. The pressure-drop over the filter is an energy loss, which translates into increased fuel consumption.

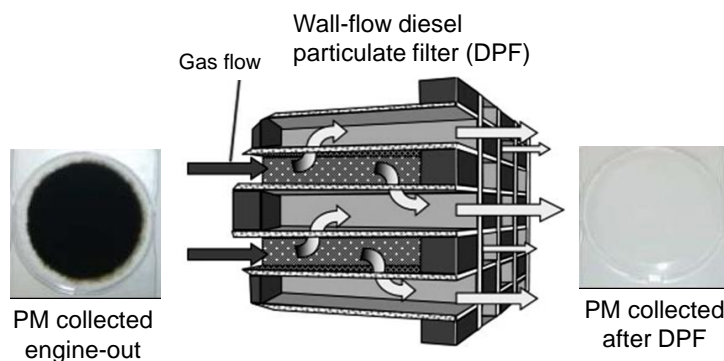


Figure 13: Wall-flow DPF in which every other channel is plugged, forcing the particulate-containing exhaust to go through the porous walls that act as a filter [52]. In the figure, particulates collected from the exhaust before and after a DPF are indicated [54]. The figure is a combination of the figure by Tsuneyoshi and Yamamoto (Energy 48 (2012) 492–499 used with permission from Elsevier [52]) and a figure from DieselNet technology guide [54].

Consequently, when the differential pressure reaches a certain limit, the DPF needs to be regenerated. In this regeneration, the combustible part of the PM, mainly the soot and condensed HC, is removed by oxidizing it into CO_2 and water. The regeneration can be done with oxygen at high temperature ($>500\text{ }^\circ\text{C}$). This process is called active regeneration, because it is done by actively increasing the temperature in the exhaust, for example injecting extra fuel before the DOC. This fuel is then oxidized over the DOC, creating an exotherm (i.e. an increase in temperature). Alternatively, the soot can be oxidized by NO_2 that has been produced by the DOC and/or by a catalytic coating (similar to the DOC) on the filter. NO_2 is a stronger oxidant than O_2 ; consequently, the regeneration can occur at a lower temperature. This means that less energy is needed, and is thus better in terms of fuel efficiency. [44]

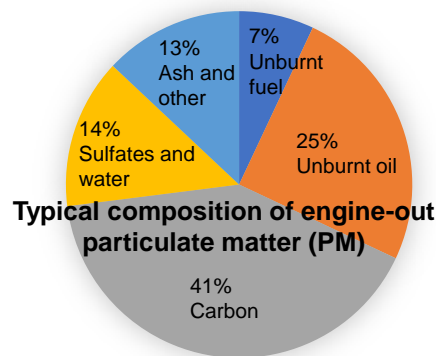


Figure 14: Example of a typical PM composition from a heavy-duty truck; however, the PM composition varies considerably with engine design, operation conditions and calibration. Based on numbers from [53]

1.5.3 Selective Catalytic Reduction, SCR

The SCR catalyst is used to reduce the NO_x in the exhaust to nitrogen and water with the help of ammonia (NH_3) that acts as a reducing agent (**Figure 15**). NH_3 is introduced to the exhaust through injection of the aqueous urea-solution (Adblue or DEF) [55].

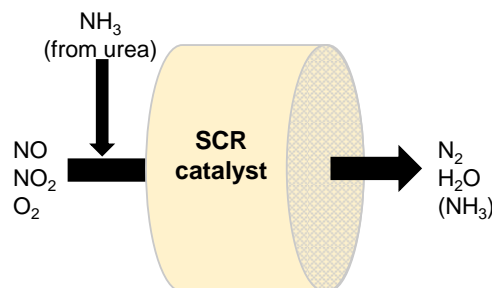
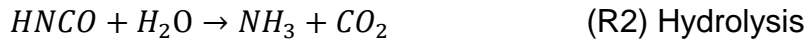
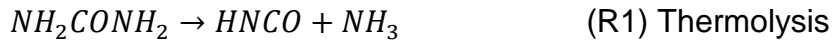


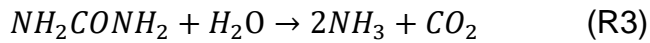
Figure 15: General description of the SCR NO_x reduction process.

1.5.3.1 Reactions relevant for the SCR catalyst

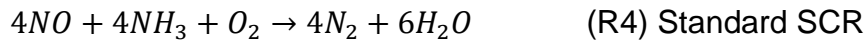
NO_x from the exhaust is converted with ammonia over the SCR catalyst. In a vehicle, the ammonia is introduced as an aqueous urea solution. This urea solution is sprayed as a fine aerosol into the exhaust, where it vaporizes and transforms into ammonia and carbon dioxide, via formation of isocyanic acid, through reactions called thermolysis and hydrolysis (Reactions **R1-R2**, respectively) [55].



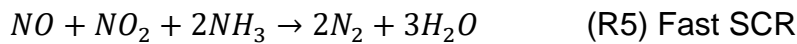
The two above equations then result in the overall reaction (**R3**). Thus, one urea molecule results in two ammonia.



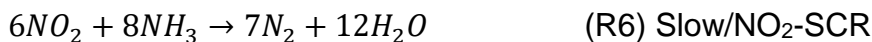
Three different NH₃-SCR reactions can occur, depending on the concentration of NO and NO₂ in the feed. These reactions are the standard (**R4**), the fast (**R5**), and the slow, or NO₂-SCR reactions (**R6**) [49]. The majority of the NO_x in the engine-out exhaust is NO (normally around 90-95 %). Therefore, the standard SCR reaction (**R4**), with NO only, will be the dominating reaction in the exhaust system if no DOC is present in front of the SCR catalyst, or at conditions where the NO oxidation rate is low.



If the amount of NO and NO₂ instead are equal, the fast SCR reaction occurs. This is called the fast SCR reaction because it generally improves the low-temperature performance of the catalyst, i.e. it is a faster reaction.[56] This is especially true for vanadium-based and iron-exchanged zeolite SCR catalysts, which are dependent on NO₂ to reach high conversion at low temperatures [57, 58]. For vanadium-based SCR catalysts, it has furthermore been observed that, even with NO₂ concentrations only half of the stoichiometry of the fast SCR reaction (i.e. NO₂/NO_x=0.25), a remarkable improvement in the SCR performance can be obtained, compared to if only NO is present [59].



In the case where all the NO_x would be in the form of NO₂, the slow or NO₂-SCR reaction will occur [49, 60]. This reaction is called the slow SCR reaction because it is normally slower than the standard SCR reaction. In reality, a pure slow/NO₂-SCR reaction would not occur, as there is no case when all the NO_x is in the form of NO₂ in real applications. However, if the NO₂/NO_x is above 0.5, the slow SCR reaction (or ammonium nitrate equilibrium reaction, depending on the temperature) can also take part [59].



Different types of SCR catalysts show different responses to the NO_2/NO_x ratio, and what is optimal for one type of catalyst may not be optimal for another type [58].

Besides from the desired SCR reactions mentioned above, side reactions that lowers the SCR performance of the catalyst can occur [61]. These unselective side-reactions should be kept as low as possible, i.e. the catalyst should have a high selectivity towards the wanted SCR reactions. What kind of side reaction that occur depends on the type of catalyst, catalyst formulation, and exhaust conditions, such as temperature and NO_2/NO_x ratio. Example of important, unwanted side reactions are formation of N_2O and ammonia oxidation [61].

A reaction that might be of importance for the SCR performance is the NO oxidation (**R7**). However, there are different opinions regarding the importance of this reaction for the SCR activity, and there appears to be no clear consensus about it [62].



Other important properties for SCR catalysts are the ammonia storage capacity and the redox ability. Ammonia storage is important as the SCR mechanism includes reaction of NO with adsorbed NH_3 , and furthermore ammonia stored on other sites of the catalyst can act as a reservoir if the ammonia supply is low. The dynamics of the ammonia adsorption and desorption are important to know for adequate urea dosing [55]. The redox potential is important because the SCR mechanisms include cycling between different oxidation states. [63]

1.5.4 Ammonia Slip Catalyst, ASC

The ammonia slip catalyst (ASC) is used to convert any remaining NH_3 that has not reacted over the SCR catalyst, i.e. NH_3 that has slipped through it. To ensure high NO_x conversion, a slight excess of NH_3 might be used under operation, and thus some NH_3 slip is likely to occur. [49, 64] Ammonia has an unpleasant odor, and the Euro VI emission standard limits the maximum slip of NH_3 to 10 ppm.

The ASC is basically an oxidation catalyst, in which the ammonia is selectively oxidized to nitrogen and water. Another name of this type of catalyst is ammonia oxidation catalyst (AMOX or AOC) [65]. Pt particles supported on e.g. Al_2O_3 , have a high NH_3 oxidation activity. However, the selectivity towards N_2 formation is rather low; significant amounts of NO and N_2O can be formed in addition to N_2 . As a solution to this selectivity issue, the oxidizing part can be combined with an SCR catalyst. One way of practically realizing this is to use a so-called dual-layer catalyst/architecture. In this architecture, the catalyst consists of an oxidation catalyst in the bottom layer and an SCR layer on top of this, as illustrated in

Figure 16. [65] In the oxidation layer of this catalyst, ammonia is oxidized to NO_x or N_2 . The formed NO_x can then react selectively with incoming NH_3 in the SCR layer (e.g. Cu- or Fe-zeolite). [66, 67] Again, the selectivity towards N_2O needs to be low. Currently there are no emission regulations on N_2O in the European Union, but it will likely be introduced in future standards, either as an N_2O limit or included in the GHG emission limits. In the US, on the other hand, EPA limits the N_2O emissions to 0.1 g/bhp-hr [18].

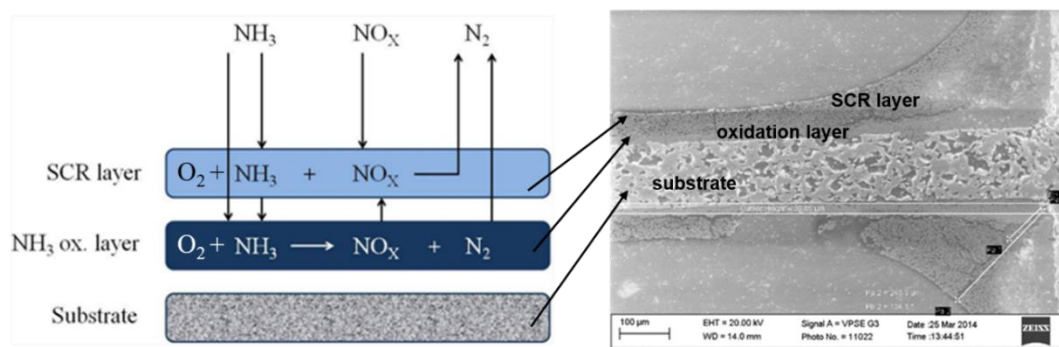


Figure 16: Principle of a dual-layer ammonia slip catalyst (ASC) to the left, and SEM-image of such a catalyst showing the cordierite wall and the two different catalytic layers: an oxidation layer and an SCR layer. The figure is adapted and based on figures from the Master Thesis of P. Wikholm 20 [68].

1.6 SCR catalysts: Cu-SSZ-13 and $\text{V}_2\text{O}_5\text{-WO}_3/\text{TiO}_2$

Different types of materials can be used as SCR catalysts, but the catalysts most commonly used commercially today are based on vanadium ($\text{V}_2\text{O}_5\text{-WO}_3/\text{TiO}_2$) and small-pore zeolites exchanged with copper (Cu-SSZ-13). Cu-SSZ-13 has better low-temperature NO_x reduction activity, but this performance is negatively affected by SO_x in the exhaust. VWTi on the other hand is tolerant to SO_x , but has a lower hydrothermal stability than Cu-SSZ-13. A potential concern about vanadium-based catalysts is their hydrothermal stability in terms of a potential loss of toxic vanadia to the surroundings. This is highly undesired both due to the toxicity of vanadia (V_2O_5), and to the loss of active material thus occurring [69, 70]. Some markets therefore demand vanadia-free catalysts [69-71], or proof that evaporation of vanadia cannot occur during operation.

1.6.1 $\text{V}_2\text{O}_5\text{-WO}_3/\text{TiO}_2$

The vanadium-based catalyst has been used for selective catalytic reduction of NO_x by NH_3 since the 70's in Japan where it was used for stationary applications, abating emissions from e.g. nitric acid plants. In Europe it has been used for stationary applications since the 80's. [72] In the 90's, it was investigated for the use in mobile applications, especially heavy-duty diesel trucks. Instead of gaseous

ammonia, which would be difficult to handle on a truck, an aqueous solution with urea was used as a precursor for NH_3 . In 2005/2006, vanadium-based SCR was introduced at a large scale in Europe, with the introduction of Euro IV. [49]

In this catalyst, vanadium pentoxide, or vanadia (V_2O_5), is the active component (typically 1-2.5 wt%), promoted by tungsten trioxide, tungsta (WO_3 , typically 6-10 wt%), and supported on titanium dioxide, titania (TiO_2). WO_3 increases the low-temperature activity of the catalysts by increasing its acidity. It furthermore increases the durability of the catalysts, both towards hydrothermal aging and chemical deactivation by sulfur and alkali metals. Advantages of the vanadium-based SCR catalyst include the price and the good sulfur tolerance.

Depending on the V_2O_5 loading of the catalyst, different vanadium sites can form on the catalyst: monomeric vanadyls, polymeric vanadates (see **Figure 17**) and/or crystalline vanadia [73]. Furthermore, thermal treatment of the catalyst may transform sites from one kind to another. At vanadia loadings below the monolayer capacity, the vanadium usually exists as the monomeric and polymeric species [73]. It is generally agreed that polymeric sites are the most active for the SCR reaction [73, 74].

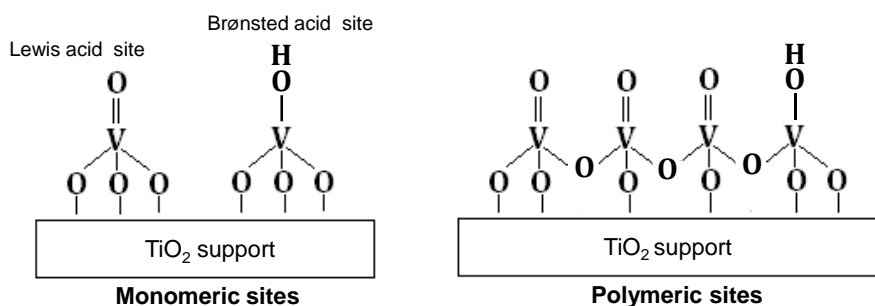


Figure 17: A simplified illustration of monomeric and polymeric vanadium-sites in V_2O_5 -based SCR catalysts.

In the mechanism for the SCR reaction on vanadium-based catalysts, it is generally agreed that ammonia is adsorbed on the catalyst and then reacts with gas-phase or weakly adsorbed NO [75, 76]. It is also agreed that the SCR reaction occurs through a redox mechanism in which vanadium sites cycle between two different oxidation states [77, 78]. However, the exact mechanism and nature and role of the different sites are not completely agreed on. Tronconi et al. [77] showed that both ammonia and NO are required to reduce the vanadium from 5^+ to 4^+ . Concurrent with this reduction, N_2 and H_2O are formed (see **Figure 18**). Oxygen is then used to re-oxidize the vanadium from 4^+ to 5^+ . This re-oxidation is considered as the rate-limiting step for low-temperature standard SCR ($<300^\circ\text{C}$) [59, 77, 79, 80]. In the fast SCR reaction this re-oxidation is facilitated by surface nitrates formed from NO_2 in the feed, and re-oxidizes the vanadium considerably faster [59, 77]. The rate limiting step for the fast SCR reaction at low temperature, is instead the reaction between HNO_3 and NO [59]. A schematic of this is shown in **Figure 18**.

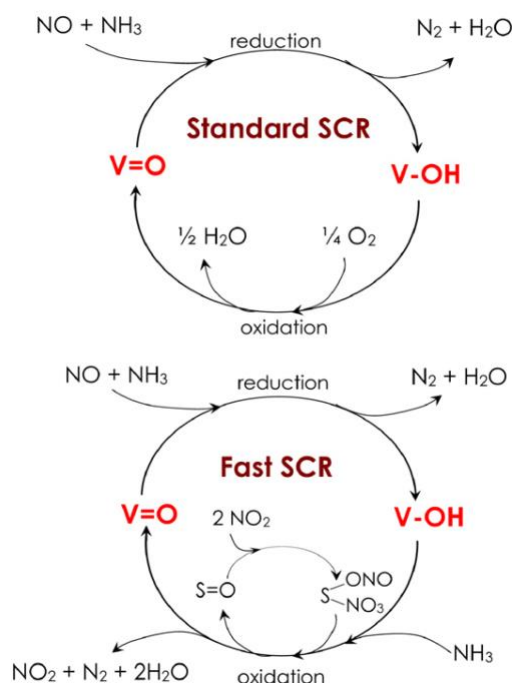


Figure 18: Proposed schematic of standard and fast SCR mechanism over a vanadia-tungsta-titania SCR catalyst, reprinted from Tronconi et al. J. Catal. 245 (2007) 1-10 [77] with permission from Elsevier (license number 4753640238659). S=O denotes a non-reducible oxidic site on the catalyst.

1.6.2 Cu-SSZ-13

The first copper-exchanged zeolite investigated for SCR was Cu-ZSM-5, and Cu-beta has also been investigated [81-83]. However, these materials suffered from insufficient hydrothermal stability and hydrocarbon poisoning, which hindered their commercial application. Nevertheless, in 2009, a new Cu-zeolite SCR catalyst was patented [84]. This catalyst was the small-pore copper-exchanged SSZ-13 zeolite, Cu-SSZ-13, and the zeotype Cu-SAPO-34, with the same framework [84]. As opposed to the earlier Cu-zeolites, this catalyst has a high hydrothermal stability and low susceptibility to hydrocarbon poisoning. Additionally, it has an excellent low-temperature performance and a wide temperature operating window. Due to these features, Cu-SSZ-13 is now widely used in markets with stringent emission standards. However, fuels with a very low sulfur content must be used, due to their sensitivity to sulfur-poisoning when exposed to SO_x. In addition, an important durability issue has been revealed for Cu-SAPO-34 catalysts: this type of material can severely and irreversibly deactivate as a result of exposure to water at low temperatures (<100 °C) [85-87].

The zeolite SSZ-13 is a small-pore zeolite with chabazite (CHA) framework. It consists of a CHA cage, constructed by 8- and 4-membered rings (8mr, 4mr), which are connected to double 6-membered rings (d6mr) (see **Figure 19**). These units are then connected in a three-dimensional structure. The pore openings of the CHA cages are 3.8 Å [88]. The hydrothermal stability and low susceptibility

towards HC poisoning of the Cu-SSZ-13 catalyst, is considered to be due to this small pore size.

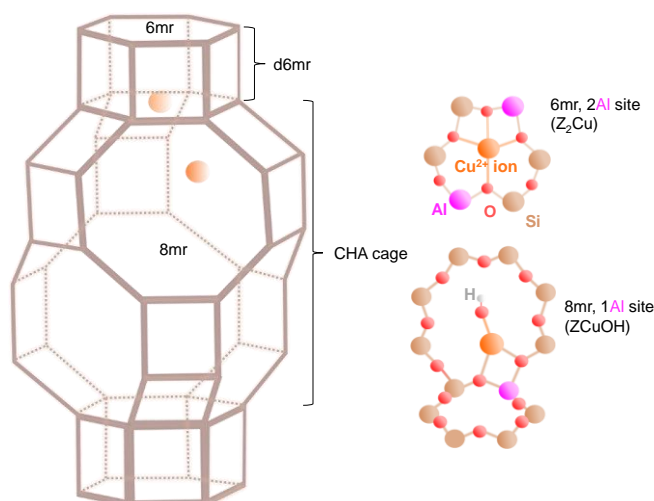


Figure 19: Schematic of a unit cell of a Cu-SSZ-13 catalyst consisting of double 6-membered rings connected by a CHA cage. In the figure, each corner represents a tetrahedral Si or Al, and in-between these corners is an oxygen atom. Cu^{2+} ions are coordinated to the zeolite by the negative charge induced by Al in the zeolite structure. The 6- and 8mr rings can contain either one or two Al, which $[\text{CuOH}]^+$ and Cu^{2+} , respectively, can be coordinated to.

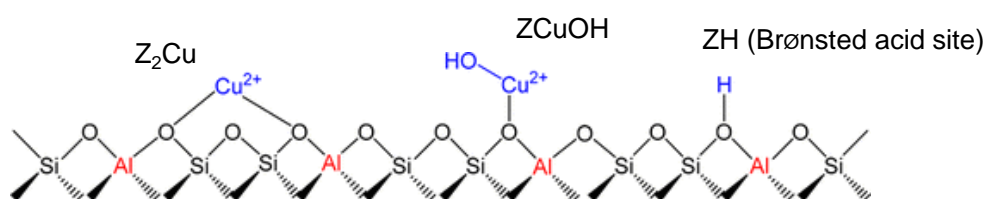


Figure 20: Simplified schematic of different cationic Cu (Lewis acid) and Brønsted acid sites in the Cu-SSZ-13 catalyst. Adapted with permission from Song et al. ACS Catal. 7 (2017) 8214 [89], Copyright 2017 American Chemical Society.

During the past decade, Cu-CHA materials for both NH_3 -SCR and the partial oxidation of methane have been studied extensively. A significantly increased understanding about the copper sites and the standard SCR reaction mechanism has been achieved through a combination of catalytic studies, in-situ and in-operando characterization techniques (e.g. XAS, DRIFTS) and computational investigations of a range of well-defined samples, nicely summarized in the reviews by Paolucci et al. [90], Borfecchia et al. [91], and Gao and Peden [92].

It is now well-established that the type of Cu species that exists in the catalyst is highly dependent on the sample composition (Si/Al and Cu/Al) and on the external conditions the catalyst is subjected to, such as gas atmosphere and temperature. The synthesis route can be of relevance as well. Some important findings are that both water (at ambient conditions) and ammonia (at low SCR reaction temperatures) solvate the copper sites; instead of being strongly coordinated to the framework as e.g. Z_2Cu , paired Al exchange sites, and ZCuOH , isolated Al exchange

sites (as shown in **Figure 19-20**), the Cu ions become mobile within the zeolite. A facile movement of Cu ions in the zeolite framework occurs upon interaction with strongly adsorbing molecules [90-93].

The standard SCR mechanism consists of a reduction half-cycle and an oxidation half-cycle, in which Cu changes oxidation state between 2^+ and 1^+ . In the low-temperature reduction half-cycle, ammonia-solvated Cu^{2+} ions are efficiently reduced to Cu^+ by NO [94]. According to the current understanding of the standard SCR reaction, the re-oxidation of Cu^+ to Cu^{2+} by oxygen at low temperature, requires the formation of dimeric copper oxygen species, which forms from highly mobile $[\text{Cu}(\text{NH}_3)_2]^+$ species. At low Cu loadings, the low-temperature SCR reaction is limited by the ability of Cu to form these dimeric copper species [95, 96]. At higher Cu loadings, the reaction is limited by O_2 dissociation on the formed Cu pairs [95-97]. **Figure 21** shows a proposed catalytic cycle for the standard SCR reaction at low temperature.

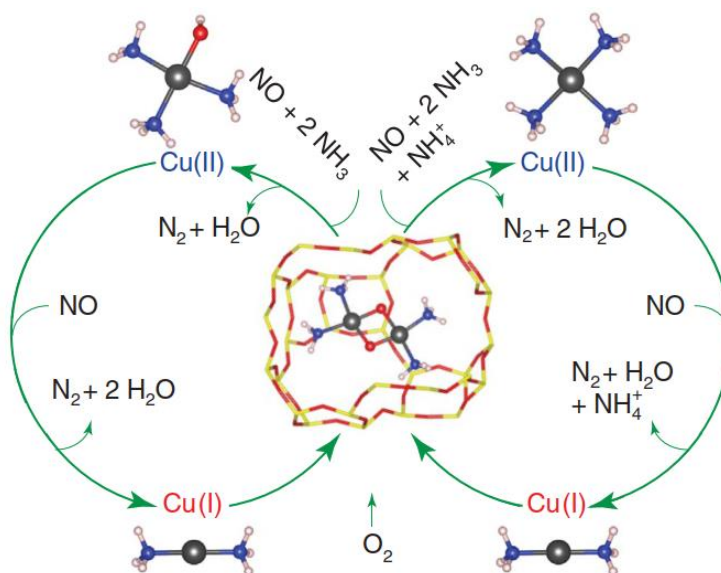


Figure 21: Low-temperature catalytic cycle for the standard SCR reaction over Cu-SSZ-13 proposed by Paolucci et al. [96] The re-oxidation of Cu^+ to Cu^{2+} requires the meeting of two ammonia-solvated Cu^+ ions. Reprinted from Paolucci et al. Science 357 (2017) 898-903 with permission from Science AAAS (license number 4753640740238).

Mechanisms that include NO_2 in the feed gas, e.g. fast SCR, are less well-understood, probably due to some experimental difficulties. These difficulties include background reactivity of SSZ-13 support, accumulation of ammonium nitrate on the surface of the catalyst at low temperature, while at high temperature, the reaction occurs too fast to obtain kinetic data [92]. Whether or not the fast SCR follows a redox mechanism is not established. Only Cu^{2+} has been detected during in-situ XAS studies of the fast SCR reaction [94, 98]. However, this does not necessarily imply that the reaction is not redox-based. It could as well be that the re-oxidation of the Cu^+ is so fast that these ions are not detected.[94]

The formation and accumulation of ammonium nitrates at low temperature may inhibit the fast SCR reaction, rendering it no faster but even slower than the standard SCR reaction [99, 100]. However, in a recent study by Bendrich et al. [101], the inhibitory effect observed by these ammonium nitrates for steady-state experiments, was not observed during transient tests, which were more similar to the conditions in real engine exhaust.

1.7 Catalyst deactivation

In theory, a catalyst is neither consumed nor irreversibly changed with time; that is, the activity and selectivity of the catalyst would be constant. However, in reality the activity and/or selectivity of the catalyst can change/decrease with time due to catalyst deactivation. This deactivation can be related to high temperatures, with sintering, vapor phase formation of active phase, or support phase transformation as a result.

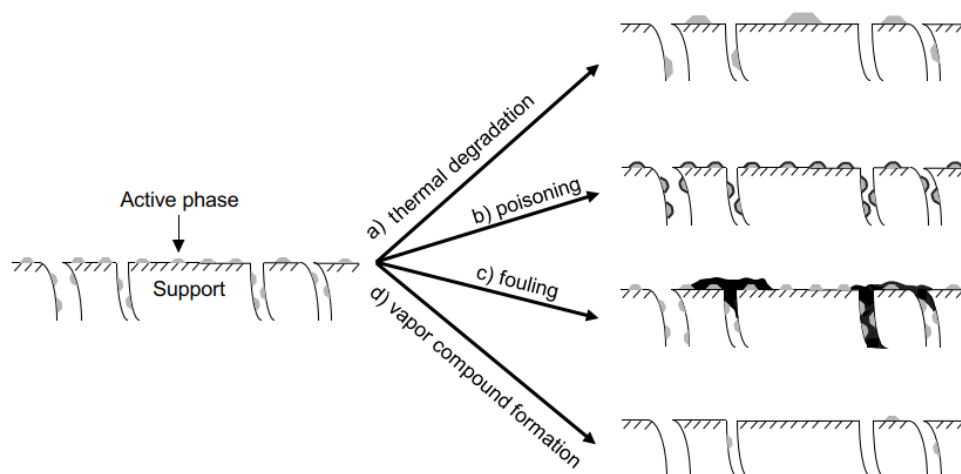


Figure 22: Conceptual figure of different deactivation mechanisms for supported catalysts. a) thermal aging by sintering/agglomeration of the active sites with formation of larger catalyst particles with less active surface area; b) poisoning of active phase by e.g. chemisorption of a compound binding strongly to the active site; c) fouling of active site and support, pore filling, covering support, pores and active sites; d) vapor phase formation of active phase resulting in loss of catalytic sites. Figure reprinted with permission from P. Velin [102].

Another cause of deactivation is due to components in the feed (e.g. contaminants from the fuel or lube oil in the exhaust). It can furthermore be due to mechanical damage. A conceptual model of some of these deactivation mechanisms is pictured in **Figure 22**. [103]

The focus of this thesis is chemical deactivation, mainly about SCR catalysts, but also oxidation catalysts. Therefore, a discussion of the effect of different contaminants on the catalytic performance of vanadium-based and Cu-SSZ-13 (or CHA) SCR catalysts is given below. Deactivation by hydrothermal aging is also briefly discussed, as this mechanism is often present, at least to some extent, in real applications.

1.7.1 Deactivation by various fuel- and lube oil-derived components

The following discussion is based on the review in **Paper II**, and a more thorough description of the different contaminants and their effect on both SCR catalysts and DOCs can be found therein [35]. However, some additional, newer results and insights, especially about chemical deactivation of Cu-SSZ-13 catalysts, are presented in the following sections.

1.7.1.1 Sulfur/SO_x

Sulfur will always be present to some extent in the exhausts due to its presence in both fuels and lube-oils. In ULSD and biodiesel, the maximum allowed limit for sulfur is 10-15 ppm. This translates into a SO₂ content in the exhaust of around 0.5-1.5 ppm. In lower-quality diesel, the sulfur content can be considerably higher [104]. The lube-oil normally contains around 0.3-0.7 wt% sulfur [105], with normal oil consumption rates around 0.075% of the fuel consumption [106]. The sulfur tolerance of the catalyst is thus of high importance.

V₂O₅-WO₃/TiO₂

The V₂O₅-WO₃/TiO₂ catalyst has been shown to be sulfur tolerant, unless high SO₂/SO₃ concentrations are present in combination with ammonia at low temperatures. In this case, ammonium bisulfate can form and deactivate the catalyst by fouling. Depending on the concentration, SO₂ can even promote the SCR performance of this type of catalyst. [35] For example, both these phenomena have been observed when testing a VWTi SCR catalyst in an engine-bench with ULSD after aging cycles using fuels with two different sulfur contents, 350 ppm and 3600 ppm, respectively [107]. The test after the 350 ppm S fuel had been used resulted in a slightly improved SCR performance, while the test after aging with the 3600 ppm S-fuel, resulted in deactivation at temperatures up to 375 °C. When repeating this performance test, after the first test had been done, almost full activity was regained, and the deactivation was proposed to be due both to sulfur and heavy hydrocarbons [107].

Cu-SSZ-13

As opposed to the VWTi catalyst, Cu-SSZ-13 catalysts are severely deactivated by sulfur. SO_x severely affects the activity of Cu-SSZ-13 (and Cu-SAPO-34) in the low and mid-temperature range (up to around 300-350 °C), as shown in several papers [104, 108-125].

As an example, at a reaction temperature of 220 °C, the rate constant under standard SCR conditions have been shown to decrease to values between 2 and 54% of that of prior to the SO_x-exposure. In these experiments, the effect of SO_x under various conditions was investigated, e.g. different temperatures [108, 109], type of SO_x (SO₂ or SO₂+SO₃), and presence or absence of H₂O [109].

At temperatures higher than 300-350 °C, the performance of Cu-SSZ-13 is not affected, or could even be slightly increased [108]. Furthermore, SO_x poison Cu-CHA catalysts no matter if the SO₂ exposure is performed in the presence of SCR gases or not; however, the temperature dependence of the sulfur uptake, and the extent of poisoning, appears to differ [126]. It has also been shown that deactivation by SO_x is rapid; most of the deactivation occurs within the first hour of SO_x exposure. However, saturating the catalyst completely with sulfur takes a long time [108]

Partial regeneration to reach a rate constant (at 220 °C) of around 75-95% of that of fresh catalyst could be realized if the catalyst is heated to 550 °C in oxidizing conditions [109]. Heating the catalyst further up to around 600-700 °C has been observed to result in complete regeneration [127]. However, this high regeneration, or deSO_x, temperature is not feasible in a vehicle since it would result in an excessive fuel penalty. Regeneration in a partially reducing atmosphere (e.g. ammonia-containing exhaust), on the other hand, appears to be easier, i.e. sulfur is released at a lower temperature, as compared to a fully oxidizing atmosphere [119].

SO_x is proposed to deactivate the Cu-CHA catalysts by interacting with Cu sites, forming some kind of Cu-(H_vSO_w)_x(NH_y)_z species [111, 122, 126, 128]. Thus, less Cu ions are likely available for formation of Cu pairs, and the low-temperature performance is consequently affected. According to recent findings, ZCuOH sites have been shown to be more sensitive to sulfur-poisoning than Z₂Cu sites [111, 121, 122, 126]. DFT calculations have shown that both SO₂ and SO₃ can adsorb on ZCuOH/ZCu sites, while they cannot adsorb on Z₂Cu. However, the presence of water and/or NH₃ may change this, resulting in interaction with SO_x also on these sites [111, 126]. DFT calculations also indicated that SO₂ interacts more strongly with Cu⁺ than Cu²⁺ while the opposite is true for SO₃. Furthermore, these calculations indicated that SO_x do not bind to the mobile [Cu(NH₃)₂]⁺ species that form under SCR reaction [126]. Some proposed sulfur-copper structures are shown in **Figure 23**.

Another observation is that the presence of NO₂ in the feed during the SCR reaction for a SO₂-poisoned catalyst has been shown to result in an alleviated effect of the SO₂-poisoning compared to standard SCR conditions [114].

Several SO_x deactivation studies have been performed; although all studies agree upon the severe poisoning effect on the low-temperature NO_x reduction performance, some contradictory results exist, and the sulfur poisoning mechanism is still not completely understood. One example of such contradictory results is the effect of SO_x-exposure temperature. In some studies, a higher degree of deactivation is observed when the sulfation occurs at high temperatures compared

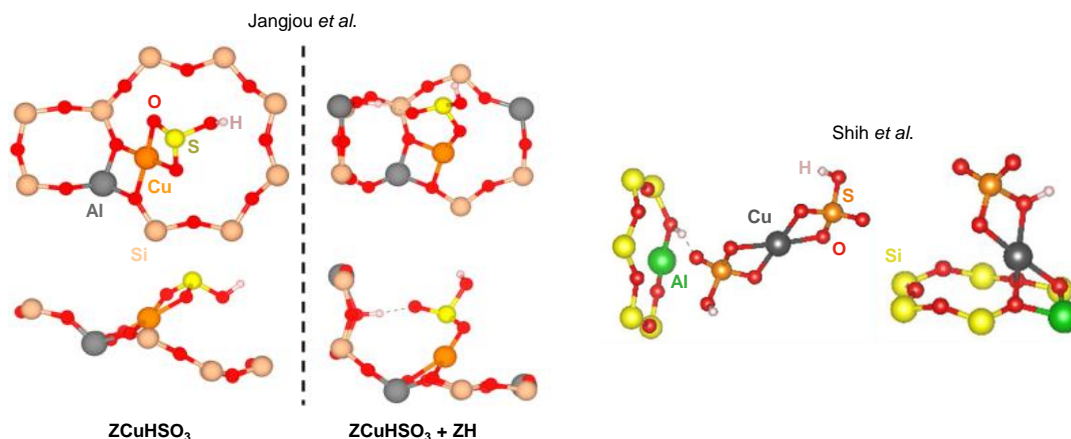


Figure 23: Some proposed structures of SO_x-poisoned Cu-sites in Cu-SSZ-13. Adapted with permission from Jangjou et al. ACS Catal. 8 (2018) 1325 [111] (copyright 2018 American Chemical Society), and Shih et al. Appl. Catal. A 574 (2019) 122 [122] with permission from Elsevier (license number: 4753641351768)

to at low temperatures. In other studies, the opposite effect has been observed. Such differences could be related to different gas atmospheres during the SO_x-exposure. Nevertheless, even with similar gas compositions, different results have been obtained. Another reason could be differences in the copper speciation in the investigated samples, which in turn may affect the SO_x poisoning, as different Cu species have been shown to have different sensitivities towards sulfur. Even a similar Cu/Al and Si/Al does not necessarily imply that the Cu species on the catalysts are the same. Another thing that might be of importance is the state of the catalyst prior to the SO_x poisoning.

1.7.1.2 Phosphorus

Phosphorus can be found in biofuels and originates from the raw material used for biofuel production. It is additionally present at rather high concentrations in lube oils.

V₂O₅-WO₃/TiO₂

The effect of P on V₂O₅-WO₃/TiO₂ has been studied by several authors [129-135]. In general, the V₂O₅-WO₃/TiO₂ catalyst appears to be rather tolerant towards phosphorus; severe deactivation is normally only observed at high P concentrations (around 2 wt% and above) [35]. However, most of these studies were done using wet impregnation for the phosphorus-exposure, and notably, some studies showed that for similar phosphorus loading, aerosol aging resulted in more severe deactivation than wet impregnation [130, 133]. Additionally, a severe deactivation has been observed for a truck operated on FAME for around 10,000 h, and high concentration of phosphorus was found on this catalyst [16].

Cu-SSZ-13

A few studies related to phosphorus exposure of Cu-SSZ-13 SCR catalysts are available in the open literature, of which most use wet impregnation for the phosphorus-exposure [118, 136, 137]. Wet impregnation is a simple and exact method for introducing poisons, but it may not reflect the deactivation mechanism that occurs in real operation. The combined conclusions from these studies suggest that the deactivation of Cu-SSZ-13 by phosphorus could be severe; however, it appears to depend on the concentration of phosphorus on the catalyst, or more importantly, the molar P/Cu ratio. Low P/Cu ratios appear to result in a suppression of NH_3 and NO oxidation reactions while the standard SCR reaction is unaffected, or even slightly promoted at high temperatures [118, 136, 138]. Higher P/Cu ratios, on the other hand, could be detrimental [118, 137, 138]. Furthermore, there are indications that vapor-phase deposition of phosphorus [138] results in a more severe deactivation than do wet impregnation methods [136]. Furthermore, sulfur poisoning of P-exposed Cu-SSZ-13 catalyst by SO_2 has been observed to be accelerated, due to a lower amount of active copper ions in the P-poisoned catalysts [118].

1.7.1.3 Alkali metals and alkaline earth metals

Alkali and alkaline earth metals can be found in biodiesel and originates from the biodiesel production process.

$\text{V}_2\text{O}_5\text{-WO}_3/\text{TiO}_2$

Deactivation of vanadium-based SCR catalysts have been studied extensively. This type of SCR catalyst is very sensitive to deactivation by alkali metals, and alkaline earth metals. The degree of deactivation follows the basicity of the alkali or alkaline earth metal, with potassium being the strongest poison, followed by sodium. A corresponding decrease in ammonia storage capacity is usually observed upon exposure to alkali metals. [130-132, 139-148]

Cu-SSZ-13

The studies performed on the effect of alkali and alkaline earth metals on Cu-SSZ-13 [137, 149-151], Cu-SAPO-34 [152-155], and other Cu-zeolites [144, 156] imply that Cu-zeolites are significantly more resistant towards these contaminants than are VWTi catalysts. Severe deactivation is generally only observed at high loadings of the alkali/alkaline earth metal. A high contaminant load could in this case be e.g. above around 1 wt% or around 1-1.5 mmol contaminant per gram catalyst. Compared to the vanadium-based catalysts, the poisoning strength of the alkali/alkaline earth metals also appears to be different. In all studies on Cu-CHA catalysts, in which both alkali metals and alkaline earth metals were investigated, Mg had the strongest poison effect [149, 153]. This is similar to what has been observed for some Fe-exchanged zeolites [157, 158]. As a contrast, K or Na is the

worst poison for VWTi catalysts. Comparing the deactivating effect of alkali metals with that of SO₂-exposure for Cu-CHA catalysts, the deactivating effect of alkali metals is significantly lower [154]. In addition, an improvement in SCR performance in the high-temperature range, due to an inhibited ammonia oxidation, has been observed in some of the studies [151, 154].

Exchange of the isolated Cu ions with the alkali or alkaline earth metal, and concurrent formation of CuO_x (or CuAl₂O₄-like species [150, 152]), which could block the pores of the catalyst, have been proposed as deactivation mechanisms [137]. Pore blocking by oxides of the contaminant may also contribute significantly to the deactivation [137]. Disruption of zeolite framework may additionally occur at high poison concentrations [153].

In a study by Gao et al. [159] it was observed that co-impregnation with an alkali metal can actually improve the thermal stability and may also increase both low- and high-temperature SCR performance. An increase in the low-temperature reducibility and an inhibition of the high-temperature ammonia oxidation reaction were the explanations for these effects. In addition, a lower N₂O formation was observed over the entire temperature range [159]. On the other hand, Wang et al. [150] observed a stronger poisoning effect of alkali metals after mild hydrothermal aging (600 °C), compared to what had previously been observed for similar alkali loading (0.5 mmol/g catalyst) in other studies. In addition, the hydrothermal stability at 700 and 800 °C decreased after this alkali contamination.

The effect of different types of potassium salts on a Cu-SSZ-13 (2.6 wt% Cu) was investigated by Liu et al. [151]. It was shown that these salts displayed significantly different degrees of deactivation on the catalyst. 2 wt% K from K₂CO₃ resulted in a significant deactivation over the whole temperature range, whereas for 2 wt% K in the form of K₂SO₄ or K₃PO₄, only the low-temperature performance was negatively affected while the high-temperature performance was improved due to an inhibited NH₃ oxidation [151].

Applying fast SCR conditions has been observed to result in a lower decrease in the NO_x reduction performance compared to during standard SCR conditions [144].

All the above studies were made by wet-impregnation methods. In addition to these studies, deactivation of a Cu-BEA was observed after engine aging with Na-doped fuel using a light-duty exhaust treatment configuration. In this configuration, the SCR catalyst was positioned downstream of the DOC but upstream of the DPF. In contrast, for a similar aging performed with a heavy-duty configuration, with both a DOC and a DPF before the SCR catalyst, no Na-related deactivation was observed due to the DPF capturing the sodium [160].

1.7.1.4 Zinc

Zinc is present in the lubrication oil in the form of Zinc dialkyldithiophosphates (ZDDP). It could additionally be present in biodiesel, from the production process using a heterogeneous catalyst, but the concentration is expected to be rather low (below around 1 ppm).

V₂O₅-WO₃/TiO₂

In most studies that have investigated the effect of zinc on the SCR performance of VWTi catalysts, using a wet impregnation or an aerosol method, a deactivating effect has been observed [130-132, 161, 162]. The deactivating effect appears to be stronger than that of phosphorus, but weaker than that of alkali metals [130, 131].

Cu-SSZ-13

Only one study that investigates the effect of zinc on Cu-SSZ-13 SCR catalysts has been found [137]. In this study, which was performed by wet impregnation (0.34-1.35 mmol Zn/g catalyst), a significant deactivation was observed during the standard SCR reaction at 250 and 350 °C. However, the deactivating effect was lower as compared to phosphorus at the same loadings. The deactivation was concluded to be due to mainly pore blocking and pore filling, but a decrease in isolated Cu²⁺ and formation of CuO upon contamination was also observed. [137]

Although no more studies on the effect of Zn on Cu-CHA materials were found, an interesting result was obtained in a study on an iron-zeolite (Fe-MFI) [158]. In this research paper, the authors investigated the effect of Zn using different contamination procedures, wet impregnation and aerosol aging. While the impregnation method (0.1-0.3 mmol Zn/g catalyst) resulted in a strong deactivation under standard SCR conditions, the aerosol method caused only slight deactivation. This was likely related to the low capture efficiency of Zn on the catalyst during this the aerosol aging. [158]

1.7.2 Hydrothermal aging

In this thesis, no studies with focus only on hydrothermal (HT) aging have been performed. However, this kind of deactivation/aging is important to understand as it will always be present some extent in real conditions. Furthermore, some of the samples evaluated in this thesis are engine-aged samples. During the operation in the truck or engine, these samples may have been subjected to conditions such that HT aging cannot be fully excluded.

1.7.2.1 V₂O₅-WO₃/TiO₂

Vanadium-based SCR catalyst has a rather low hydrothermal stability. The thermal deactivation can occur by formation of crystalline vanadia, transformation of the TiO₂ support from high-surface area anatase to the low-surface area rutile, and

through evaporation of vanadia. This evaporation may occur around 670 °C and is highly undesired, both due to loss of active material and to that V₂O₅ is a toxic compound [69, 70].

1.7.2.2 Cu-SSZ-13

Cu-SSZ-13 catalysts have a rather high hydrothermal stability. However, it appears to be more sensitive towards high-temperature aging in rich/reducing conditions, and metallic copper may form [163]. ZCuOH sites are less thermally stable, and can convert into Z₂Cu, and eventually also CuO_x if the temperature is high enough [164]. When CuO_x has formed, destruction of the zeolite framework is facilitated [92] .

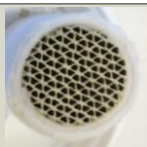
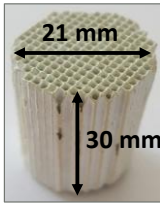
Another important deactivation phenomenon observed is that Cu-SAPO-34, another Cu-CHA material, can deactivate severely and irreversibly when it is exposed to wet exhaust, not at high temperature, but at low (<100 °C) [85-87, 165].

Part II: Experimental

2.1 Catalyst samples

Several different catalysts were included in this project. The focus was on SCR catalysts, including investigations of both Cu-SSZ-13 and V_2O_5 - WO_3 /TiO₂ catalysts. Additionally, some studies included bimetallic Pt-Pd/Al₂O₃ oxidation catalysts (**Paper V-VI**). Fresh and lab-aged, as well as engine or vehicle-aged samples, have been evaluated. All catalysts samples were commercial or close to commercial, and received from catalysts manufacturers, delivered as small cores drilled out from full-size (truck) catalysts.

Details regarding the fresh SCR catalysts used for various aging experiments are displayed in **Figure 24**. The vanadium-based catalyst has been used in **Paper I** and **V**. Cu-SSZ-13 Cat A1 was evaluated in **Paper III-IV**, while Cat B were included in **Paper III**, and Cat A2 was used in for **Paper V**.

V₂O₅-WO₃/TiO₂			
260 cpsi, corrugated substrate			
Commercial			
Spec: 2.3 wt% V ₂ O ₅ ; 8 wt% WO ₃			

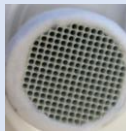
Cu-SSZ-13	400 cpsi, washcoated monolith		
	Cat A1	Cat A2	Cat B
Cu content in crushed monolit:	0.69 wt%	0.78 wt%	0.67 wt%
Cu content in washcoat:	2.5 wt%	3 wt%	
Si/Al: ~15	~7	~15	
Coat load (g/dm3):	~150	~143	

Figure 24: Fresh SCR catalyst samples used for various aging experiments. Small cores (typically $\varnothing = 21$ mm, L = 30 mm) were drilled out from full-size catalysts. Cu-SSZ-13-A1 and -A2 are from the same supplier, while Cu-SSZ-13-B is from another supplier. 25x45 mm in Paper I.

Information regarding the engine- and vehicle-aged SCR catalysts that were evaluated in this project is provided in **Table 3**. The vehicle-aged VWTi catalysts are the same type, or similar, as the fresh V_2O_5 - WO_3 /TiO₂, while the engine-aged Cu-SSZ-13 is the same type as Cat B. However, they are not from the same batches as the fresh catalysts. Details about the DOCs that have been investigated are provided in **Table 4**.

Table 3: Vehicle- or engine-aged SCR catalyst samples used in various papers. Small cores ($\varnothing = 21$ mm, L = 30 mm) were drilled out from full-size catalysts.

Catalyst sample	Description
V ₂ O ₅ -WO ₃ /TiO ₂ EuVI 700 kkm (Paper I)	SCR catalyst from 480 hp long-haulage field test truck operated for 700,000 km on biodiesel (100% RME). Euro VI configuration (DOC-DPF-SCR-ASC) (Paper I)
V ₂ O ₅ -WO ₃ /TiO ₂ EuV 120 kkm (Paper I)	SCR catalyst from 250 hp long-haulage field-test truck operated for 130,000 km on conventional diesel in Brazil. Euro V configuration (SCR only) (Paper I)
Cu-SSZ-13-B Engine-aged, samples from inlet and outlet part of the catalyst (Paper III)	SCR catalyst from a 500 h, standard test cycle in an engine-bench, using a 500 hp Scania DC13 Euro V engine, ULSD fuel Peak temperature before the SCR catalyst during the test was 530 °C, but in average a higher than normal temperature during the test. Eu V configuration (SCR only) (Paper III)

Table 4: Oxidation catalyst samples used in various aging experiments. Small cores (either $\varnothing = 21$ mm, L = 30 mm, or $\varnothing = 11$ mm, L = 19 mm) were drilled out from full-size catalyst bricks.

Catalyst sample	Description
Pt-Pd/Al ₂ O ₃ (Paper V)	Pt-Pd/Al ₂ O ₃ washcoat coated on cordierite, 400 cpsi 20 g PGM/ft ³ , Pt:Pt=2:1 (mass-based), designed for diesel fuel operation
Pd-Pt/Al ₂ O ₃ fresh and samples from inlet and outlet of an engine-aged catalyst (Paper VI)	Pt-Pd/Al ₂ O ₃ washcoat coated on cordierite, 400 cpsi 100 g PGM/ft ³ , Pt:Pt=1:2 (mass-based), designed for biogas operation engine bench consisting of a Volvo G13C 460 hp engine, Euro VI compliant emission control system, dual-fuel type engine, powered with 90 % biogas and 10 % diesel for 900 hours, mixed driving simulated

2.2 Evaluation of catalytic performance using laboratory flow reactors

The performance of fresh and aged catalyst samples was evaluated in laboratory bench-flow reactors. A description of the different test protocols used for these tests follows below.

2.2.1 Test protocol for SCR catalyst samples

Three different SCR test protocols have been used for the different aging studies in this thesis. The first test protocol (**Table 5**), which was used in **Paper I**, aimed to investigate the effect of different biodiesel-derived contaminants on a V₂O₅-WO₃/TiO₂ SCR catalyst in a typical Euro VI system. That is, with a functioning DOC in front of the SCR catalyst, providing NO₂ to the SCR catalyst in order to yield fast SCR conditions. Therefore, the NO_x reduction performance during the fast SCR reaction (NO₂/NO_x = 0.5) was investigated in this case. The performance of most of the fresh catalyst samples was tested before the samples were exposed to contaminants. After this, the performance of all contaminated catalysts was evaluated.

Table 5: Conditions for Test protocol 1 (Paper I). Prior to performance tests of fresh catalyst samples, a degreening (450 °C, 5h, in air) was done to ensure stable performance.

Inlet gas concentrations	Test temperatures	GHSV _{NTP}
1000 vol-ppm NO, 1000 vol-ppm NO ₂ , 2000 vol-ppm NH ₃ , 8 vol% O ₂ , 6.5 vol% H ₂ O	375, 300, 250 °C	50,000 h ⁻¹

The other two test protocols (Test protocol 2 and 3), used in **Paper III-V** for evaluation of performance effects of sulfur and phosphorus, were more extensive: at each tested temperature, they included (1) an NO oxidation step or NO_x reference concentration step, (2) an NH₃ saturation step from which the total ammonia storage capacity at the specific temperature could be determined, (3) different SCR steps, and finally (4) a step in which adsorbed ammonia could react with gas-phase NO and O₂. Details from these two test protocols are displayed in **Figure 25** and **Table 6**.

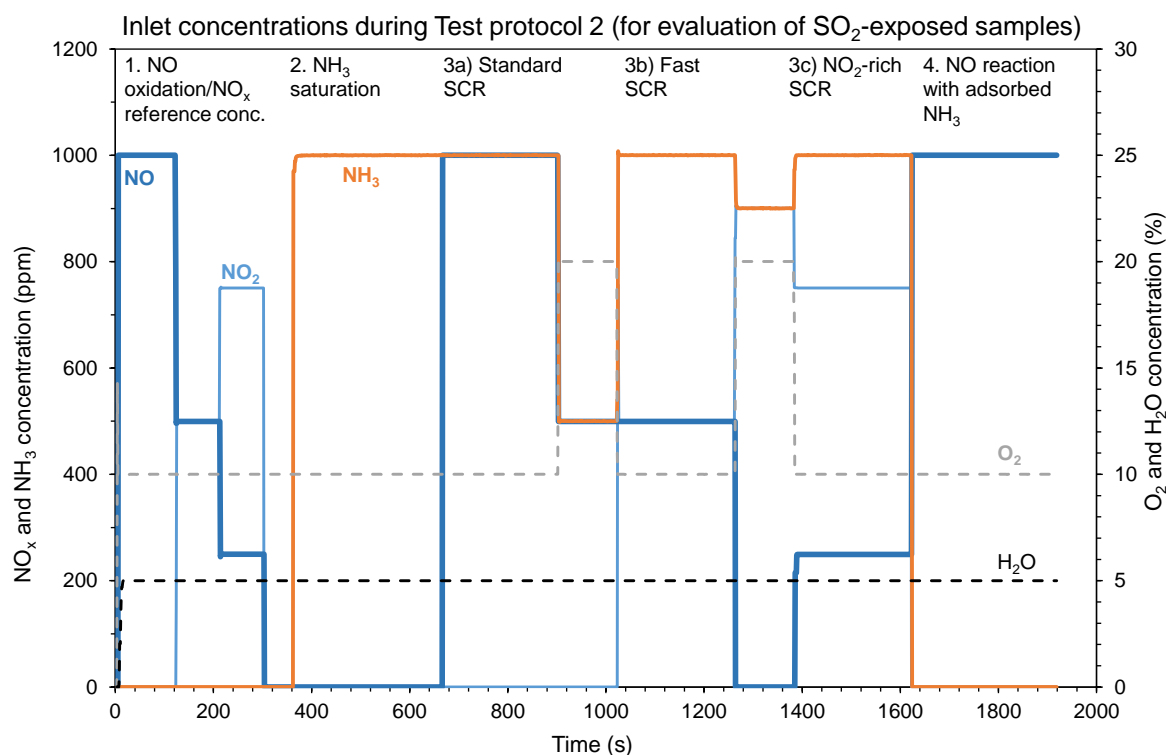


Figure 25: Test protocol 2, used for SCR test of fresh, SO₂-exposed, engine-aged, and regenerated SCR catalyst samples, showing the feed concentrations of NO_x, NH₃, O₂, and H₂O. The test sequence is performed first at 220 and then at 280 °C, with a GHSV 120,000 h⁻¹, total flow of 21 dm³/min (N₂ as balance).

Table 6: Experimental conditions during degreening and SCR performance tests according to Test protocol 3. H₂O was present at all steps except for during the temperature ramps, which were performed in N₂ only.

Experimental step	Test conditions
Degreening of fresh catalysts	1h, 500 °C, 10% O ₂ , 5% H ₂ O, GHSV 120,000 h ⁻¹
SCR performance test of fresh and aged catalysts	<p>The following steps were performed at each temperature (200, 250, 300, 350, 400, 500 °C) with a GHSV of 120,000 h⁻¹</p> <ol style="list-style-type: none"> 1. 500 ppm and 1000 ppm NO, 2, 5, and 10% O₂ 2. NH₃ saturation (1200 ppm, 1000 ppm, in absence of O₂ in Paper IV-V. In Paper IV-V, additionally a step with 500 ppm NH₃) 3. Standard SCR reaction at 200, 250, 300, 350, 400, 500 °C with: <ol style="list-style-type: none"> a) 2% O₂, 1000 ppm NO and NH₃ b) 5% O₂, 1000 ppm NO and NH₃ c) 10% O₂, 1000 ppm NO and NH₃ d) 5% O₂, 500 ppm NO and NH₃ 4. Reaction with adsorbed NH₃: 1000 ppm NO, 10% O₂

2.2.2 Test protocol for DOC samples

The NO, CO, and C₃H₆ oxidation performance of all the fresh, degreened Pt-Pd/Al₂O₃ catalyst cores, which were used for aging experiments with biodiesel exhausts (**Paper V**), was tested in a bench flow reactor at KTH prior to the aging experiments. This was done in order to be sure that any observed decreased performance would be related to the aging experiment, and not due to an inferior performance as a starting point. From these tests, it was noticed that one of the tested DOCs displayed a poorer fresh performance; consequently, this core was not used for the aging experiments. Instead, an additional DOC core was tested and used for the experiments. In the test of these fresh DOCs, a GHSV of 80,000 h⁻¹, 100 ppm CO, 100 ppm C₃H₆, and 1000 ppm NO, 10% O₂ and 5% H₂O, balance N₂ was used. The steady-state conversion at 4-5 different temperatures between around 50 and 375 °C was measured. Additionally, we measured the conversion during the cooling. Prior to the activity tests, all cores were degreened for 1h at 500 °C in 10% O₂, 7% H₂O, balance N₂ with a GHSV of 40,000 h⁻¹.

The ability of biogas-aged oxidation catalyst samples (**Paper VI**) to oxidize CH₄, CO, and NO during heating and cooling was tested in a bench-flow reactor at Chalmers (described elsewhere [166]). **Table 7** provides information regarding the performance test used for this catalyst.

Table 7: Experimental test protocol for oxidation catalyst. In all steps, 8 vol% O₂, 5 vol% H₂O, balance Ar was used. GHSV: 45,000 h⁻¹. The temperature was ramped linearly by 5 °C/min.

Temperature (°C)	CO (vol-ppm)	CH ₄ (vol-ppm)	NO (vol-ppm)	SO ₂ (vol-ppm)	Description
100-450↑↓	1000	-	-	-	CO oxidation
100-450↑↓	-	1000	-	-	CH ₄ oxidation
100-450↑↓	-	-	1000	-	NO oxidation
100-450↑↓	1000	1000	1000	-	Oxidation in complex gas mixture

2.3 Aging experiments and construction of an aging rig

2.3.1 Screening of the poisoning effect of biodiesel-related contaminants by wet impregnation using a DoE (Paper I)

P, S, Na, K, Mg, Zn are contaminants that can be present in the exhaust when operating the engine on biodiesel. These contaminants could have a poisoning effect on exhaust treatment catalysts. To elucidate which of these contaminants that impact the NH₃-SCR performance of a VWTi catalyst, and reveal important interaction effects between the contaminants, a design of experiment (DoE) in the form of a screening design was constructed. This design was constructed to resolve main effects of each contaminant, as well as interaction effects between contaminants, at least for any poison in combination with either sulfur or phosphorus. S and P were considered to be most important poisons for interaction effects, as these are normally more abundant than any of the other potential poisons in real engine applications. A reduced factorial design in the form of 2⁶⁻¹ was considered to fulfill the design criteria. In this design, the combined effect of the six potential catalyst poisons was investigated using two different contamination levels (contaminant concentrations) for each poison: one high concentration and one low concentration. With the two different contamination levels for each of the six contaminants, plus six replicates, this design resulted in totally 38 observations, i.e. 38 samples to be poisoned and evaluated. Contamination of the catalyst samples was performed by wet impregnation. The activity (NO_x conversion during the fast SCR reaction) of the poisoned catalyst samples were analyzed with respect to the concentrations of the different contaminants in the samples.

Wet impregnation was chosen as contamination method, as this is a simple, fast, and precise method. This was required since the number of catalyst samples that were poisoned and analyzed was high. For the wet impregnation, nitrate salts of Na, K, Zn, and Mg, and ammonium salts of P and S, in aqueous solutions were used. Two contamination levels of poisons in the catalyst samples were targeted: 0.25 and 1 wt% of each contaminant, for the low and high level, respectively. After

this, the SCR performance of the contaminated samples were tested. Prior to the contamination, all catalyst samples were degreened, and the SCR activity (NO_x conversion) of fresh samples was tested for most of the samples. In order to save time, some fresh samples were not tested. This was motivated by observing that the NO_x conversions of all tested fresh catalysts were very similar.

2.3.2 Construction of an aging rig

In this project, an aging rig for chemical and hydrothermal aging was designed and constructed (see **Figure 26**). The rig consists of a setup where gases and aerosol particles are fed to a multi-channel reactor positioned in a furnace. The flow through each channel is controlled by rotameters (heated by an oven lamp), to ensure equal flows through all channels that are in use. A static mixer is used to ensure mixing of the gases prior to the reactor. The flow of various gases and water (currently air, nitrogen, SO_2 , but also prepared for one or two additional gases, eg NH_3) is controlled by MFCs, and the water is evaporated with a controlled evaporation and mixing (CEM) system from Bronkhorst. The aerosol is provided by a TSI3076 constant output atomizer (COA), including a filtered air supply (FAS) and a diffusion dryer (DD). The flows are programmed via iTools with using Eurotherm 3508 and 3504 controllers. All lines after water introduction are heated (to above the dew point) to avoid water condensation. The heating of the gas lines is done by heating tapes connected to an adjustable electric power source, in which the temperature is controlled by the voltage and the dimensions of the heating tape.

For aging experiments in which the aerosol generator was used, the rotameters were unfortunately easily clogged by precipitated salt. Furthermore, the time needed to reach a desired poison concentration was considered to be too long when several channels were in use at the same time, since the aerosol flow, and thus the total amount of contaminant, was split into several sub-flows. Therefore, a bypass to only one of the channels in the reactor was constructed to mitigate these problems. A schematic of the aging rig is displayed in **Figure 27**.

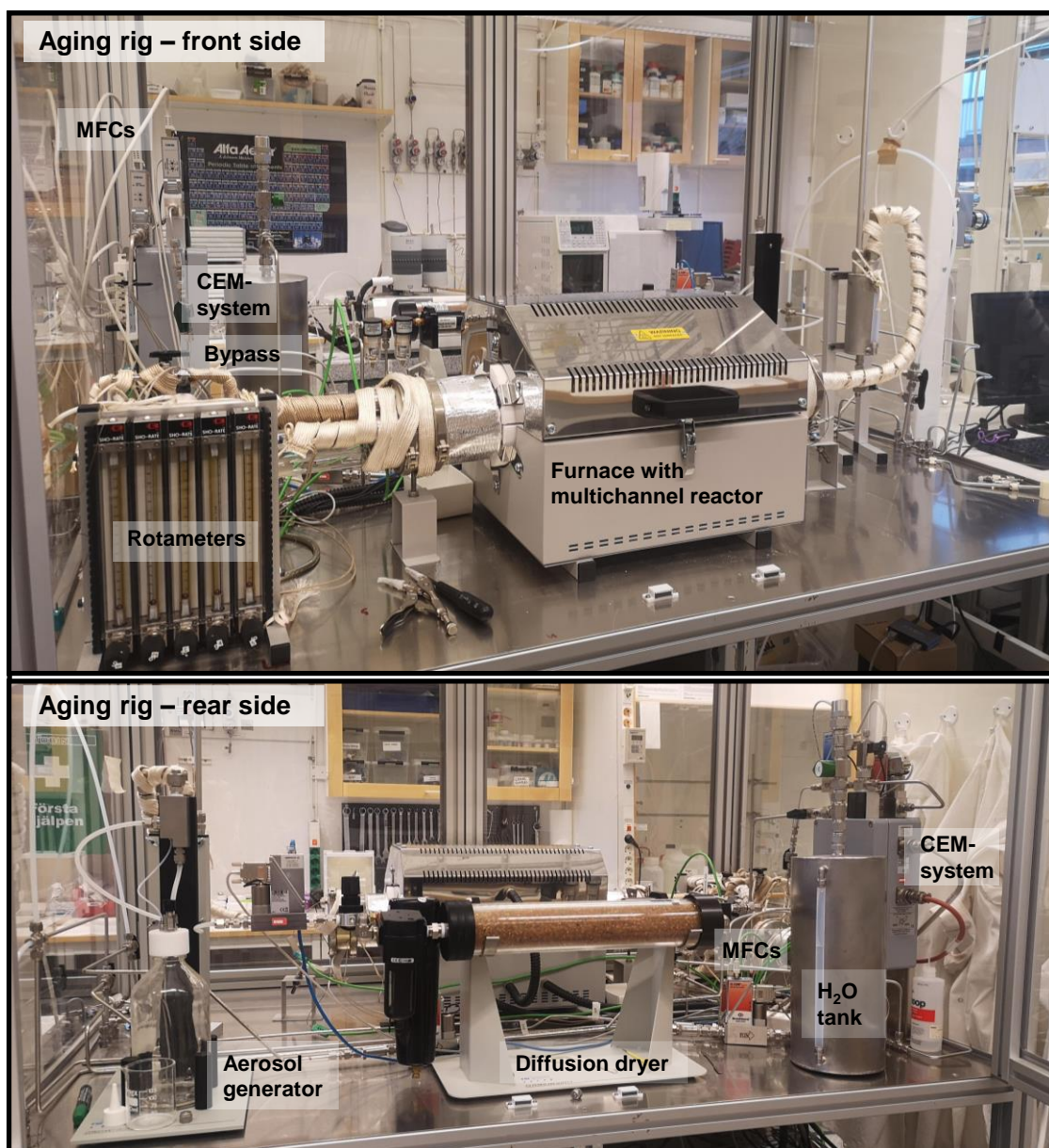


Figure 26: Aging rig for hydrothermal and chemical aging using aerosol and/or gases.

Preliminary aging experiments on DOC and Cu-SSZ-13 SCR samples with a phosphorus-containing aerosol were performed in the rig. The phosphorus came from an aqueous solution of $(\text{NH}_4)_2\text{HPO}_4$. In these tests, the aging temperature was approximately 200 °C, 2-4 g/dm³ $(\text{NH}_4)_2\text{HPO}_4$, and the aging time 8-24 h. The results for the aged DOC will briefly be discussed in **Chapter 3.5.6**.

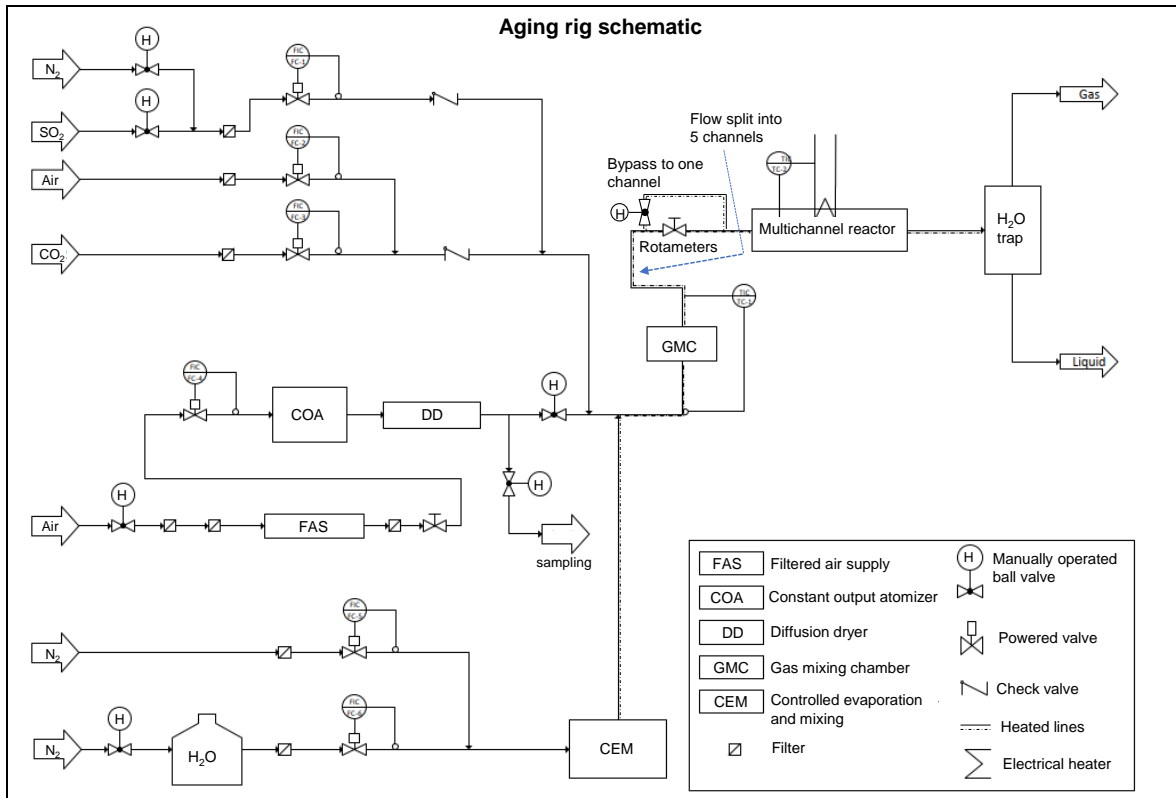


Figure 27: Simplified schematic for the aging rig for hydrothermal and chemical aging using aerosol and/or gases.

2.3.3 SO₂-exposure and regeneration in lab-reactor (Paper III-IV)

The effect of sulfur on Cu-SSZ-13 catalysts were studied by exposing the catalyst samples to SO₂ in a wet oxidizing flow in bench flow reactors. In most of the SO₂-aging experiments, the synthetic catalyst activity test (SCAT) rig at Scania was used for the SO₂-exposure. In this rig, regeneration of the catalyst was also performed, and SCR performance tests were conducted prior to and after SO₂-exposure and regeneration. The regeneration was performed at first 500 and then 700 °C in a wet oxidizing flow, with an SCR test in between. For the SO₂-exposure of the catalyst sample used for characterization in **Paper IV**, the aging rig was used. The conditions for the SO₂-exposures and regenerations are shown in **Table 8**.

Table 8: Conditions during SO₂-exposure and regenerations (notation within brackets). 10% O₂ and 5% H₂O, balanced by N₂, was present all the time during both SO₂-exposure and regeneration.

Experimental step	Conditions
SO ₂ -exposure (SXY0, where XY0 denotes the temperature e.g. S220)	50 ppm SO ₂ , GHSV 60,000 h ⁻¹ , 8h, T = 210*, 220, 280, 350, or 400 °C
Regeneration 500 °C (R500)	GHSV 120,000 h ⁻¹ , 30 min, T = 500 °C
Regeneration 700 °C (R700)	GHSV 120,000 h ⁻¹ , 30 min, T = 630-670 °C (constant increase during the regeneration time)

* Paper IV, SO₂-exposure in the aging rig

2.3.4 Exposure of DOC and SCR catalysts to FAME-exhausts with phosphorus and/or sulfur using a diesel burner rig (Paper V)

In this aging study, a diesel burner rig (see **Figure 28**) at Umicore in Copenhagen was used to expose DOC and SCR catalyst samples to pure, P-, S-, and P+S-doped biodiesel exhaust. Four different aging experiments were conducted: One with pure FAME, one with P-doped FAME, one with S-doped FAME, and finally one with P- and S-doped FAME. In each aging experiment, two DOCs and 4 SCR (two VWTi and two Cu-SSZ-13) catalysts were aged in four separate channels (see **Figure 28**). The DOCs were positioned upstream of two of the SCR catalysts, while a dummy (cordierite core with no coating) was positioned upstream of the other two SCR catalysts. The effect of having a DOC in front of the SCR catalyst is two-fold: it is expected to protect the SCR catalyst against chemical deactivation by acting as a trap, and it could additionally oxidize SO₂ in the exhaust into SO₃. The dummies were included to yield similar flow restrictions in all channels, but was not expected to trap significant amounts of contaminants.

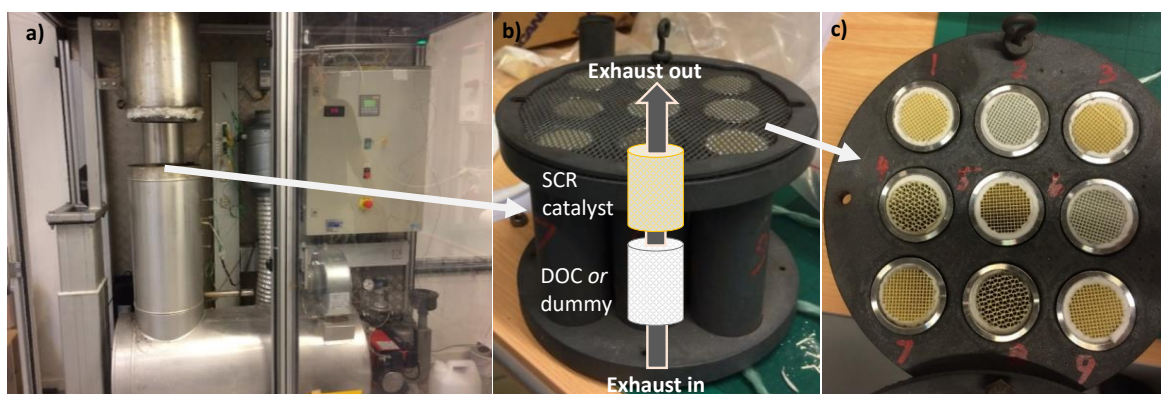


Figure 28: The diesel burner aging rig (a) and sample holder (b and c). For each aging, the sample holder was loaded with 4 SCR catalyst cores, 2 DOC cores (in front of two of the SCR catalysts) and the remaining channels (1, 3, 5, 7, 9) were filled with dummies.

The phosphorus and sulfur concentrations in the aging experiments with only P or S were targeting a full-useful lifetime-exposure (FUL) of P and S respectively, while the concentrations in the 4th experiment with both P and S were decreased to around 1/10th of a FUL exposure. Details for the different aging experiments are shown in **Figure 29**.

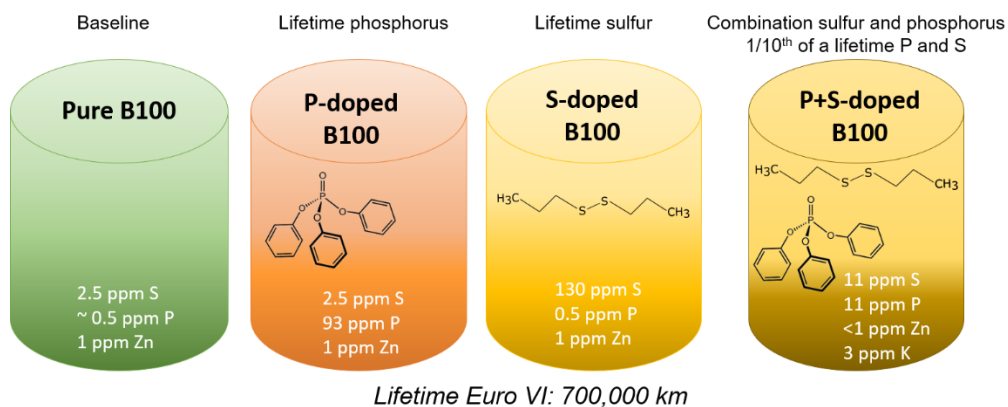


Figure 29: Details regarding the different aging experiments in the diesel burner rig. B100 = 100% biodiesel (rape methyl ester, RME). The inlet temperature to the samples was around 450 °C and the oxygen content in the biodiesel exhaust around 7% during all aging experiments. The aging time was around 170 h, using approximately one barrel (200 dm³) of biodiesel in each aging.

2.3.5 Aging of a Pd-Pt/Al₂O₃ oxidation catalyst in an engine operated on biogas (Paper VI)

In this part, a Euro VI emission control system was aged in an engine-bench using a dual-fuel engine (Volvo GC13C 460 hp) operated on 90% biogas and 10% diesel (<10 ppm S). The exhaust treatment system consisted of an oxidation catalyst (DOC) followed by a DPF, urea injection, three SCR catalysts in series and finally an ASC (see **Figure 30**). The oxidation catalyst in this system was optimized for biogas operation, and was described in **Chapter 2.1**.

900 h of aging in the engine-bench was performed by repeating a 700 s cycle until 900 h of aging was reached. The exhaust gas flows and temperatures (170-550 °C) in this cycle represented mixed driving conditions. After the aging, the exhaust treatment system was dismantled and the different components in it were tested separately. In this thesis, only the results of the DOC are included.

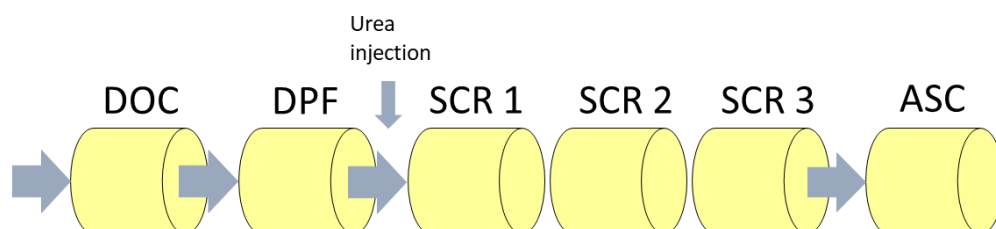


Figure 30: Euro VI exhaust treatment system with an oxidation catalyst (DOC), a particulate filter (DPF), urea injection, SCR catalysts (SCR1-3), and ammonia slip catalyst (ASC). From Englund et al. Catalysts 9 (2019) 1014 [167].

2. 4 Catalyst characterization

2.4.1 Copper oxidation state and coordination by in-situ Synchrotron X-ray absorption spectroscopy (XAS)

Spectroscopic techniques using X-rays are based on that each element has a characteristic set of excitation or fluorescence energies, and thus, identification of elements can be performed using such techniques [168]. In X-ray absorption spectroscopy (XAS), the interaction of the X-rays with the element of interest is dependent on the oxidation state and the coordination environment of the element. This technique is thus widely used for identifying oxidation state and coordination environment of a selected element. Due to the possibility to perform the XAS measurement in-situ, and in-operando, important information about element speciation during e.g. reaction can be obtained [90].

In an XAS experiment, the sample is bombarded with X-rays of a fixed energy. Some of these X-rays are absorbed by atoms in the sample, which results in excitation or ejection of a core electron. This absorption can be quantified by

different means: 1) by comparing the intensity of the incident beam to that of the transmitted (transmission); 2) by measuring fluorescence from the excited atoms that results when electrons fill the now-vacant core-orbital/core-hole (fluorescence), and 3) by measuring electrons that are ejected as the core-hole fills (Auger electrons). Once the absorption for one energy of the bombarding X-rays is quantified, the energy of the X-rays is slightly changed, and the process is repeated. In this way, an XAS-spectra is created by stepping through a range of energies.[169] A synchrotron light source provides tunable and intense X-ray beams, improving the speed and quality of data collection [168].

An example of a normalized, background subtracted XAS spectra is shown in **Figure 31**. In this figure, the different data regions of interest are shown. The X-ray absorption near edge structure (XANES) is the portion of XAS spectra measurement in the vicinity of the absorption edge. This part mainly provides information about oxidation state, but can also give information regarding the coordination environment. [169]

The extended x-ray absorption fine structure (EXAFS) is the oscillatory data measured hundreds of electron volts above the edge. The spacing of these oscillations depends on the distance, D , between absorbing and scattering atoms, and provides data regarding coordination number and bond distances. [169]

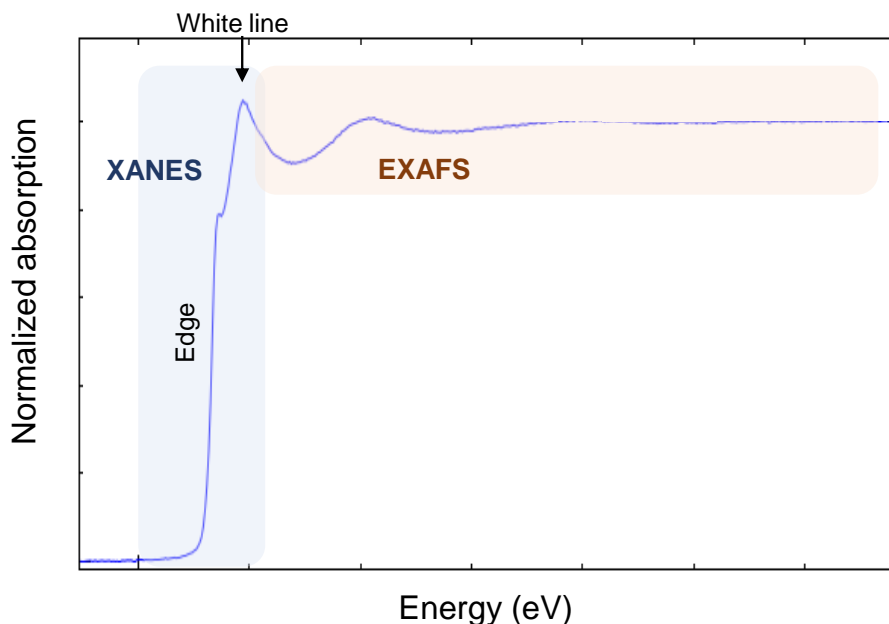


Figure 31: Example of a normalized, background-subtracted XAS spectrum, showing different data regions.

In **Paper IV**, we performed in-situ XAS in oxidative and reducing atmosphere between room temperature and 400 °C to obtain information about the copper species in fresh and sulfur-poisoned Cu-SSZ-13 (Cat A1), and the response of these species to different conditions.

2.4.2 Bulk elemental analyses by XRF and ICP

X-ray fluorescence spectroscopy (XRF) is a simple and quick way of analyzing a range of elements in various types of samples, both liquids and solids. In this technique, X-rays are used to irradiate the sample and the fluorescence coming from the sample due to this interaction is measured by an energy dispersive (ED) detector. This detector measures the different energies of the characteristic fluorescence radiation coming from the sample. All elements are excited simultaneously. Each element has a unique atomic structure giving rise to a unique set of peaks in its electromagnetic spectrum. A wavelength dispersive detector can also be used.

Inductively coupled plasma optical emission spectroscopy (ICP-OES) is a widely applied technique for determining concentrations of different elements in a sample. As with the XRF, a high number of elements can be quantified with this technique. In this technique, a liquid sample is turned into an aerosol of fine droplets. These droplets are drawn into an extremely hot plasma, which causes the droplets to vaporize and the atoms and ions in the sample become excited while emitting light (electromagnetic radiation) with a characteristic wavelength for each element. The intensity of the emitted radiation is related to the concentration of the specific element. For solid samples, it is important to dissolve the sample completely for an accurate analysis.

ICP-OES and energy-dispersive XRF have been used to perform bulk elemental analyses of fresh and aged/contaminated catalyst samples in all papers throughout this thesis.

For the ICP-analyses, samples were ground and digested in $\text{HNO}_3 + \text{HCl} + \text{HF}$ in a microwave furnace prior to analysis to ensure complete dissolution of the sample. For the XRF analyses in **Paper II** and **IV**, the samples were ground in a ball mill, mixed with a binder and pressed into flat briquettes, which then were analyzed. For these analyses, the concentration of elements might not be exact as no references were used. However, for comparison of concentrations of e.g. active material and contaminants, and ratios of different elements, in samples of similar compositions, the method is considered acceptable. For the SCR samples in **Paper V**, the samples were instead analyzed as fusion beads, and calibration against references had been performed. Thus, these analyses resulted in more precise quantification results.

In all the elemental analyses, unless something other is stated, the analysis is performed on a part of a catalyst core, i.e. the sample is a mixture of both the substrate (cordierite) and the washcoat.

2.4.3 Surface species by XPS

X-ray photoelectron spectroscopy (XPS) is a method widely used to evaluate the surface elemental composition and chemical states of the species at the surface of a solid sample. A beam of monochromatic, soft X-rays is used to irradiate the sample. This causes electrons to be emitted from a few surface layers (1-10 nm) of the sample. The number and kinetic energy of these emitted electrons are measured over a range of electron kinetic energies, which results in a spectrum with electron counts versus binding energy. The binding energy of the core electrons is unique for each element; consequently, different elements can be identified through this binding energy. Furthermore, this binding energy will depend on the chemical state of the element, thus additionally providing information regarding the oxidation state of the element. An example of an XPS survey spectra is shown **Figure 32**.

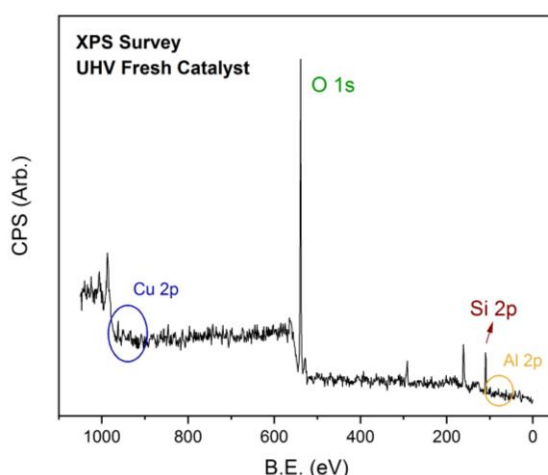


Figure 32: Example of an XPS survey (wide scan) spectra for a fresh Cu-SSZ-13 sample. Smaller regions of interest are then scanned additionally to provide more detailed information.

In **Paper I** and **IV**, XPS was used to compare the surface composition and chemical state of the surface species of fresh, lab-aged, and engine-aged V_2O_5 - WO_3 /TiO₂ and fresh and engine-aged Pt-Pd/Al₂O₃ oxidation catalyst samples, respectively.

2.4.4 Electron microscopy to study the morphology of DOC and SCR catalyst samples

The wavelength of light limits the resolution of a light microscope. In an electron microscope, considerably higher resolutions are reached due to the shorter wavelength of electrons, the so-called de Broglie wavelength. Resolution even down to the atomic scale can be achieved using high-resolution instruments. [170, 171]

In a scanning electron microscope (SEM), a magnified, three-dimensional like image, in the micro- to nanometer scale, of the sample is created by scanning the surface of the sample with a focused electron beam [172].

Similar to SEM, scanning transmission electron microscopy (STEM) uses electrons instead of light to form an image of a sample. However, as opposed to SEM, the image from STEM forms by electrons that interact with the sufficiently thin sample as they pass through it. The sample must thus be very thin, usually <100 nm thick or a suspension on a grid. In STEM, the electron beam is focused on a fine spot (spot size normally 0.05-0.2 nm), and then scanned over the sample in a rectangular pattern (raster scan), as in SEM, to create an image of the whole sample. [171]

Examples of high-resolution transmission electron (HR-TEM) and high angle annular dark field (HAADF) STEM micrographs on DOC samples are shown in **Figure 33**, where Pt particles are shown by the black and white spots, respectively. This is due to that the image contrast is strongly dependent on the atomic number (Z) of the elements in the sample, meaning that particles of high-Z elements on a low-Z element support will appear as dark (or bright) spots [171].

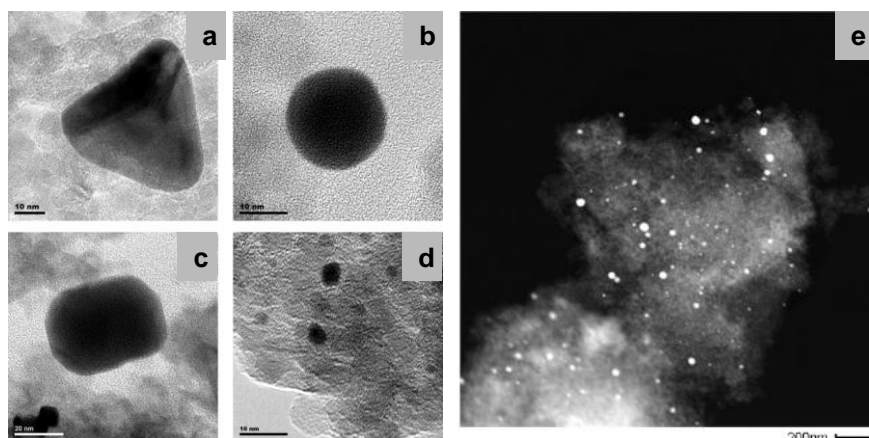


Figure 33: Example HR-TEM (a-d) and STEM-HAADF (e) micrographs of fresh (d), hydrothermally (a) and engine-aged DOC samples (b, c, e). Black and white dots, respectively, indicate Pt particles. Adapted from Winkler et al. Appl. Catal. B 93 (2009) 177 [173] with permission from Elsevier (license number 4752960738745).

Combining SEM or STEM with an energy-dispersive X-ray spectroscopy (EDX) detector, the elemental composition of the sample can also be determined (semi-quantitatively). A mapping over a certain surface of the sample can be performed to show elemental distributions in different regions of the sample

2.4.4.1 Elemental mapping/quantification by SEM-EDX

SEM-EDX has been used in **Paper I** and **V**, to identify elements, and their distributions, on the analyzed surface of some of the SCR catalyst samples from these studies. A cross-section of some of the samples were casted in epoxy to obtain a flat, smooth surface, which is preferable for the elemental mapping as height differences in the samples otherwise give rise to different intensity regions in the sample. Examples of the epoxy-casted samples and SEM images from them are shown in **Figure 34**.

Cross-sections of epoxy-casted Cu-SSZ-13 and V_2O_5 - WO_3 /TiO₂ samples

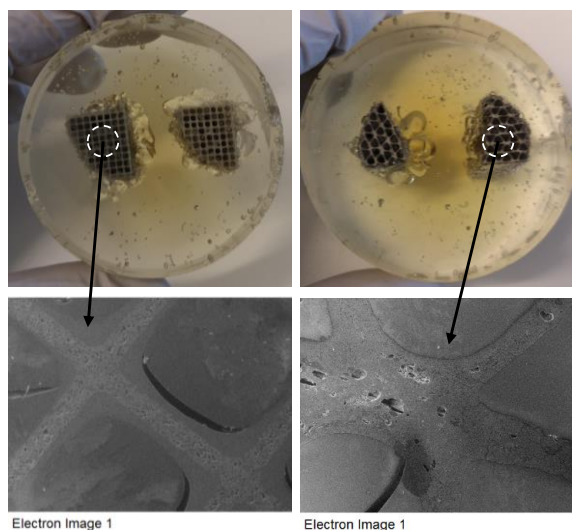


Figure 34: Epoxy-casted SCR samples and corresponding electron images

2.4.4.2 Nanoparticle size by STEM

STEM was used to study the morphology of one of the Cu-SSZ-13 samples (CatA1, **Paper IV**). It was also used to estimate the Pt and Pd nanoparticle size in fresh and biogas-aged DOC samples (**Paper VI**) to investigate if thermal aging had occurred. Particles consisting of heavy elements can be observed as dark or bright spots, depending on which mode the element operates in.

2.4.5 Determination of sulfur content by TGA-MS or using a LECO sulfur analyzer

In **Paper IV**, the sulfur content in the SO₂-poisoned Cu-SSZ-13 sample before and after the XAS measurement was determined by a thermogravimetric analyzer in combination with an MS. In this method, the sample is heated with a linear heating rate, and the weight of the sample is measured simultaneously. The weight loss is related to different species desorbing or decomposing from the sample. The different species, e.g. H₂O and SO₂, will desorb from the sample at different temperatures due to different adsorption strengths. To determine which weight loss that is related to sulfur (i.e. SO₂), the MS is used.

The sulfur content in the catalyst samples investigated in **Paper V** has been analyzed by a Leco sulfur analyzer. In this analyzer, the sample is combusted in pure oxygen whereupon the sulfur in the sample is oxidized to gaseous SO₂. This SO₂ is then detected and quantified by a non-dispersive infrared detector.

2.4.6 Acidity by NH₃-TPD

The acidity of a material can be determined by NH₃-temperature programmed desorption (TPD), where ammonia (or some other molecule with basicity) is allowed to saturate the material whereupon the sample is heated linearly to desorb

the adsorbed ammonia. This desorbed ammonia is quantified by a TCD detector. From the TPD measurement, acid site strength and total acidity/number of acid sites can be obtained. Ammonia adsorbed on weak acid sites will desorb at a lower temperature, while stronger acid sites will desorb the ammonia at a higher temperature. By integrating the ammonia signal versus time, the total amount of ammonia adsorbed and desorbed from the sample can be calculated. For SCR catalysts, in which ammonia is one of the reactants, NH_3 -TPD is specifically useful

For a subset of the samples in **Paper I**, NH_3 -TPD measurements were performed to see if any correlation between total acidity and contaminants and/or NO_x conversion could be found. The total acidity was quantified and the acidic strength was compared qualitatively.

2.4.7 Reducibility and copper speciation by H_2 -TPR

Another temperature programmed method is temperature programmed reduction (TPR). In this method, a sample is exposed to a reductant, commonly hydrogen (H_2), and the H_2 consumption is measured as the sample is heated at a linear rate. Using this method, reducible species in a material can be characterized. Different detectors, e.g. MS or TCD, can be used for measuring the H_2 consumption. An MS provides, in addition to measuring the H_2 consumption, the ability to identify the evolving gases during the TPR, while a TCD detector is simpler and cheaper but only determines the H_2 consumption.

Using H_2 -TPR, different copper species in the Cu-SSZ-13 catalyst sample can be identified and quantified in relation to each other. In 2012, Kwak et al. [174] noted two different reduction peaks in the TPR-profile of Cu-SSZ-13 samples, and that the ratio between these peaks changed with different exchange levels (see **Figure 35**). This analysis, which was also supported by FTIR results, showed that Cu-species with different reducibility existed in the Cu-zeolite; and that the relative quantity of these species was dependent on the exchange level. These species were later associated with Cu^{2+} charge-balanced by coordination to a 2Al position in the zeolite (often considered to be related to the 6mr) and $[\text{CuOH}]^+$ coordinated to a 1Al position in the zeolite (often considered to be related to the 8mr, or CHA cage). The latter, which in this thesis is defined as ZCuOH, is easier to reduce than the former, defined as Z_2Cu .

In **Paper IV**, H_2 -TPR with a TCD detector was used to characterize Cu-species in a fresh Cu-SSZ-13 samples (Cat A, batch 1).

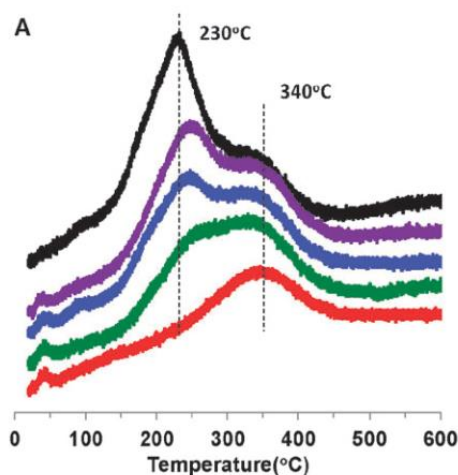


Figure 35: H₂-TPR profile of Cu-SSZ-13 samples with different ion exchange levels (increasing from the red curve, 20%, to the black curve, 100%) showing that two different cationic Cu-species are present in the samples. It furthermore shows that the relative concentration of these species depends on the exchange level. Reproduced from Kwak et al. [174] with permission from the Royal Society of Chemistry.

2.4.8 Surface area measurements by N₂ physisorption

Gas physisorption, using e.g. N₂, is a widely used method for measuring specific surface area, pore volumes and pore size distributions of porous materials. The sample is exposed to N₂ at 196 °C (liquid nitrogen temperature, 77 K) at increasing (and decreasing) partial pressures of N₂. The volume of N₂ adsorbed and desorbed during this process is measured, resulting in adsorption and desorption isotherms. To determine the specific surface area of the sample, a model accompanied with certain assumptions must be used. Commonly, the BET method is used, in which a simple physisorption mechanism is assumed, where all surface sites are populated equally, and no interaction between the adsorbate molecules occur [175].

The specific surface area of fresh and contaminated samples (**Paper I**) was measured by N₂ physisorption at -196 °C, using the BET model, to investigate if the contaminants had any effect on the surface area. Prior to the measurement, samples were degassed (evacuated at an elevated temperature a couple of hours) to remove adsorbed (physisorbed) species, mainly water, which otherwise could block pores in the material.

2.4.9 Powder X-ray diffraction (XRD)

XRD is a method that is commonly applied to detect and quantify crystalline phases in a powder material.

In **Paper VI** we have used XRD to evaluate thermal aging effects of Pd-Pt/Al₂O₃ oxidation catalyst. As a crystalline particle grows, e.g. due to sintering, an increase in the measured intensity is observed in the diffractogram. XRD was also used to see if any CuO could be detected in Cu-SSZ-13 Cat A1 in **Paper IV**.

2.5 Calculations/Theory

2.5.1 Evaluation of the screening design using Multiple Linear Regression (Paper I)

Multiple Linear Regression (MLR) [176] was used to evaluate the results of the screening design. The investigated factors were the main contaminants (P, S, Na, K, Mg, Zn) as well as interaction effects between S or P with any other poison (e.g. P x Na, S x Na, P x S).

MLR models the linear relationship between the independent variables, the matrix X in Equation (1), and the responses, Y in Equation (1). In our case, X is the measured contaminant concentration in the samples, and Y is the NO_x conversion of all the contaminated samples. In the matrix X , all the design parameters (main factors and interaction effects of interest) from the screening design are included. The regression matrix β contains the regression coefficients. This parameter is calculated based on the measured concentrations and NO_x conversions, and it describes the magnitude of the poisoning effect on the NO_x conversion, relative to the model mean. That is, for each poison and poison interactions, a β coefficient that describes the poisoning effect is obtained. ϵ is the residual (error) matrix.

$$Y = X\beta + \epsilon \quad (1)$$

Analysis of variance (ANOVA) was used to calculate the probability that each factor, i.e. main contaminant and interaction, explained more of the variation in the response variable (NO_x conversion) than would be expected from random phenomena. Only main factors and interactions with a p-value <0.05 (i.e. 95% confidence or higher), were then used in the final model.

In addition to the poison concentration, the specific surface area (BET) for all samples, and the total acidity, measured for a chosen subset of the samples, were used in the model, to investigate if there were any correlations between these two factors and the NO_x conversion and/or poison concentration.

2.5.2 Evaluation of aging using a relative rate constant

For most of the aging experiments, a relative rate constant has been used for evaluating the deactivating effect on the low-temperature performance of the SCR catalysts. This constant is defined as the rate constant of the aged catalyst, divided by the corresponding rate constant of the fresh catalysts, and is calculated using the NO_x conversion (X) of aged and fresh catalyst, respectively, as in Equation (2).

$$k_{rel} = \frac{k_{aged}}{k_{fresh}} = \ln(1 - X_{aged}) / \ln(1 - X_{fresh}) \quad (2)$$

Using this equation, it has been assumed that the rate of NO_x reduction is 1st order with respect to NO, and 0th order with respect to NH₃, resulting in the Equation (3). The true NH₃ dependence is actually not zero, but normally weaker than 1 [78, 122, 177]. When used for comparison between two similar samples, the error resulting from this simplification is likely similar for both samples, assuming that the aging does not considerably change the NH₃ dependence of the reaction. We did not investigate this, but according to Shih et al. [122], sulfation of two different model Cu-SSZ-13 samples did not change the reaction order for NH₃ as compared to the fresh state of the catalysts.

$$k = -\frac{F_{NO,in}}{C_{NO,in} \cdot V} * \ln(1 - X) \quad (3)$$

k = 1st order rate constant (s⁻¹)

$F_{NO,in}$ = molar flow rate of NO in the feed (mol s⁻¹)

$C_{NO,in}$ = concentration of NO in the feed (mol dm⁻³)

V = catalyst volume (dm³)

X = NO conversion of fresh and aged catalyst

2.5.3 MCR-ALS for analysis of in-situ temperature dependent XAS spectra and DFT-assisted theoretical XANES

Analysis of Cu-K edge spectra of samples with several unknown different Cu species, in unknown concentrations, is not straightforward. Linear Combination Fitting (LCF) using normal reference compounds is difficult for framework-Cu species, as the spectra of such species cannot be described by commonly available reference materials [178]. Furthermore, the intensity and position of edge features depend not only on oxidation state, but also on the coordination environment. This is especially true for copper(I) ions [179]. Therefore, an approach using multivariate curve resolution alternating least square (MCR-ALS) was utilized, inspired by the work of Martini et al. [178]. In this technique, all normalized Cu K-edge XANES spectra collected in oxidizing (O_2/N_2) and reducing (H_2/He) flows, at temperatures between room-temperature and 400 °C, were analyzed by an MCR-ALS code [180] to obtain a number of pure components (spectra) that can reconstruct the full set of spectra. The optimal number of components was based on principal component analysis (PCA) [178, 181].

The pure components of fresh and SO_2 -poisoned Cu-SSZ-13 samples were compared with calculated theoretical XANES spectra [182]. The structures for the theoretical spectra were chosen based on density functional theory (DFT) calculations. DFT-optimization was performed for Cu-structures in the 6- and 8-membered rings, and the most energetically favored species were chosen.

In addition to the analysis of the XANES data, a part of the EXAFS data was analyzed using continuous Cauchy wavelet transforms (CCWT). These transforms were used for visualization of the EXAFS spectra in three dimensions: the wavenumber, k ; the interatomic distance, R ; and the CCWT modulus, which decompose the EXAFS amplitude terms continuously. By using this analysis, it is possible to identify overlapping contributions from different neighbor atoms or scattering events that are impossible or difficult in the Fourier transform data, for example the nuclearity in different Cu oxo species.

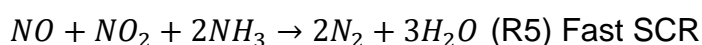
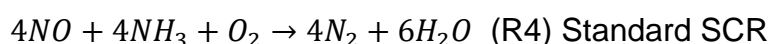
Part III: Results and Discussion

3.1 Performance of fresh SCR catalysts

The standard SCR reaction for fresh Cu-SSZ-13 (Cat A1 and A2) and V₂O₅-WO₃/TiO₂ catalyst samples was evaluated with three different oxygen concentrations (2-10%) at temperatures between 200 and 500 °C. In addition, the effect of NO₂/NO_x ratio (0, 0.5, and 0.75) was investigated as the Euro VI exhaust treatment systems have a DOC is positioned upstream of the SCR catalyst to produce NO₂. This NO₂ is used to apply the so-called fast SCR condition, for which equimolar amounts of NO and NO₂ is fed to the SCR catalyst, as this could improve the low-temperature performance [49]. This effect was evaluated at two different temperatures: 220 and 280 °C, with 10% O₂. A third Cu-SSZ-13 catalyst (Cat B) was also evaluated with this test. In all the above described experiments, the GHSV was 120,000 h⁻¹, and the following inlet concentrations were used: 1000 ppm NO_x, 1000 ppm NH₃, and 5% water was present for all SCR reactions.

3.1.1 V₂O₅-WO₃/TiO₂

For the vanadium-based SCR catalyst, the conversion of NO and NH₃ during standard SCR conditions (R4) is quite low at temperatures below around 300 °C (see **Figure 36a-b**); only around 10-15% is converted at 200 °C. However, when applying fast SCR conditions (R2), this low-temperature performance can be significantly improved: the conversion at 220 °C increases from around 20 to around 80%, without any increase in N₂O concentration, by adding NO₂ at equimolar concentration as NO. Thus, the selectivity towards the desired SCR reaction is excellent. The reason for the improved performance with equimolar amounts of NO and NO₂ in the feed, has been proposed to be related to the faster re-oxidation of active vanadium sites, which is considered as the rate limiting step for the standard SCR at low temperatures [77].



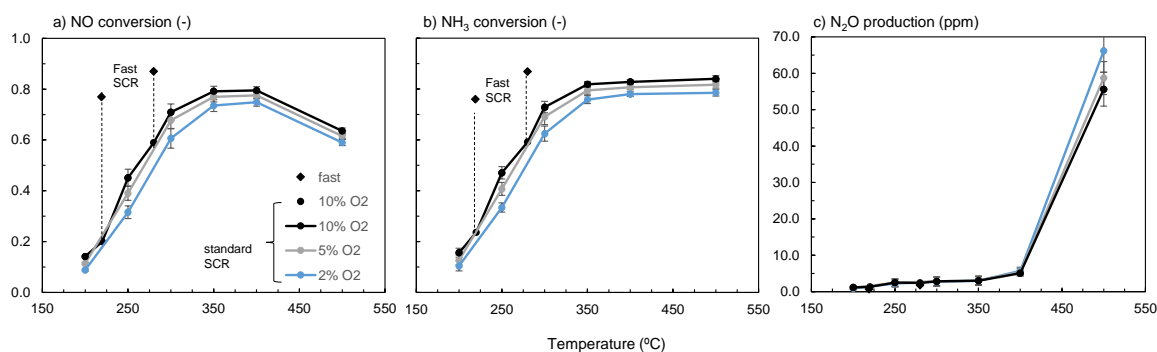
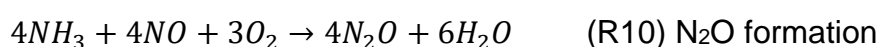


Figure 36: NO conversion, NH₃ conversion and N₂O production of the fresh V₂O₅-WO₃/TiO₂ SCR catalysts. Average of 8 fresh samples, +/- 1 standard deviation as error bars. Test conditions: 1000 ppm NO, 1000 ppm NH₃, 2-10% O₂, 5% H₂O, GHSV 120,000 h⁻¹. Two points (220 and 280 °C) with fast SCR conditions (10% O₂, 5% H₂O) are included as well.

Another feature observed for the catalytic performance of this vanadium-based catalyst is that at temperatures up to around 400 °C, ammonia and NO are equally converted, in a stoichiometry in agreement with the standard SCR reaction. On the other hand, at higher temperatures (500 °C), the conversion of NO and NH₃ differs: the NO conversion decreases while the NH₃ conversion stays at the same high value. This difference demonstrates that undesired side-reaction(s) occur, competing with the SCR reaction, and is also shown by the high N₂O production at this temperature (**Figure 36c**). N₂O is vastly undesired as it is a strong greenhouse gas and additionally contributes to depletion of the ozone layer [183]. As opposed to at high temperature, the N₂O formation for this catalyst at lower temperatures (<400 °C) is negligible, both for standard and fast SCR conditions. This agrees with previous observations [61].

Besides from reacting in the standard SCR reaction, ammonia can be oxidized to N₂, NO, and/or N₂O, according to reactions **R7-R10**. In both reactions **R7** and **R8**, ammonia is consumed in a reaction not including reaction with NO. **R7** is also called selective catalytic oxidation (SCO) [184], however, in this case, it is not a selective reaction as NH₃ is consumed not reacting with NO, thus less ammonia is available for NO reduction. The same applies in reaction **R8**, but in this reaction the problem is not only the unselective ammonia consumption, but NO is also formed, resulting in negative conversion. [61]



High-temperature N₂O formation occurs due to ammonia oxidation [60]. As N₂O is formed at high temperature for this catalyst, one of the reactions **R9-R10** is likely

to occur. In reaction R6, nitrous oxide is formed directly from oxidation of ammonia by oxygen, which agrees with the observed NO and NH₃ conversion. However, it would also be possible that reaction **R9** occurs, in combination with **R8** in which NO is formed from ammonia.

Another observation is that the standard SCR reaction is slightly promoted by oxygen, displayed by the small, gradual increase in NO and NH₃ conversion as the O₂ content is increased (**Figure 36a-b**, blue, gray and black curves are 2, 5, and 10% O₂, respectively). This applies over the entire temperature range. In a previous study, oxygen was shown to have an enhancing effect on NO conversion, at least at concentrations up to around 10% [143]. Unlike the NO_x reduction, the highest N₂O yield is obtained for the lowest oxygen concentration, which is easiest observed at 500 °C where high amounts of N₂O is produced. Oxygen thus has a slightly inhibiting effect on the reaction that forms N₂O over this catalyst.

It should be noted that the space velocity is rather high in these tests, 120,000 h⁻¹, which is a challenging condition for this catalyst. Thus, full conversion is not reached even at the highest temperature. More commonly applied GHSVs for this type of catalyst in heavy-duty applications are between 20,000 and 70,000 h⁻¹, and would have yielded higher conversions [49, 185]. At intermediate to high temperatures, the reaction rate of the catalyst is mainly limited by pore-diffusion and external diffusion (film transfer), respectively. The performance of the catalyst in the film-transfer limited regime can be improved by increasing the surface area for gas-solid mass transfer, i.e. the geometrical surface area (GSA), by increasing the cell density. [49]

3.1.2 Cu-SSZ-13

For the Cu-SSZ-13 samples, a clear difference in performance is observed, with Cat A2 having a considerably better performance than Cat A1 (see **Figure 37**). This is especially true for the NO conversion, which is significantly higher for Cat A2, both at high and low temperatures. Concurrently, no increase in N₂O formation is observed for this catalyst compared to Cat A1; instead, the N₂O production at high temperature is actually slightly lower. Consequently, Cat A2 is not only more active, but also more SCR-selective than Cat A1.

Applying fast SCR conditions by adding NO₂ to the feed, result in an improvement of the NO and NH₃ conversion for Cat A1, especially at 220 °C. However, this conversion improvement is accompanied by a substantial increase in the N₂O formation, as opposed to for the VWTi catalyst. For Cat A2, full conversion is almost already reached at 220 °C; but a slightly higher conversion is reached for the fast SCR reaction. As for the Cat A1, this is also accompanied by a higher N₂O production, though, not as high as for Cat A1.

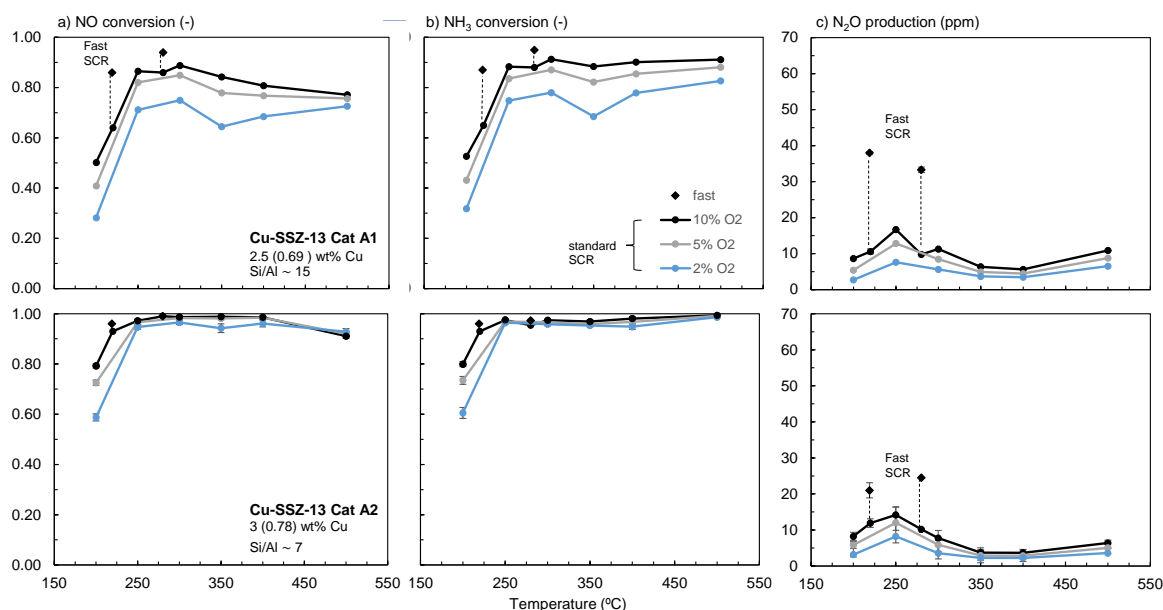


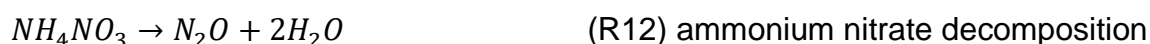
Figure 37: NO conversion, NH₃ conversion and N₂O production of the fresh Cu-SSZ-13 catalysts (top panels: CatA1; lower panels: Cat A2). For Cat A2, the values are an average of 8 fresh samples, with error bars corresponding to +/- 1 standard deviation. For Cat A1, the values are based on one catalyst sample. Test conditions: 1000 ppm NO, 1000 ppm NH₃, 2-10% O₂, 5% H₂O, GHSV 120,000 h⁻¹.

At temperatures higher than 300 °C, Cat A1 displays a decrease in selectivity to the SCR reaction, as shown by the decreased NO conversion at this temperature, while the conversion of NH₃ still is high. This is probably related mainly to the competing reaction in which ammonia is oxidized into N₂ (R7), while only a small part is converted to N₂O. Cat A2 on the other hand, has a selectivity-drop only at temperatures above 400 °C. The selectivity-decrease above 300 °C for the Cat A1 could be related to that a part of the Cu occurs as CuO_x particles instead of being ion-exchanged to the zeolite (supported by STEM results, **Chapter 3.4**). CuO_x clusters are generally considered to have low NO_x reduction performance at low temperature, although some authors argue that they could oxidize NO into NO₂ at rather low temperature, which then could improve the low-temperature performance through the fast SCR reaction [186-188]. However, most authors agree that a higher SCR activity is obtained on Cu ions exchanged to the zeolite. Moreover, CuO_x is active for ammonia oxidation, especially at higher temperatures, thus competing with the desired SCR reaction [60]. This is consistent with the observed results for Cat A1.

Both Cu-SSZ-13 samples show similar N₂O production profiles (**Figure 37**, to the right), which are quite different from the profile of the VWTi catalyst. The Cu-zeolites have one maximum at low temperature (around 250 °C), where the vanadium-based catalyst has insignificant N₂O formation. Additionally, a 2nd maxima appear at high temperature (around 500 °C), as for the VWTi catalyst. However, the N₂O produced at this temperature is considerably lower than that for the vanadium-based catalyst. This indicates that the main side reaction occurring

at high temperature is the oxidation of NH_3 by oxygen to N_2 and water (R4), while only a small part is oxidized to N_2O . This agrees with the results of a previous study of a Cu-zeolite, where the ammonia oxidation (in absence of NO) was observed to yield mainly N_2 ; ammonia oxidation was also noted during the standard SCR, especially at temperatures $>450^\circ\text{C}$ [58].

The N_2O production maximum at low-temperature for the Cu-SSZ-13 samples is consistent with the work of others [58, 114, 189]. The mechanism of N_2O formation depends on the temperature: at low temperatures (below around 300°C), the formation of N_2O is generally considered to occur through decomposition of ammonium nitrates formed on the surface of the catalyst, reactions (R11) and (R12) [57, 189]. This N_2O production is favored if NO_2 is present in the feed [24, 58, 60, 113], which agrees with our results.



Combining the two reactions above results in the global reaction for N_2O formation (R13):



With NO present in the feed, the formed ammonium nitrates can instead be reduced according to reaction (R14). For the VWTi catalyst, this is likely the case as its N_2O production at low temperature is insignificant. Alternatively, the formation of ammonium nitrates is low for this catalyst. For the Cu-SSZ-13 catalysts on the other hand, reduction of ammonium nitrates by NO appears to be less efficient.



As displayed by the different curves (black, gray, blue) in **Figure 37**, both Cu-SSZ-13 catalysts shows a dependence on the oxygen concentration in the feed; a lower O_2 concentration results in a lower NO and NH_3 conversion, especially at the lowest temperature evaluated (200°C). For Cat A1, the oxygen dependence is observed over the whole temperature range, while it for Cat A2 is noted mainly at 200°C . However, for the lowest O_2 concentration (2%) it is observed at 350°C as well. At this concentration, the NO conversion profiles of both Cu-zeolites display the characteristic seagull shape. This means that the curve has first the normal increase in NO conversion with temperature at low temperatures, but it is then followed by a decrease in conversion at intermediate temperatures (here seen at 350°C). Finally, the conversion increases again at higher temperatures. This shape is often seen for Cu-SSZ-13 at demanding conditions, such as low Cu content, high space velocity, and low oxygen concentration [190]. A promoting effect of oxygen has previously been reported for a Cu-zeolite by Colombo et al. [58], who performed SCR tests

with 2-8% O₂ in the feed and estimated the reaction order to be approximately 0.45.

The oxygen dependence at the highest temperature (500 °C), appears to be different than that at lower temperatures. Contrary to at low temperatures, the NO conversion at 500 °C is slightly higher for the lowest oxygen concentration for Cat A2; the small drop in NO conversion observed at this temperature is lowest when only 2% O₂ is present in the feed gas. A similar trend is noted for Cat A1; in fact, the NO conversion does not decrease at all at high temperature, as opposed to with 5 and 10% O₂ present. Consequently, at high temperature, the oxidation of ammonia appears to be favored by a higher oxygen concentration, while the oxygen concentration seems less important for the SCR reaction.

3.1.3 Summary of NO₂/NO_x ratio effect on the SCR performance: NO_x conversion and N₂O selectivity/production

Different types of SCR catalysts response differently to NO₂ in the feed, as is shown in **Figure 38-39**. These figures show the NO_x conversion and N₂O selectivity at 220 and 280 °C for three different NO₂/NO_x ratios: 1) NO₂/NO_x=0, i.e. the standard SCR reaction; 2) NO₂/NO_x=0.5, i.e. the fast SCR reaction; and 3) NO₂/NO_x=0.75, i.e. a mix of fast SCR and slow or NO₂-SCR.

In this thesis, I have defined the N₂O selectivity as the amount of N₂O produced divided by amount of NO converted. This is not a true definition of selectivity, as the true selectivity depends on the reaction through which N₂O is formed (e.g. if the nitrogen originates from both NO and NH₃ or only one of those), which is not always known, and beyond the scope of my studies. However, the definition I have chosen to use in this thesis is a good measure in terms of the SCR performance, as it in an easy way shows how much N₂O that is produced for a certain feed concentration and conversion level of NO_x.

The VWTi catalyst indeed shows a great improvement when NO₂ is present in the feed, especially for fast SCR conditions in which the low-temperature NO_x conversion is significantly higher, whereas the amount of N₂O produced is the same, or lower, as at standard SCR conditions. Increasing the NO₂ concentration beyond fast SCR conditions, to an NO₂/NO_x ratio of 0.75, also results in a significantly improved NO_x conversion at 220 °C. However, this increase is less pronounced than with fast SCR conditions. Moreover, at 280 °C, the NO_x conversion is slightly lower than for standard SCR conditions. Additionally, the selectivity to N₂O is higher than for fast SCR conditions at both temperatures, while compared to the standard SCR reaction, it is higher only at 280 °C. Consequently, the NO₂/NO_x ratio should not be higher than 0.5 for optimal SCR performance of this catalyst.

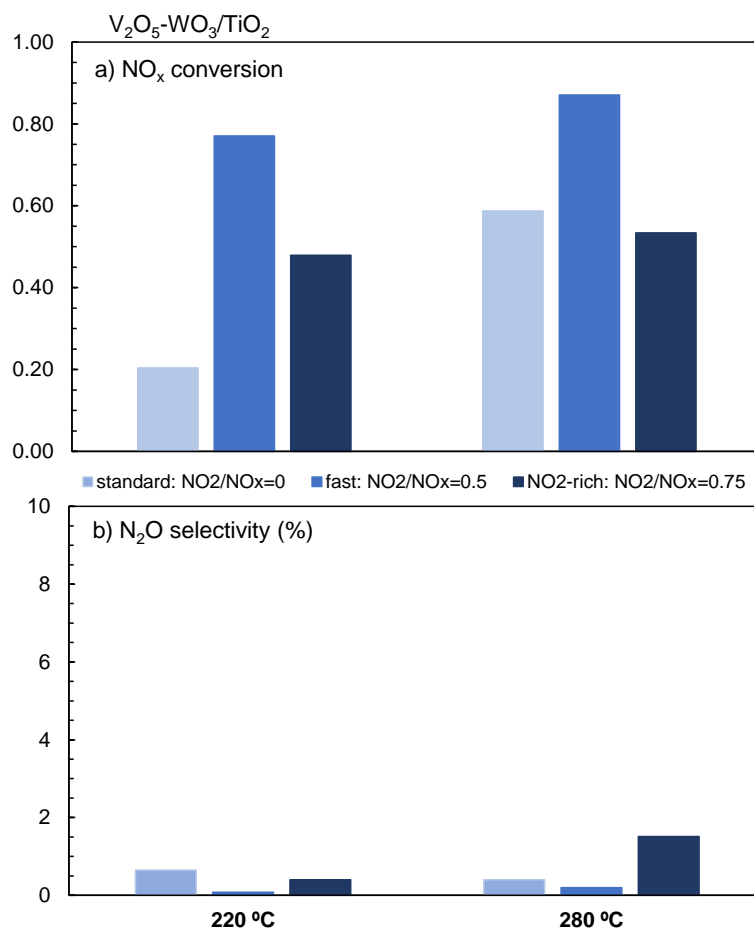


Figure 38: Effect of NO₂ in the feed (NO₂/NO_x=0, 0.5, or 0.75) on the NO_x conversion and N₂O selectivity of the V₂O₅-WO₃/TiO₂ catalyst at 220 and 280 °C. NO₂ present in the feed, especially at equimolar amounts with NO, improves the low-temperature NO_x reduction by increasing the NO_x conversion at 220 °C considerably, and decreasing the N₂O selectivity. Test conditions: 1000 ppm NO_x, 1000 ppm NH₃, 10% O₂, 5% H₂O, GHSV 120,000 h⁻¹.

As opposed to the vanadium-bases catalyst, the copper-zeolites display only a slight increase in NO_x conversion when applying fast SCR conditions, but a considerable increase in N₂O selectivity. Increasing the NO₂ concentration further results in a slightly decreased NO_x conversion, compared to standard SCR conditions, and a substantial increase in N₂O. The N₂O selectivity increases to at least twice of what is observed for the fast SCR condition. The increase in N₂O production with increasing NO₂ content in the feed has been observed previously for a Cu-CHA catalyst [189]. In that study, the fast SCR reaction was actually observed to be slower than the standard SCR reaction at very low temperatures (150 and 200 °C)[189]. This has also been shown previously in another study [99], and was suggested to be due to blocking of the pores by ammonium nitrates [99, 189]. For Cu-SSZ-13 SCR catalysts, it is thus of high importance not to exceed an NO₂/NO_x ratio of 0.5, and for fresh catalysts it is questionable if even a ratio of 0.5 should be reached.

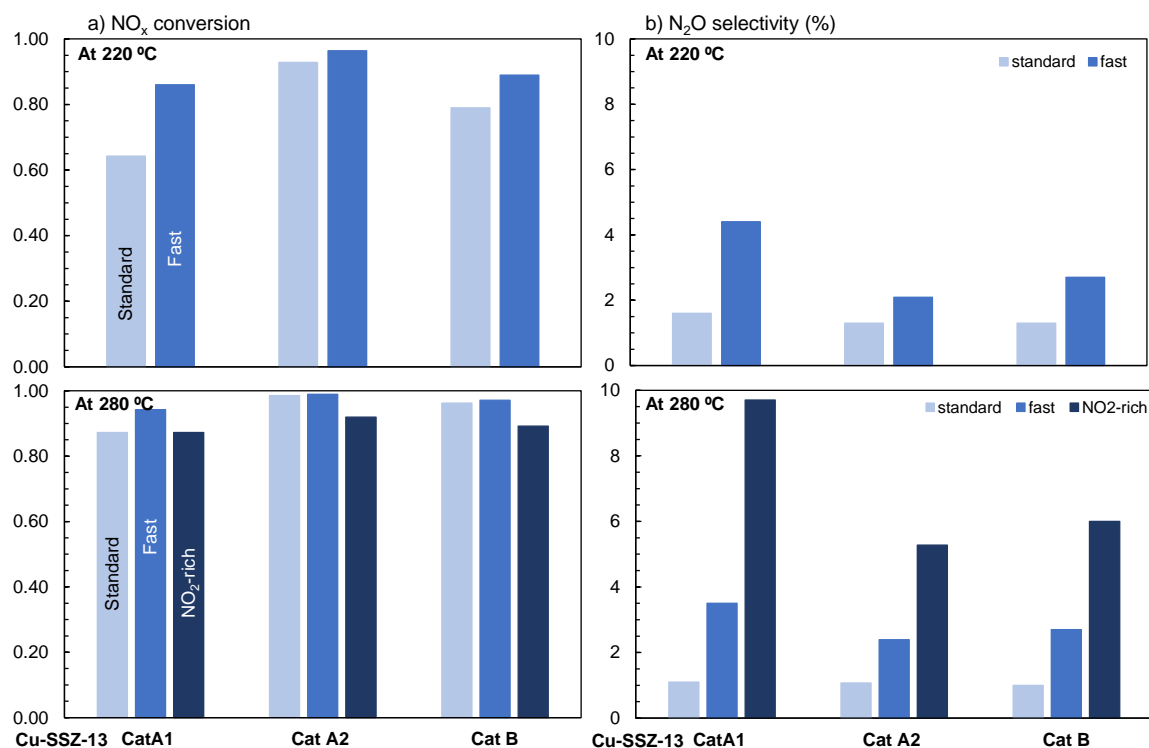


Figure 39: Effect of NO₂ in the feed (NO₂/NO_x=0, 0.5, or 0.75) on the NO_x conversion and N₂O selectivity of the different Cu-SSZ-13 catalysts at 220 °C. Fast SCR conditions result in a moderate increase NO_x conversion for all samples, but the N₂O selectivity is significantly increased. A further increase in the NO₂ concentration results in substantial amounts of N₂O being produced. Test conditions: 1000 ppm NO_x, 1000 ppm NH₃, 10% O₂, 5% H₂O, GHSV 120,000 h⁻¹. At 220 °C, the NO₂-rich SCR did not reach steady-state.

3.2 The effect of biodiesel-derived contaminants on V₂O₅-WO₃/TiO₂ SCR catalysts – a screening study (Paper I)

The influence of 6 different potential catalyst poisons (P, S, Na, K, Mg, Zn) related to biodiesel-operation was studied for a commercial vanadia-tungsta-titania SCR catalyst using a screening design. In this experiment, the catalyst samples were wet impregnated with aqueous solutions containing all the contaminants. In these contamination solutions, each specific contaminant was present either in a low, or a high, contamination level. These two levels were targeted to be around 0.25 and 1 wt%, respectively. In addition to the lab-aged samples, two engine-aged SCR catalysts were included in the study: one from a truck with Euro VI system that had been operated 700,000 km on 100% biodiesel; the other from a truck with a Euro V system, operated 130,000 km in Brazil. Both these trucks had been operated in long-haulage.

Evaluation of the accelerated lab-aging method was performed using various characterization techniques (ICP-OES, SEM-EDX, and XPS). The ICP-OES results (**Figure 40**) showed that the aging method resulted in reproducible contamination levels in the catalysts samples, although both levels were slightly lower than targeted. Importantly, a significant difference was obtained between high and low concentration levels, and the variation within each concentration level was low. These features are important for successful use of the experimental data in the model.

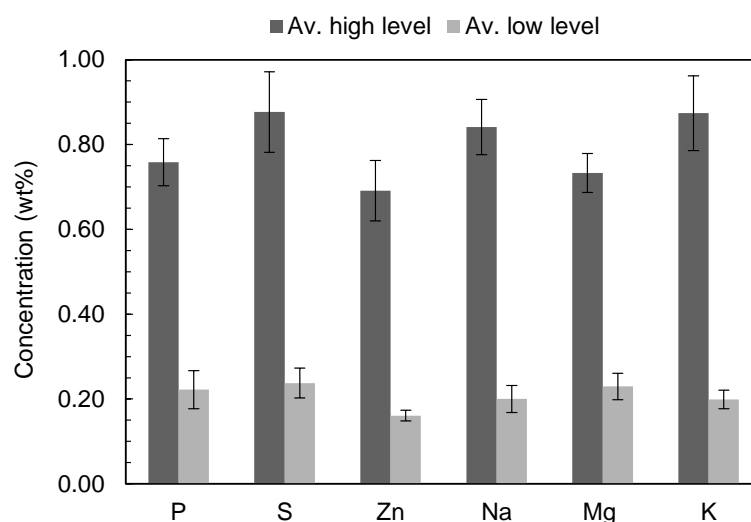


Figure 40: Concentrations of contaminants in the lab-aged samples, measured by ICP-OES. Target levels were 0.25 and 1 wt% for the high and low level, respectively. The error bars correspond to \pm one standard deviation. From Paper I, Dahlin *et al.* Appl. Catal. B 183 (2016) 377 [191].

Analysis of the surface elemental composition and binding energy of each contaminant in the fresh, lab-aged and vehicle-aged samples by XPS showed the contaminants P, S, Na to be present as similar surface compounds on both lab- and engine-aged samples. However, the concentrations were significantly lower for the engine-aged samples. K and Zn were detected only on the surface of the lab-aged samples. The binding energy of sodium, which was detected on the lab-aged and engine-aged catalysts but not on the fresh (see **Figure 41**), was 1071.7-1071.9 eV and indicates that it is in the form of pyrophosphate ($\text{Na}_4\text{P}_2\text{O}_7$) or sodium sulfate (Na_2SO_4). The binding energy of the sulfur was 169.7 eV, thus likely a sulfate; the phosphorus detected in all samples, fresh as well as aged, had a binding energy between 133.4 and 134.1 eV, agreeing well with phosphate (PO_4^{3-}) or metaphosphate (PO_3^-). These compounds, and additionally phosphorus pentoxide (P_2O_5), have been reported previously in studies of aged SCR catalysts [192, 193]. The molar P/V ratio of the lab-aged samples ranged between 0.3-1.5, while it was 0.48, 0.33, and 0.26 in vehicle-aged Euro V and VI, and fresh catalyst, respectively.

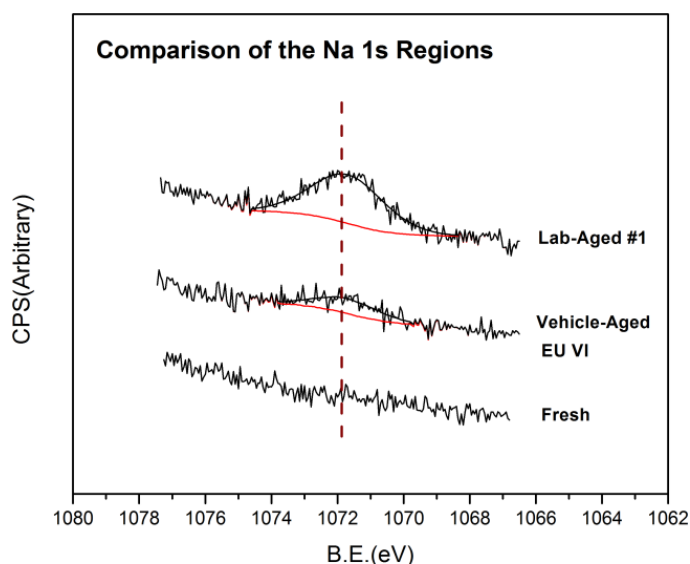


Figure 41. Na 1s XPS spectra for a lab-aged compared to vehicle-aged and fresh sample. From Paper I, Dahlin *et al.* Appl. Catal. B 183 (2016) 377 [191].

The SCR performance of fresh and lab-aged catalyst samples was evaluated in a laboratory bench-flow reactor. In this test, the fast SCR reaction ($\text{NO}_2/\text{NO}_x=0.5$) was evaluated at 250, 300, and 375 °C. NO_x conversion values in the range of 54-113% of that of fresh catalysts were obtained for the lab-aged samples. Thus, not all contamination resulted in poisoning effects. The NO_x conversions of all contaminated samples, together with measured contaminant concentrations, were evaluated using a multivariate technique (MLR) with the aim of acquiring a model able to describe the poisoning effect of each contaminant. **Figure 42**, indeed shows that the model obtained for the NO_x conversion correlates well with the actual NO_x conversion. R^2 -values of 0.92 and 0.85 were obtained for the calibrated

and cross-validated model, respectively. Consequently, we can use this model to predict the effect of various contaminants and contaminant interactions. These effects are described by the β -coefficients (see **Figure 42b**), which describe the poisoning effect of each contaminant and interaction that were significant on a 95% confidence level. A negative value means a more poisoning effect than the model mean, while a positive value means an improvement compared to the model mean. The larger the absolute value of the β -coefficient, the stronger is the effect. Contaminants that significantly affect the NO_x conversion are P, S, Na, Mg, and K. Additionally, the interactions P*Na, P*K, and S*Na have a significant effect. Notably, Zn did not show any significant effect. A poisoning effect was obtained for Na, Mg, K, P*Na, and P*K, with Na and K being the strongest poisons. This agrees with several other deactivation studies, which show the strong poisoning effect of Na and K [130-132, 139, 141-145, 148, 162, 194, 195]. The poisoning effect of the alkali metals was lowered in presence of phosphorus, and, particularly, sulfur. For S, P, and the S*Na interaction, NO_x conversions instead became better than the model mean. The alleviated effect of alkali in the presence of sulfur and phosphorus is likely due to formation of sodium/potassium phosphates and sulfates, which might prevent, or decrease, the interaction of the alkali metal with the active vanadium sites. Previous studies on deactivation of vanadium-based SCR catalysts by phosphorus, indicate that the deactivating effect is rather low at P concentrations below around 2 wt%, while higher concentrations are needed for more significant deactivation [129-132]. In these studies, the standard SCR reaction was evaluated. In our study, the phosphorus is in a concentration range where a low negative effect of P is expected, and the fast SCR reaction was evaluated.

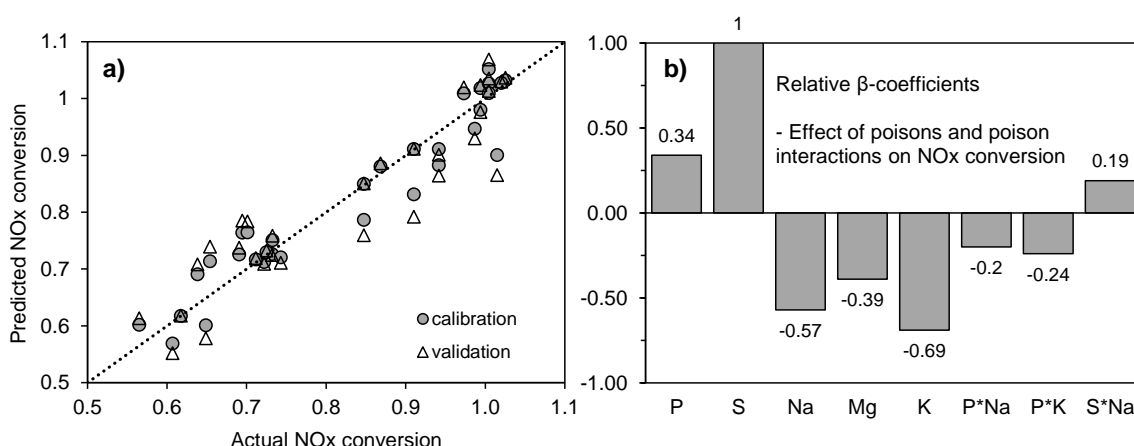


Figure 42: Centered and scaled β -coefficients for all significant main contaminant and interaction effects, i.e. effect on the SCR performance in comparison to model mean. A negative value means a poisoning effect, and the more negative the value is, the stronger the poisoning effect. A positive value means that the performance is better than the mean value from the model. No significant effect was observed for Zn. Adapted from Paper I, Dahlin *et al.* Appl. Catal. B 183 (2016) 377 [191].

To investigate if the NO_x conversion or any specific contaminants present in the samples could be correlated to the specific surface area or acidity of the aged catalyst, N₂ physisorption and NH₃-TPD were performed. The specific surface area of all samples was measured, while the acidity was measured on a subset (8 samples) of the samples. The specific surface area and acidity were also measured for fresh and engine-aged samples.

From these results, it was concluded that all aged samples had a lower surface area compared to the fresh catalysts, around 50-67% of that of a fresh catalyst. However, no correlation was found between the surface area and the NO_x reduction performance; the R² value of the model was only 0.44, which is poor. Possibly, a weak tendency towards a decreased surface area for P and Mg could be observed. This is reasonable as these contaminants often contaminate the catalyst by fouling [130, 143, 196].

The total acidity of the lab-aged samples was also lower than that of fresh catalyst samples, as shown by the NH₃ desorption profiles in **Figure 43**. In this figure, the position of the peak(s) is an indication of the acid site strength, sites with stronger acidity release ammonia at higher temperatures than sites with weaker acidity. The area under the curve is related to the total number of acid sites, that is, the total acidity.

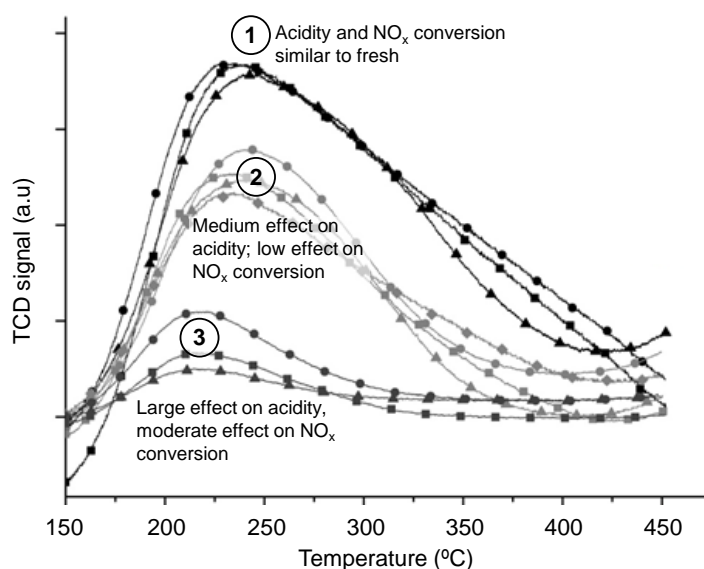


Figure 43: NH₃-TPD profiles of fresh and lab-aged catalyst samples together with the total acidity calculated from the profiles, and NO_x conversion at 300 °C (both acidity and conversion as % of fresh), total contaminant concentration. In the samples, the contaminants that are in a high contamination level are shown. Adapted from Paper I, Dahlin *et al.* Appl. Catal. B 183 (2016) 377 [191].

Based on the NH₃ desorption profiles, the lab-aged samples could be divided into three groups with respect to the effect on the acidity: (1) slight decrease - the

relative acidity is around 80%, (2) medium decrease - the relative acidity is around 50%, (3) considerable decrease, relative acidity of around 15%. For the samples with a large decrease in acidity, the peak maximum was also shifted to a lower temperature, indicating a decrease in acid strength for these samples. These samples also displayed the largest decrease in NO_x conversion (63-81% of that of fresh catalyst) while samples belonging to the other two groups had relative NO_x conversions in the range of 89-99%. Common to the samples with the largest effect on the acidity was that they had high levels of Na, K, and P. To determine whether there were actually any significant correlations between the total acidity, specific poisons and NO conversion, partial least square (PLS) regression was used. A correlation was found for Na and K, resulting in a Q²-value (corresponding to the R² value in the validated model) of 0.77, which is acceptable.

For the vehicle-aged catalyst, no (or very minor) effect on the fast SCR performance was observed, while a slight decrease in surface area and ammonia storage capacity was observed. The surface area and total ammonia storage was around 87-88%, and 84%, respectively, relative to that of a fresh catalyst.

To summarize, some important conclusions from this study are:

- The strongest poisons for the NO_x reduction performance during the fast SCR reaction for the V₂O₅-WO₃/TiO₂ catalyst are sodium and potassium. The decreased NO_x conversion is accompanied with a significant decrease in acidity for these contaminants.
- The interaction of Na and K with P also resulted in significant deactivation, although, alleviated compared to the effect of only the alkali metals. The interaction of sulfur with sodium, S*Na, on the other hand, results in a better NO_x conversion than the model mean.
- A deactivating effect was also seen for Mg, while no significant effect could be observed for Zn. P and S resulted in an improved NO_x reduction performance, compared to the mean value of the model.
- Although the surface area was decreased for all aged samples, no correlation to the NO_x reduction activity was obtained.

3. 3 The effect of SO₂ and engine-aging on the performance of Cu-SSZ-13 SCR catalyst (Paper III)

In this chapter, the effects of SO₂ on three different Cu-SSZ-13 and the V₂O₅-WO₃/TiO₂ catalyst are summarized. In addition, some results from an engine-aged Cu-SSZ-13 are included. The major part of this chapter is based on **Paper III**, although some additional results (not presented in **Paper III**) are included as well.

3.3.1 Effect of lab-scale SO₂-exposure

The poisoning effect of SO₂ on the SCR catalysts was investigated by exposing the catalysts to 50 ppm SO₂ for 8h in a bench-flow reactor (a total sulfur throughput of 34 g/dm³ SCR catalyst). The influence of the SO₂-exposure temperature was investigated for the Cu-SSZ-13 samples (mainly for Cat A1). For all samples, the standard, fast, and NO₂-rich SCR performance was tested at 220 and 280 °C, using Test Protocol 2. Furthermore, the effect of regeneration in a wet oxidizing atmosphere at two different temperatures, 500 and 700 °C was evaluated. The 500 °C-regeneration temperature was chosen as a realistic deSO_x temperature applicable during operation of a truck. The additional regeneration at 700 °C was included as a step in which total regeneration was expected [104, 127]. However, in real applications, this temperature would result in an excessive fuel penalty.

When a Cu-SSZ-13 catalyst is exposed to SO₂, sulfur accumulates on the catalyst, as indicated by the delayed detection of SO₂ (see **Figure 44**) in the outlet gas flow. This SO₂ uptake is rapid, as the major part of the uptake occurs within the first 1000-1500 s. After this, the uptake is slower, reaching a completely saturated catalyst takes a long time. These features have been shown previously by Hammershøi *et al.* [108], who also observed a rapid uptake in the beginning of the SO₂-exposure, followed by a continued slow accumulation of sulfur. In this study, small increase in S/Cu with increasing time was noted even after 60 h of SO₂-exposure [108].

The V₂O₅-WO₃/TiO₂ catalyst on the other hand, shows an insignificant SO₂ uptake, similar to an empty cordierite core, observed by the immediate breakthrough of SO₂. This was also confirmed by a TGA-MS analysis of the cordierite core, in which no mass loss related to sulfur was observed.

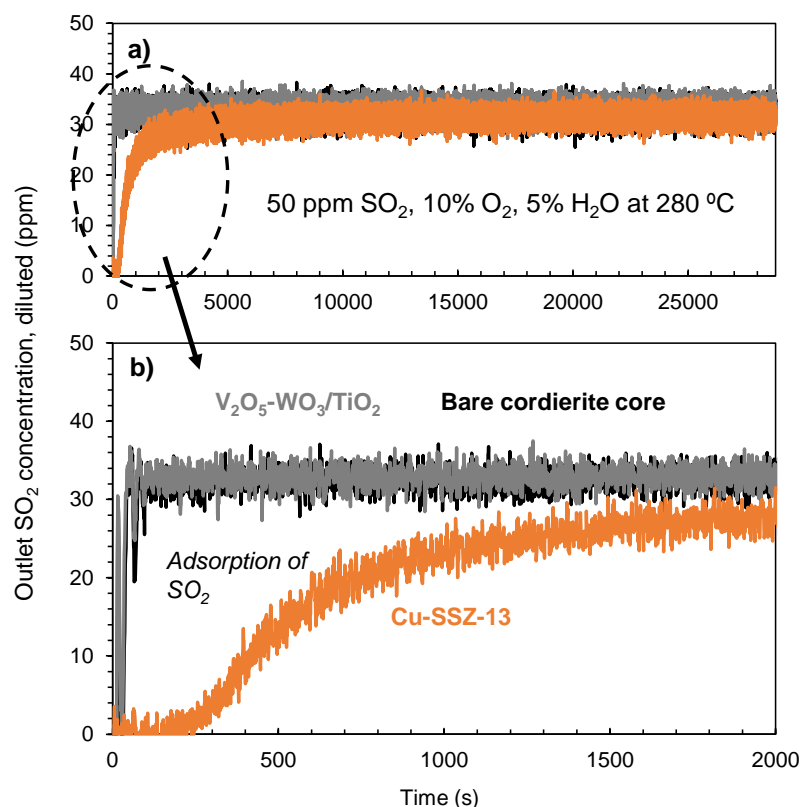


Figure 44: SO₂ outlet concentration during the 8 h SO₂-exposure of Cu-SSZ-13 (Cat A2), V₂O₅-WO₃/TiO₂, and a bare cordierite (no washcoat) core at 280 °C. The total flow is diluted prior to the FTIR analyzer to reach a flow of 20 dm³/min. Therefore, the concentration of SO₂ after saturation is lower than 50 ppm.

The effect of this SO₂-exposure on the performance of all SCR catalysts investigated in my PhD project is shown in **Figure 45**, as the relative rate constant at 220 °C for the standard SCR reaction. This constant is defined as the rate constant of the SO₂-exposed catalyst divided by that of the fresh catalyst; by this division it simplifies to be dependent only on the NO conversion (X) for the sample (assuming a first order reaction w.r.t. NO, and zero order w.r.t. NH₃):

$$k_{aged}/k_{fresh} = \ln(1-X_{aged})/\ln(1-X_{fresh}).$$

All Cu-SSZ-13 catalysts experience a severe drop in NO reduction performance, as the rate constant is only 10-25% of that of the corresponding fresh catalyst. As opposed to the Cu-zeolites, the vanadium-based catalyst instead becomes promoted by the SO₂-exposure. A positive effect of sulfur was also observed in **Paper I**, although this contamination was done with wet impregnation and only the fast SCR reaction was studied. Studies by others have also shown that SO₂ can promote the SCR reaction, especially at low temperature [141]. This effect could be explained by enhancement of both the number and strength of acid sites on the catalyst by SO₂-exposure [141, 197].

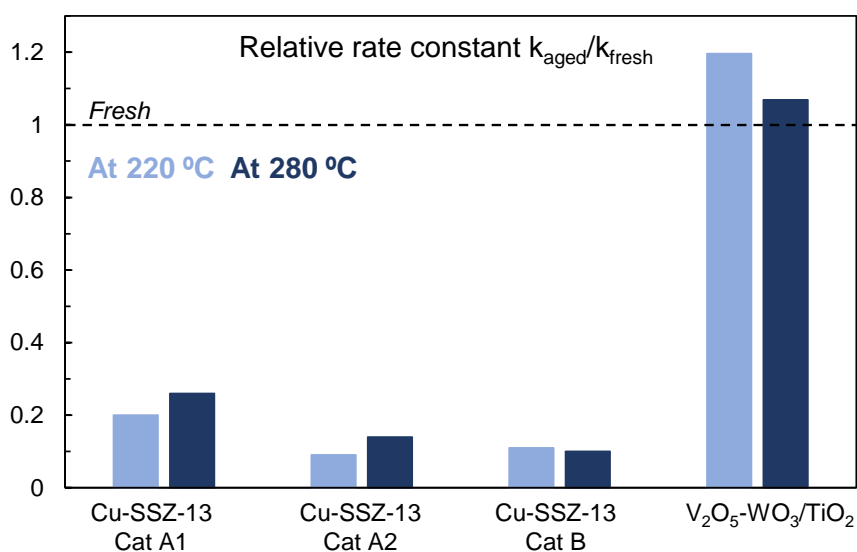


Figure 45: Relative rate constant of the standard SCR reaction for the three different Cu-zeolites and the vanadium-based SCR catalyst after SO₂-exposure (50 ppm for 8 h at 280 °C). Inlet gas concentrations: 1000 ppm NO, 1000 ppm NH₃, 10% O₂, 5% H₂O during; GHSV: 120,000 h⁻¹; test temperatures: 220 and 280 °C.

Although the performance of all the Cu-zeolites decreased upon sulfur exposure, some differences are observed between the samples. For example, Cat A2, which shows the best fresh performance, and Cat B is approximately twice as deactivated as Cat A1, which has the poorest performance when fresh. These differences become even more pronounced when the effect of sulfation temperature is investigated (**Figure 46**). For Cat A1, there is a clear dependence on the SO₂-exposure temperature: a lower exposure temperature results in a higher degree of deactivation, especially for the samples aged at 350 and 400 °C, for which the relative rate constants only decrease to around 0.4 and 0.65, respectively. For both Cat A2 and Cat B, on the other hand, the differences in the relative rate constant related to exposure-temperature are significantly smaller: for Cat A2, an aging at 400 °C results in a relative rate constant (220 °C) of around 0.14 compared to 0.09 when the SO₂-exposure temperature is 280 °C, and for Cat B the difference is even lower, 0.12 and 0.11 at aging temperatures of 400 and 280 °C, respectively. In previous studies performed by others, different results regarding sulfur-exposure temperature, both increased and decreased NO reduction performances with increasing temperature have been reported [108, 198].

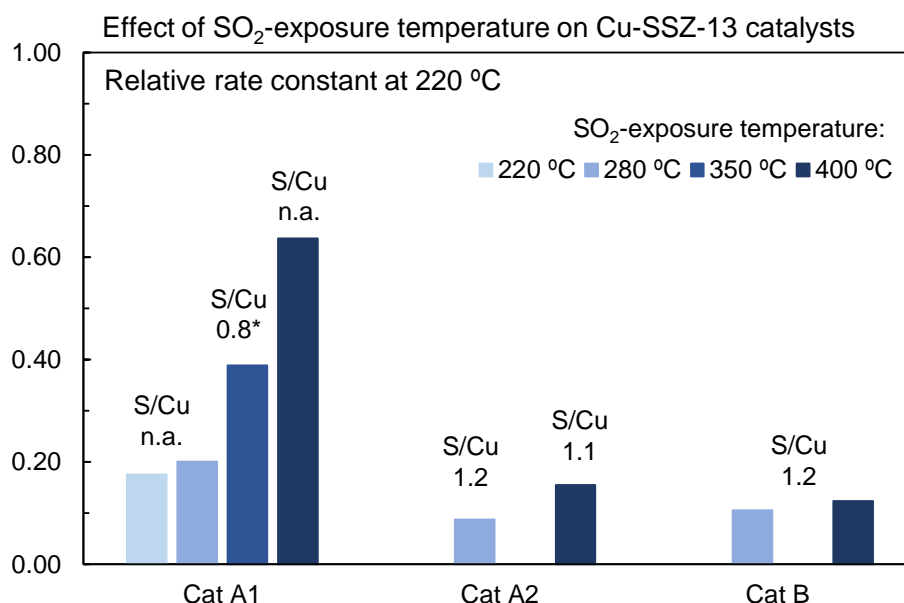


Figure 46: Relative rate constant at 220 °C for Cu-SSZ-13 samples (Cat A1, Cat A2, Cat B) exposed to SO₂ at different temperatures (220, 280, 350, and 400 °C. Cat A2 and B were exposed to SO₂ only at 280 and 400 °C. Molar S/Cu ratios after each experiment are indicated. SO₂-exposure: 50 ppm SO₂, 8 h, 10% O₂, 5% H₂O, GHSV 60,000 h⁻¹. SCR test: 1000 ppm NO, 1000 ppm NH₃, 10% O₂, 5% H₂O, GHSV 120,000 h⁻¹.

The deactivation due to SO₂ can be partially to completely reversed by exposing the Cu-zeolite to elevated temperatures, see Figure 47. Exposing the catalyst to an oxidizing stream, with water vapor present, at a temperature of 500 °C results in an increase in the relative rate constant (220 °C) from around 0.1-0.20% to around 0.65-0.85, while it increases further to 0.9-1.0 after additional regeneration at 700 °C. Again, some differences are observed between the different catalysts, with Cat A2 and Cat B appearing to be slightly harder to regenerate. Regenerating Cat A2 at 500 °C results in an increase in the relative rate constant from 0.09 to 0.75 at 220 °C, and from 0.14 to 0.85 at 280 °C. The S/Cu decreases correspondingly from 1.2 to 0.32. The same trends as stated above apply also for the relative rate constant at 280 °C, although the rate constant is generally slightly higher at this temperature compared to at 220 °C. For example, after regeneration at 700 °C, the rate constant at 280 °C for all Cat A1 samples has the same value as that of the fresh catalysts. The S/Cu in these samples after regeneration at 700 °C is 0.07-0.10, according to XRF analyses.

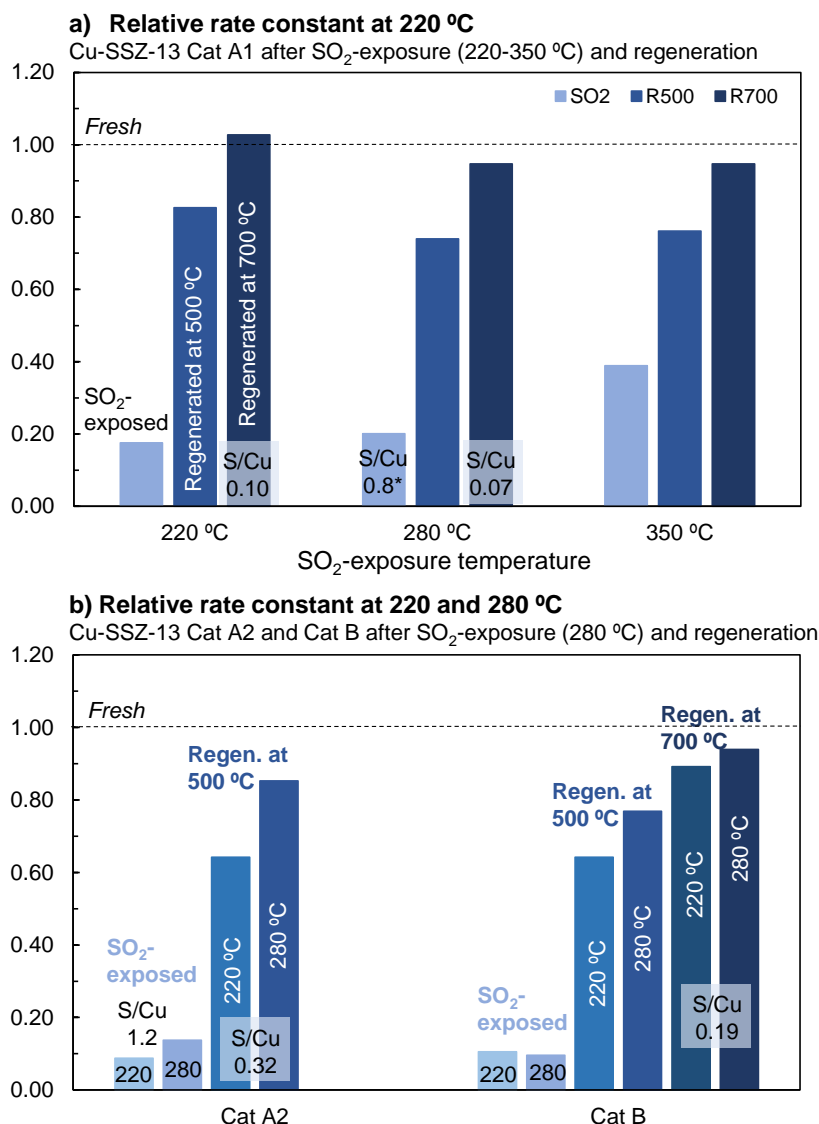


Figure 47: Effect of regeneration (500 and 700 °C in presence of O₂ and H₂O) of SO₂-exposed (50 ppm, 8h) Cu-SSZ-13 catalyst samples expressed as the relative rate constant during the standard SCR reaction: a) Cat A1 sulfated at different temperatures; b) Cat A2 and B sulfated at 280 °C, S/Cu for sulfated and regenerated Cat A2 indicated in the graph. Test conditions: during all steps 10% O₂, 5% H₂O; 1000 ppm NO, 1000 ppm NH₃, GHSV 120,000 h⁻¹, 220 and 280 °C during SCR test. * this S/Cu was done for a catalyst sulfur-exposed without prior SCR test.

We also investigated the effect of NO₂/NO_x ratio on the NO_x reduction performance of SO₂-exposed SCR catalysts. As an example, the outlet concentrations of the reactants, NO_x, and NH₃, and the unwanted by-product, N₂O, during the standard, fast, and NO₂-rich SCR reactions at 220 °C are displayed in **Figure 48**. Comparing the region of standard SCR with that of fast SCR, it is evident that adding NO₂ to the feed relieves the poisoning effect, as the outlet concentration of NO_x and NH₃ are much closer to those of the fresh catalyst.

Increasing the NO₂ concentration further, to NO₂/NO_x = 0.75, the overall performance became worse than for standard SCR, as the NO_x and NH₃ conversion is rather similar to those under standard SCR but the amount of N₂O produced is

higher. The effects of NO_2 are summarized in **Figure 49** which shows the NO_x conversion and N_2O production at 280 °C during standard, fast, and NO_2 -rich SCR for fresh, SO_2 -poisoned, and regenerated (500 °C) catalyst.

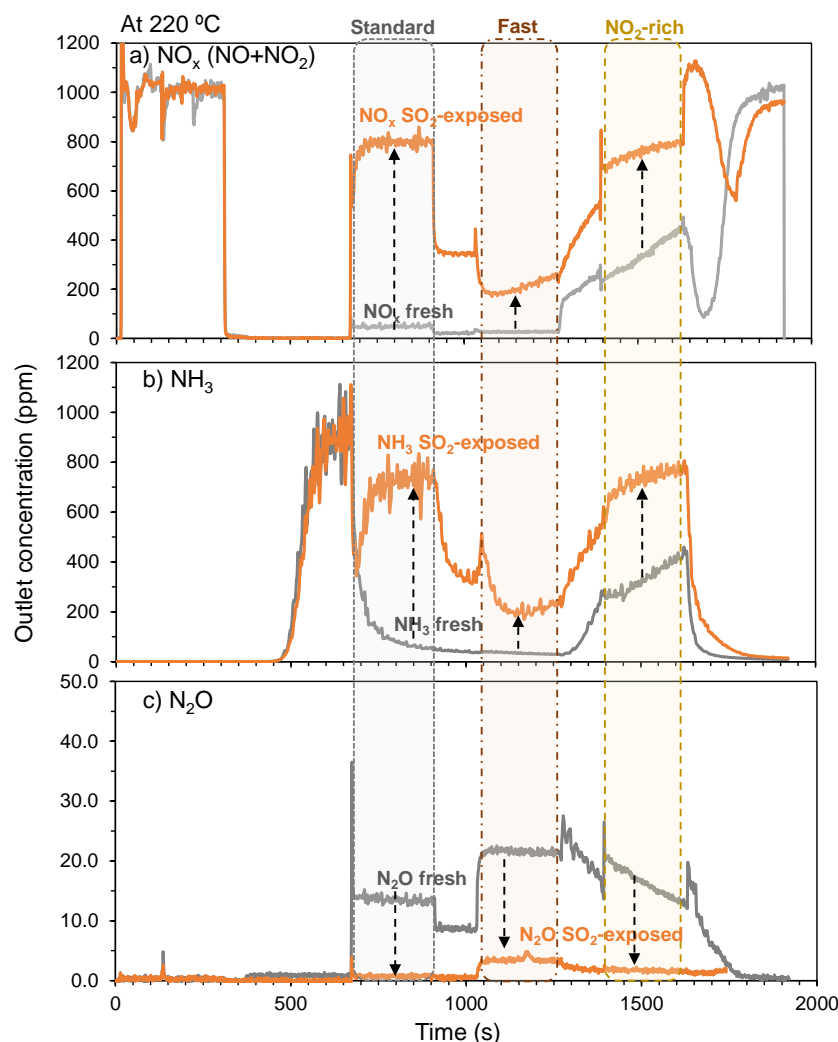


Figure 48: Outlet concentration of NO , NO_2 , NH_3 , and N_2O during SCR performance test of fresh and SO_2 -exposed Cu-SSZ-13 (Cat A2) at 220 °C. Higher outlet concentrations of reactants are observed after SO_2 -exposure, as well as decreased concentrations of the by-product N_2O . Inlet gas concentrations: 1000 ppm NO_x ($\text{NO}_2/\text{NO}_x=0, 0.5$ or 0.75), 1000 ppm NH_3 , 10% O_2 , 5% H_2O during. GHSV 120,000 h^{-1} .

It is interesting to note that the N_2O formation is suppressed by the SO_2 -exposure, and that this effect is larger than the effect on NO_x reduction. Almost no N_2O forms during the standard SCR reaction, and the amount of N_2O formed during the fast SCR reaction is considerably lower than what is produced for the fresh catalyst, although the NO_x conversion is almost the same as for the fresh one. The same applies after regeneration at 500 °C, and is applicable to all the Cu-SSZ-13 samples investigated here. For the NO_2 -rich SCR reaction however, there are some differences among the catalysts. While the same trend as stated above is true for

Cat A1, both Cat A2 and Cat B show an increase in N_2O formation at 280 °C, compared to fresh catalyst, after regeneration. Regeneration at 500 °C results in a similar, or slightly larger value than for fresh, while regeneration at 700 °C results in a considerable increase – from around 53 ppm N_2O for the fresh catalyst to around 84 ppm N_2O for the regenerated catalyst. It is thus likely that some of the copper species are transformed into other types of copper species during the regeneration. At 220 °C steady-state was not reached during the NO_2 -rich SCR reaction, for neither fresh nor poisoned or regenerated catalyst samples, which makes it difficult to draw conclusions about the effect at this temperature.

An explanation for the enhancing effect of NO_2 on the NO_x reduction performance of SO_2 -poisoned Cu-SSZ-13 catalysts might be that the fast reaction does not require two active Cu sites for the re-oxidation of the copper from Cu^+ to Cu^{2+} , as opposed to what is considered to be required for the standard SCR reaction at low temperature [95, 96].

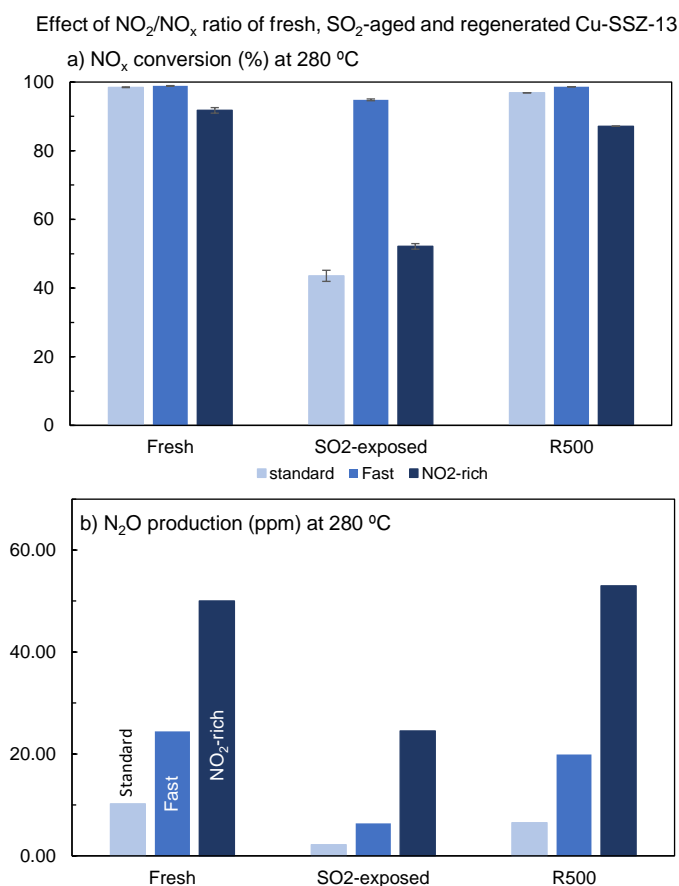


Figure 49: Effect of NO_2/NO_x ratio on NO_x reduction performance of Cu-SSZ-13 (Cat A2) - fresh, SO_2 -aged and after regeneration at 500 °C: a) NO_x conversion and b) N_2O production at 280 °C. Test conditions: 1000 ppm NO_x ($\text{NO}_2/\text{NO}_x=0, 0.5, 0.75$), 1000 ppm NH_3 , 10% O_2 , 10% H_2O , GHSV 120,000 h^{-1} . Applying fast SCR conditions at 280 °C on an SO_2 -deactivated catalyst results in a NO_x conversion close to fresh catalyst.

The effect of SO₂-exposure of NH₃ storage capacity at 220 °C depends on the sulfur-exposure temperature (see **Figure 50**), while no effect is observed on the ammonia storage capacity at 280 °C. For Cu-SSZ-13 Cat A1 samples exposed to SO₂ at 220 and 280 °C, the ammonia adsorption capacity at 220 °C appears to be slightly decreased, as indicated by the slightly earlier breakthrough of ammonia for these samples. Upon regeneration at 500 °C, the NH₃ storage increases, as indicated by the later breakthrough of ammonia. Additional regeneration at 700 °C does not induce any further difference in the NH₃ profile.

A more significant effect is observed for all Cu-SSZ-13 samples aged at higher temperatures, 350 and 400 °C. For these samples, the NH₃ storage capacity is instead considerably increased as compared to the fresh catalyst. This increase is larger for the higher exposure-temperature. After regeneration, this capacity decreases significantly; however, it is still larger than for the fresh catalyst.

The observations regarding the ammonia storage indicate that different S-species form on the catalyst depending on the temperature, and furthermore that these species might transform from one type to another upon a change in condition, such as temperature.

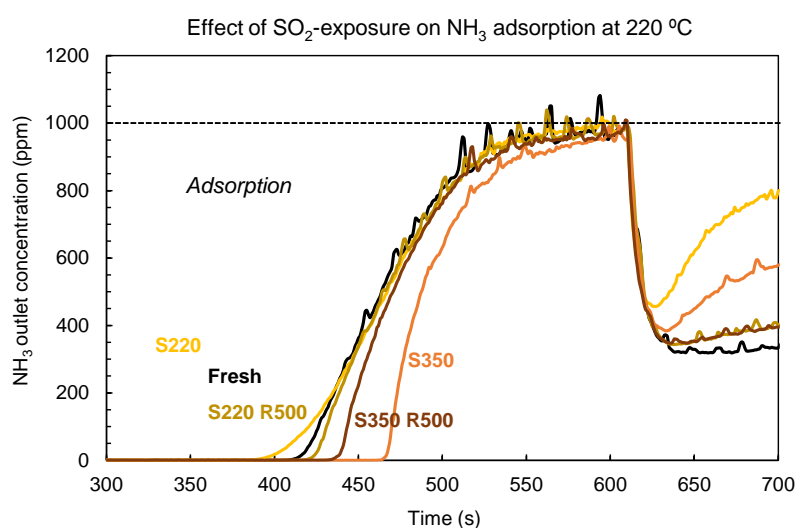


Figure 50: Outlet NH₃ concentration during the NH₃ storage step at 220 °C for Cu-SSZ-13 Cat A1 after sulfation at different temperatures (220 and 350 °C) and after regeneration at 500 °C. Test conditions: 1000 ppm NH₃, 10% O₂, 5% H₂O, GHSV 120,000 h⁻¹.

3.3.2 Effect of engine-aging

The performance of a Cu-SSZ-13 catalyst (Cat B) from a 500-h test in an engine-cell was tested with the same protocol as used for the SO₂-exposed samples. A ULSD fuel with a sulfur content of 5 ppm S, and a Euro V emission control system with only an SCR catalyst was used during this engine-test. The maximum exhaust temperature reached during the test was around 530 °C, which means that

hydrothermal aging effects should be rather low. To note though, is that the average temperature during the engine-test was higher than normal.

As shown by the decreased rate constant in **Figure 51**, the catalyst became deactivated during the engine-test. At 220 and 280 °C, the relative rate constant is only around 0.28 and 0.4, respectively.

Regeneration at 500 and 700 °C resulted in small, progressive improvements in the NO conversion, to reach a maximum relative rate constant of around 0.40 and 0.60 at 220 and 280 °C, respectively. After the regeneration at 700 °C, a small amount of the sulfur present in the catalyst had been removed.

The N₂O formation at 220 °C is as for the SO₂-exposed catalyst lower than for the fresh catalyst (**Figure 51b**), although this effect is smaller than for the SO₂-poisoned samples. However, contrary to the SO₂-poisoned samples, the N₂O production of the engine-aged sample at 280 °C was increased by around 20% compared to the fresh sample. Regeneration of the engine-aged catalyst causes this N₂O production to increase even further: after regeneration at 700 °C, the amount of N₂O formed is almost doubled compared to for fresh, 19 and 10 ppm N₂O for the engine-aged and the fresh catalyst, respectively, during the SCR reaction.

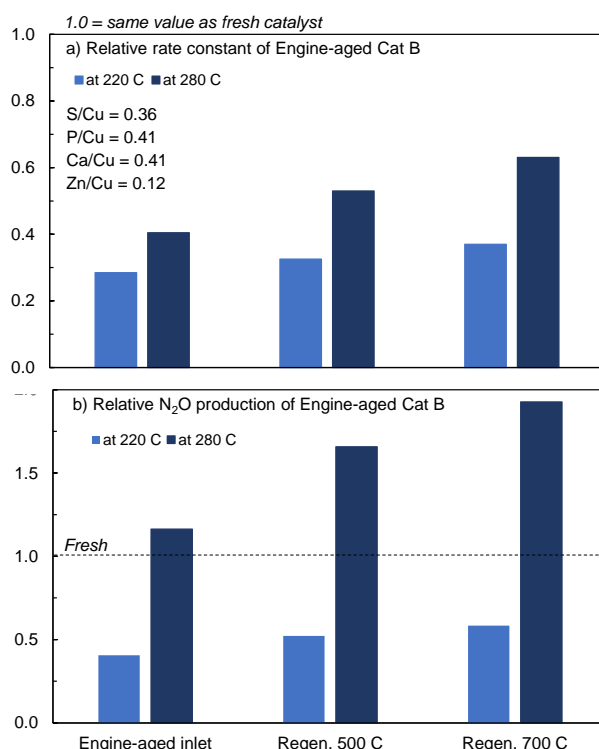


Figure 51: SCR performance of a catalyst core from the inlet part of an engine-aged catalyst (Cu-SSZ-13 Cat B) expressed as: a) the relative rate constant ($k_{\text{aged}}/k_{\text{fresh}}$), and b) the relative N₂O production (concentration of N₂O produced for aged catalyst divided by that of fresh) at 220 and 280 °C. Test conditions: standard SCR reaction, 1000 ppm NO, 1000 ppm NH₃, 10% O₂, 5% H₂O, GHSV 120,000 h⁻¹. Contaminant concentrations (molar ratios) for the engine-aged catalyst is are indicated.

As for the SO₂-exposed samples, the NO_x reduction performance in the presence of fast SCR conditions is significantly higher than under standard SCR conditions (see **Figure 52**). However, as opposed to the SO₂-poisoned catalysts, the N₂O formation during the fast SCR reaction is higher for the engine-aged catalyst than for the fresh. Another difference compared to the SO₂-exposed samples is the ammonia storage capacity, which is significantly decreased at both 220 and 280 °C for the engine-aged catalyst.

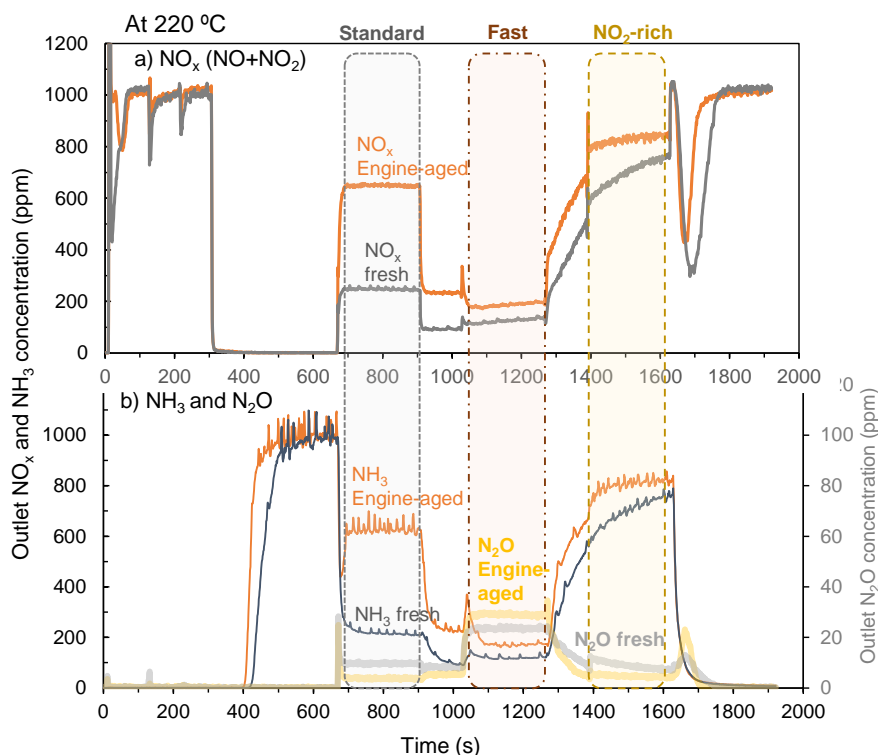


Figure 52: Outlet concentration of NO_x, NH₃, and N₂O during SCR performance test of fresh and engine-aged Cu-SSZ-13 (Cat B) at 220 °C. Higher outlet concentrations of reactants are observed for the engine-aged sample implies deactivation. Inlet gas concentrations: 1000 ppm NO_x (NO₂/NO_x=0, 0.5 or 0.75), 1000 ppm NH₃, 10% O₂, 5% H₂O during. GHSV 120,000 h⁻¹.

XRF analysis of the engine-aged catalyst shows the presence of P, Ca, and S: 0.15, 0.20, and 0.11 wt%, respectively, in the inlet part. Higher concentrations of P and Ca were detected in the inlet part of the catalyst compared to the outlet part. During the regeneration, a part of the sulfur was desorbed as the sulfur concentration decreased to 0.08 wt% after the regeneration at 700 °C.

The presence of these contaminants might be a reason, or a part of the reason, for the decreased performance of the engine-aged catalyst. However, hydrothermal effects might also be a part of the deactivation, especially since the N₂O formation is increased and the NH₃-storage capacity is decreased for this catalyst.

In summary, the following conclusions can be made from the investigation on the effect of SO₂- and engine-aging:

- SO₂ severely affects the low-temperature NO_x reduction performance of Cu-SSZ-13 catalysts, although, the exact effect varies between different samples.
- As opposed to Cu-SSZ-13, the performance of the VWTi catalyst increases by sulfur exposure.
- The standard SCR reaction is most affected – adding NO₂ to the feed to reach fast SCR conditions significantly increases the performance of an SO₂-poisoned Cu-SSZ-13 catalyst.
- Partial to full regeneration is possible by exposing the catalyst to a humid oxidizing flow at 500 and 700 °C.
- The N₂O formation is suppressed by SO₂-exposure, especially during the standard and the fast SCR reaction. For the NO₂-rich SCR condition, differences between the Cu-zeolites are observed.
- For the engine-aged catalyst, only a small is part related to sulfur (reversible), other contaminants and probably also hydrothermal aging are responsible as well.

A summary of the effect of SO₂-exposure on the relative rate constant in relation to the measured S/Cu ratio in the catalyst sample is shown in **Figure 53**. Note that the data provided in this figure are based on all three Cu-zeolites for which S/Cu data were available. Also, for several samples, mainly Cu-SSZ-13 Cat A1, no Cu/S data are available.

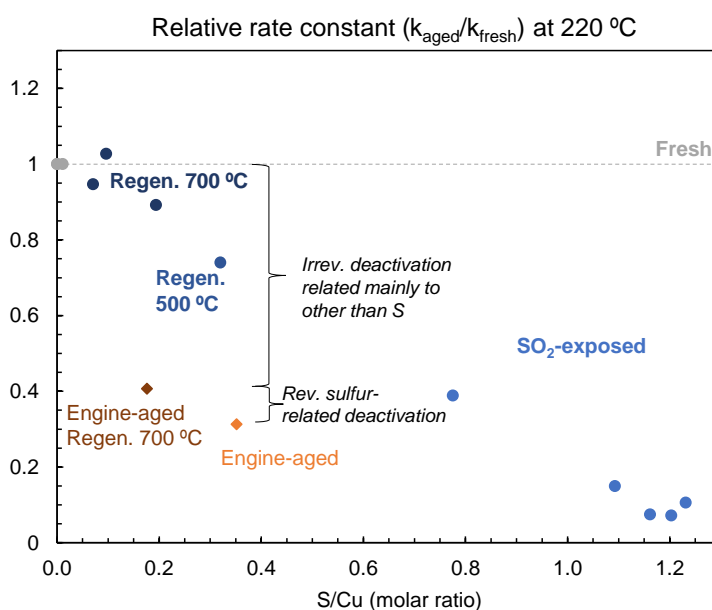


Figure 53: Relative rate constant at 220 °C as function of the measured S/Cu (mol/mol) for all SO₂-exposed, engine-aged and regenerated Cu-SSZ-13 samples (Cat A1, A2, B) for which elemental analysis data are available. Conditions during SCR test: standard SCR, 1000 ppm NO, 1000 ppm NH₃, 10% O₂, 5% H₂O, GHSV 120,000 h⁻¹.

3.4 Copper sites and oxidation and reduction behavior of fresh and SO₂-poisoned Cu-SSZ-13 catalyst by in-situ synchrotron XAS (Paper IV)

Exposing Cu-SSZ-13 catalysts to SO₂ results in a considerable decrease in their low-temperature NO_x reduction performance. However, the NO_x reduction at higher temperatures is only slightly affected or not affected at all; also, under fast SCR conditions the poisoning effect is significantly less pronounced. It is furthermore possible to regenerate the catalyst by exposing it to elevated temperatures.

To understand the nature of these effects, copper species in a fresh and an SO₂-poisoned Cu-SSZ-13 catalyst (Cat A1) were investigated using in-situ Cu K-edge XAS. These experiments were done in a temperature range from room temperature to 400 °C, in oxidizing and reducing atmosphere (20% O₂/N₂ and 5% H₂/He, respectively). TGA-MS was used to determine the sulfur content in the as-received Cu-zeolite, and after it had been exposed to different gas atmospheres during the XAS experiment. XAS is a technique that gives the average result of all Cu-species that exist in the analyzed sample, and provides information about coordination environment and oxidation states. As a compliment to the XAS experiment, additional characterization was performed with STEM and H₂-TPR (fresh catalyst only). A multivariate curve resolution alternating least squares (MCR-ALS) approach was used to evaluate the XAS data, and was compared to reference spectra of Cu-species obtained by DFT-assisted XANES calculations. In addition to the analysis of the XANES data, a part of the EXAFS data was analyzed using continuous Cauchy wavelet transforms (CCWT). This analysis can be used to enhance the sensitivity to the nuclearity of Cu-oxo species in Cu-zeolites, which otherwise could be difficult to differentiate [199].

Based on the TEM-images of the fresh Cu-SSZ-13, it is likely that this sample, in addition to exchanged Cu ions also contain CuO_x nanoparticles, as indicated by black dots (**Figure 54**). Particles with similar structures have previously been assigned to such clusters in studies performed by others [188, 200, 201]. These CuO_x clusters might be a reason for the inferior performance of the fresh Cat A1 compared to the fresh Cat B and Cat A2. The SO₂-poisoned catalyst also contained similar clusters/particles.

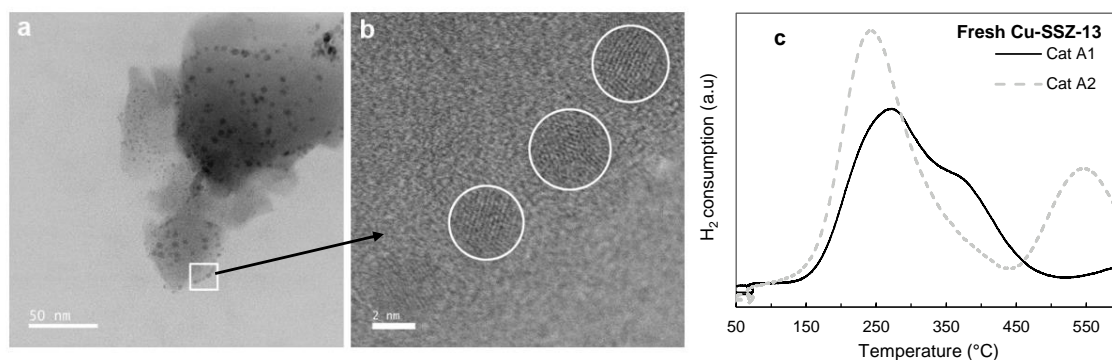


Figure 54: STEM images and H₂-TPR profile for the fresh Cu-SSZ-13 Cat A1. The H₂-TPR was conducted from 50 to 600 °C with 10% H₂ and a heating rate of 10 °C/min, after an in-situ pre-treatment step with 2.5% O₂/He 1 h at 400 °C. The profile of Cat A2 is shown for comparison.

The H₂-TPR profile of the dehydrated fresh Cu-SSZ-13 sample has two clear peaks at temperatures below 500 °C (see **Figure 54**). This shows that there are at least two Cu species with different reducibility in the catalyst, likely corresponding to ZCuOH and Z₂Cu, where the former is easier to reduce than the latter. Previous studies on well-defined Cu-SSZ-13 catalysts, for example with different Si/Al and Cu/Al ratios, have shown that Cu²⁺ in ZCuOH (or in CHA) reduce to Cu⁺ at around 230-280 °C, while Cu²⁺ in the less reducible Z₂Cu (or in the d6r) reduce to Cu⁺ at temperatures around 310-410 °C [111, 121, 123, 174, 202, 203]. The reduction temperatures depend on the experimental conditions. Although only two peaks can easily be observed in the profile, the H₂-consumption profile might as well be constructed by additional Cu species with reducibility in similar range as for the species stated above. For example, it is likely that CuO_x nanoclusters, as observed by STEM, contribute to the H₂ consumption. In previous studies, CuO_x nanoclusters have been shown to reduce at temperatures between around 210 and 300 °C [118, 200, 201, 204], with differences in reducibility depending on the size of these clusters [204].

The XAS spectra of fresh and SO₂-poisoned catalyst samples change with temperature and gas atmospheres, as shown in **Figure 55**. Analyzing all these spectra by MCR-ALS resulted in the pure components displayed in **Figure 56**. In this figure it is seen that some of the pure spectra in fresh and SO₂-poisoned catalysts are rather similar, while other are quite different from each other. Especially spectra F1 and P1 look similar, but also F2 and P2 appear quite similar. In contrast, large differences are observed for other spectra, e.g. F3, P3, and F5, P5.

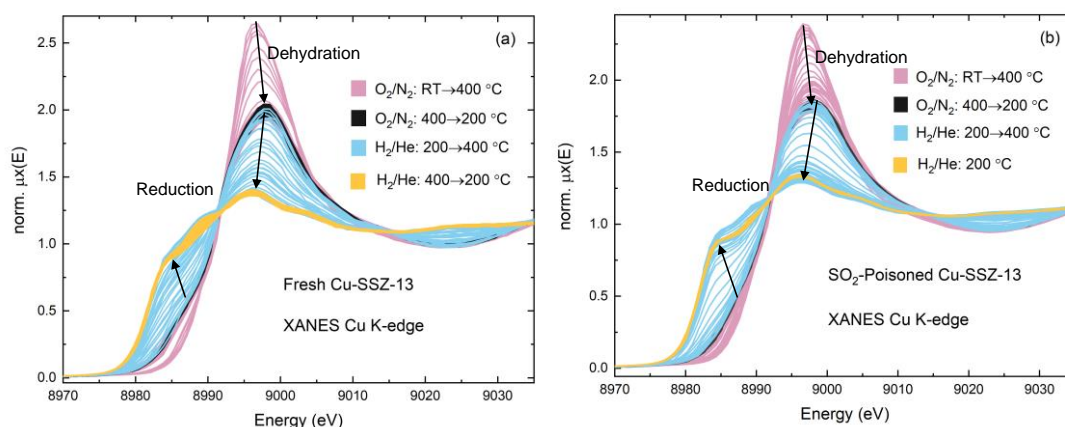


Figure 55: All XAS spectra of fresh (a) and SO₂-poisoned (b) Cu-SSZ-13 Cat A1 at temperatures between room temperature (RT) and 400 °C in oxidizing (20% O₂/N₂) and reducing atmospheres (5% H₂/He)

The change in concentration of the various components in fresh and SO₂-poisoned catalysts with time along with a comparison of the experimental spectra with theoretical XANES spectra (see **Paper IV**), is discussed below.

Oxidizing atmosphere (O₂/N₂, RT → 400 °C → 200 °C)

The spectra of F1 and P1 in fresh and poisoned catalyst, respectively, are both similar to the spectra of hydrated [Cu(H₂O)₆]²⁺. In this state, the Cu²⁺ ions are solvated by water molecules and only weakly coordinated to the zeolite framework [98, 178, 205]. The calculated XANES spectra of [Cu(H₂O)₆]²⁺ agrees well with the experimental result. The concentration of these components is highest in the beginning of the experiment (see **Paper IV**), which starts at room temperature with an oxidized, hydrated Cu-SSZ-13 sample. It then rapidly decreases with increasing temperature in O₂/N₂ atmosphere, as dehydration of the copper ions occurs. This dehydration process is evident by the decrease in intensity and broadening of the white line (the “peak” with the highest intensity) in the XAS spectra in **Figure 55**.

As the concentration of hydrated Cu²⁺ species (F1, P1) decreases, an increase in component F6 and P6 occurs. The concentration profiles with time are rather similar for fresh and poisoned catalyst, but differences in the spectra are observed. The concentration of components F6 and P6 reaches a maximum after about one quarter of the heating time in O₂/N₂. After that, it smoothly decreases until the end of heating; however, even at high temperatures in O₂/N₂, the concentration of this component is around 10-15%. These spectra are thus likely represented by dehydration intermediates, but may also be related to CuO_x, which would be supported by the STEM results. The Cu K-edge XANES spectra of CuO_x nanoparticles have smeared spectral fine structure features, as compared to bulk CuO, and could thus be rather similar to the spectra of the dehydration intermediates. This spectroscopic difference compared to bulk CuO originates from

differences in the surface-to-volume ratios [206], and absence of long-range order in the nanoparticles [206-208]. Based on similarities in the concentration profiles of component F6 and P6, but differences in the spectra, P6 likely corresponds to dehydration intermediates of sulfur-poisoned Cu^{2+} species.

As water molecules are removed from the copper ions during the dehydration process, the Cu^{2+} ions instead become coordinated to the zeolite framework and the coordination symmetry of these ions decrease. The spectra of the dehydrated, oxidized catalyst samples are shown as the black curves in **Figure 55**. In an oxidizing atmosphere these Cu^{2+} species are likely present as $\text{Z}_2\text{Cu(II)}$, ZCu(II)OH , and/or ZCu(II)-O_2 , in fresh Cu-SSZ-13. According to the concentration profile, components F3 and F4 fit with these species; as the concentration of component F3 starts to decrease at an earlier stage, i.e. a lower temperature, during the reduction part (H_2/He), this component is assigned to ZCu(II)OH (and/or ZCu(II)-O_2) as this specie is easier to reduce. Consequently, F4 is assigned to the more stable Z_2Cu .

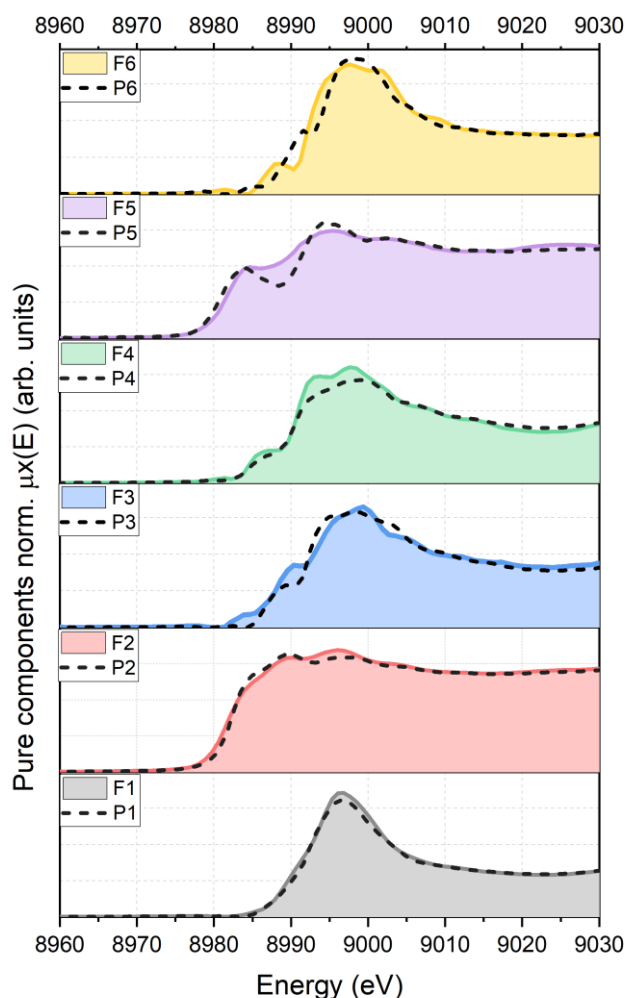


Figure 56: Pure components from the MCR-ALS analyses of the full set of spectra in oxidizing and reducing atmospheres at temperatures between room temperature and 400 °C. F (e.g. F1) indicates fresh catalyst; P (e.g. P1) indicate SO_2 -poisoned catalyst.

Significant spectral differences were observed for the components F3 and P3. Recently it has been shown that ZCuOH sites are more sensitive to SO_x poisoning than are Z₂Cu sites [111, 122, 126]. In our analysis of the spectral data of sulfur-poisoned catalyst, we therefore excluded the ZCuOH and replaced with ZH-Cu(HSO₄)₂ species. Based on our DFT calculations of several suggested Cu-S structures, these species were the thermodynamically most favored. This is also in agreement with a previous study by Shih et al. [122]. In addition, some spectral differences were also observed for component P4 compared to F4. This could thus be an indication that also these sites can be poisoned. Therefore, we also considered sulfur-poisoned Z₂Cu sites as Z₂H₂Cu(HSO₄)₂ species.

Reducing atmosphere (H₂/He, 200 °C → 400 °C → RT)

As the oxidizing gas mixture is replaced by a reducing gas mixture, substantial changes in the spectra occur (see **Figure 55**, blue curves) and reveal significant differences between spectra of fresh and poisoned samples.

In the fresh catalyst, a rapid increase in component F2 was observed upon heating in H₂/He, concurrent with a decrease in concentration of components F3 and F4. Component F2 is thus assigned to Cu⁺ in ZCu, which originates from reduction of ZCu(II)OH (and/or ZCu(II)-O₂) species). Z₂Cu sites also reduce, but at a higher temperature, to ZCu(I)/ZH. Calculated XANES spectra of these Cu⁺ species suggest that component F2 could include both of these species, as their spectra are similar.

The spectra of component P2 in the SO₂-poisoned sample looks similar to the spectra of F2 in the fresh catalyst, and is thus likely related to ZCu and/or ZCu/ZH. However, the concentration profiles of component P2 and F2 are different. Especially, the concentration of component P2 (i.e. ZCu) is significantly lower for the poisoned catalyst sample in the end part of the heating in H₂/He (holding at 400 °C). This is consistent with part of the Cu species being poisoned by sulfur, not being able to form ZCu or ZCu/ZH during this heating.

For the poisoned sample, component P5 also appear upon heating in H₂/He, already in the first half of this step. In contrast, this is not the case for component F5 in the fresh sample; the concentration of this component increases only upon cooling from 400 to 200 °C in H₂/He. Comparing the spectra of fresh and poisoned samples during the heating in H₂/He, we noted a more rapid increase in intensity in the region of 8983 eV for the poisoned sample, compared to the fresh sample. The presence of features in this region is an indication of Cu⁺. However, the spectral pre-edge features (intensity and position) of Cu⁺ species are very sensitive to the coordination environment and geometry [179, 209]. Linear two-fold coordinated Cu⁺ complexes have a sharp peak in the region of 8983-8984 eV, while three- and four-fold coordinated Cu⁺ species show less intense features. [179, 209] A distortion from the ideal linear 2-fold coordinated structure, which has an angle

of 180°, results in a decreased intensity of this pre-edge feature [209]. We therefore propose that the high intensity of the pre-edge peak in the SO₂-poisoned catalyst is due to formation of quasilinear Cu⁺-SO_x complexes. Consequently, component P5 in the SO₂-poisoned catalyst is assigned to such a quasi-linear Cu⁺ complex. This specie might be formed from the reduction of Cu-bisulfate species. According to H₂-TPR data performed by others [187, 203, 210], reduction of dispersed copper sulfate species occurs at around 230-270 °C, which agrees with the rapid increase in intensity at 8983 eV in the XANES data for the poisoned sample during the first part of heating in H₂/He. In the middle part of the heating in H₂/He, the concentration of component P5 first becomes constant, and then slightly decreases. This could be associated with the release of SO₂ from this component, liberating some of the Cu ions from the sulfur-poisoning. This agrees with the TGA-MS results, which showed that some sulfur had been removed from the catalyst during the in-situ XAS experiment.

Component F5 in the fresh catalyst, on the other hand, is not related to quasilinear Cu⁺ complexes, but could be related to Cu₂O and/or metallic Cu. Using the CCWT approach showed formation of a significant amount of metallic Cu in the fresh sample, while this effect was substantially lower in the SO₂-poisoned sample. Component F5 was therefore assigned to metallic Cu, although some contributions from Cu₂O cannot be excluded.

Based on the time-temperature-atmosphere dependent concentrations of different components in fresh and SO₂-poisoned catalyst, the following was concluded:

- Besides exchanged Cu ions, copper exists also as CuO_x nanoparticles in the investigated Cu-SSZ-13 catalyst (Cat A1).
- The SO₂-poisoned catalyst contains both Cu-species that are similar to, and Cu-species that are significantly different than, those in the fresh sample.
- The response of the Cu-species in fresh and poisoned samples to various conditions differs, especially to a reducing atmosphere.
- Differences in reducibility are related to the formation of quasi-linear complexes in the SO₂-poisoned catalyst formed during heating in H₂/He, while no such complex is formed in the fresh catalyst.
- Heating in H₂/He to 400 °C leads to partial removal of sulfur from the catalyst, as confirmed by TGA-MS, and corresponds to a regeneration of parts of the sulfur-poisoned Cu-ions.
- The CCWT analysis showed that cooling in H₂/He after heating to 400 °C leads to formation of Cu-metal clusters, which are more easily formed in the fresh catalyst than in the SO₂-poisoned. This could be an indication of Cu species in the fresh catalyst being more mobile than those in the poisoned catalyst.

3.5 The effect of phosphorus and sulfur in biodiesel exhaust on Cu-SSZ-13 and V₂O₅-WO₃/TiO₂ SCR catalysts (Paper V)

In this chapter the aging experiments are a step closer to real conditions as the catalysts were exposed to real biodiesel exhausts, generated by a diesel burner. Four different aging experiments were performed: one with pure biodiesel, and the other three with either phosphorus-, sulfur-, or phosphorus- plus sulfur-doped biodiesel. The average temperature during the aging experiments was around 450 °C. The aging with pure biodiesel served as a baseline aging while the experiments with only phosphorus or sulfur was targeting a full lifetime exposure of the catalysts to phosphorus and sulfur, respectively. In the fourth aging with both P and S added to the fuel, the concentration of the contaminants corresponded to approximately 1/10th of a lifetime. During the aging experiments, the SCR catalysts were aged in two different configurations, either with an upstream DOC, or with an upstream dummy (empty cordierite core).

3.5.1 Aging effects on the V₂O₅-WO₃/TiO₂ catalyst

The different aging experiments resulted in different effects on the VWTi catalyst – from a promoting effect to a severely deactivating effect (see **Figure 57**). The most noticeable effect is observed for exposure to the exhausts of the phosphorus-doped biodiesel (orange curve). This aging resulted in a severe deactivation of the VWTi catalyst over the whole temperature range, no matter if a DOC or dummy was present upstream of the SCR catalyst sample during the aging. Only at 500 °C, a significant difference is observed between the two samples. An interesting observation is that at 500 °C the NH₃ conversion is more affected than the NO conversion, as compared with the conversion of these reactants for the fresh catalyst. This indicates that also the non-selective oxidation of NH₃, which is quite significant in the fresh catalyst, is also inhibited, and is also supported by the decreased amount of N₂O formed (<25 ppm compared to 55 ppm) by the P-aged catalyst.

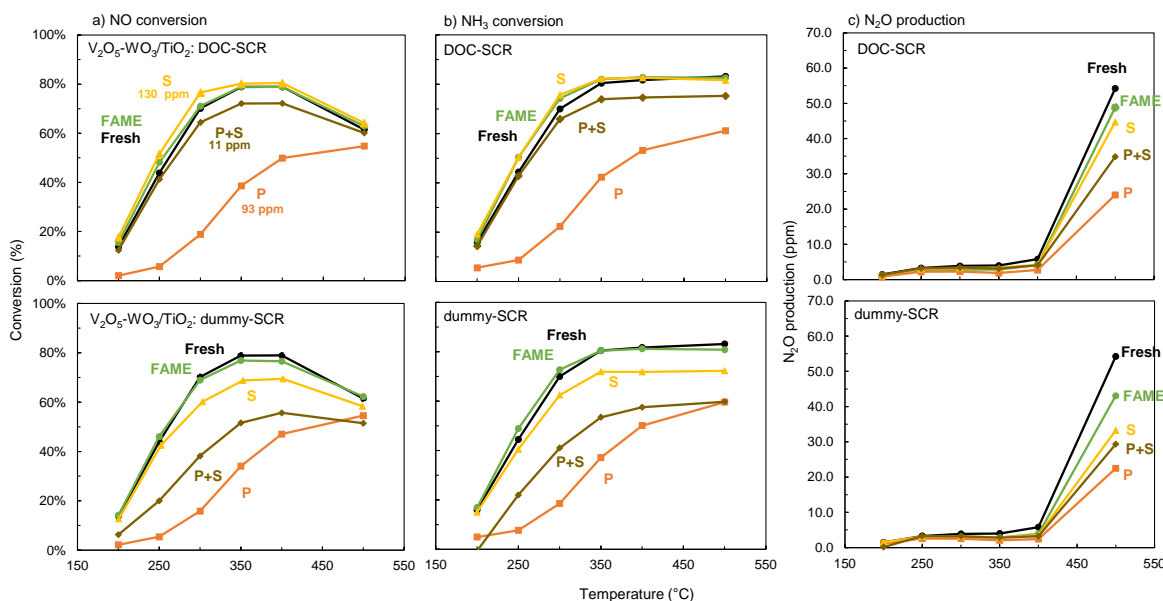


Figure 57: Effect of exposure to pure (green), P- (orange), S- (yellow), and S+P-doped (brown) FAME exhaust on NO and NH₃ conversion and N₂O production of V₂O₅-WO₃/TiO₂. DOC-SCR or dummy-SCR during aging. Test conditions: 10% O₂, 1000 ppm NO and NH₃, 5% H₂O, GHSV 120,000 h⁻¹.

Deactivation by phosphorus over the whole temperature range of a VWTi SCR catalyst has previously been observed by for example Kamata et al. [129].

Furthermore, England [16] observed a severe deactivation, also this time over the entire temperature range, for a catalyst that had been in a truck operated on biodiesel around 120,000 h. High concentrations of phosphorus was found in this catalyst [16], and hence might be the reason for the observed deactivation.

For the aging experiment with both phosphorus and sulfur added to the biodiesel (**Figure 57**, brown curve), but at lower concentrations, it is clear that an upstream DOC could considerably protect the SCR catalyst. For the sample exposed to the exhaust with a DOC in front, only a slight deactivation was observed. Furthermore, this sample appears to have an increased selectivity towards the desired SCR reaction, and decreased selectivity towards unwanted ammonia oxidation, as shown by the smaller difference between the NO and NH₃ conversion at 500 °C, and the significantly decreased N₂O production. The sample with a dummy, on the other hand, shows a high degree of deactivation. This deactivation is observed over the whole temperature range, as for the samples exposed to the exhaust with high phosphorus concentration. Also for this sample, the selectivity towards non-selective ammonia oxidation appears to be lower.

As opposed to the experiments that included phosphorus, the aging with sulfur-doped biodiesel resulted in a promotion of the NO_x reduction performance. This promotion was observed for the VWTi catalyst that had a DOC in front during the aging. A slight increase in NO conversion is observed, as well as a significant decrease in N₂O production (decrease from 55 to 45 ppm). Consequently, the

selectivity towards the unwanted N_2O is significantly decreased. However, at high temperature, ammonia is still oxidized in a reaction that does not include NO, as the NH_3 conversion is higher than the NO conversion. The VWTi sample aged with a dummy in front, instead shows a moderate deactivation in the NO_x reduction performance, primarily noticed at 300 °C and above. Similar to the sample with the DOC upstream, the N_2O production at 500 °C is decreased. Only 35 ppm N_2O was produced for this sample.

A slightly promoting effect of the aging was also noted for the experiment with pure FAME (**Figure 57**, green curve), especially in terms of decreased N_2O selectivity. This applies for both the samples, but the decrease in N_2O formation is most significant for the sample with the dummy in front during the aging. Slight increases could also be noted in the conversion of both NO and NH_3 for the sample with a DOC in front during the aging.

3.5.2 Aging effects on the Cu-SSZ-13 catalyst

As opposed to the VWTi catalyst, the Cu-zeolite experienced deactivation, to a higher or lower extent, due to all of the aging experiments (see **Figure 58**). As for the VWTi, the most pronounced effect is the severe deactivation resulting from the aging with P in high concentration (**Figure 58**, orange curves). Almost no conversion is observed for both P-aged Cu-SSZ-13 samples at temperatures up to 350 °C. After this, the NO and NH_3 conversion gradually increase with temperature, but even at 500 °C, the conversion does not reach the value of the fresh sample. This effect is especially pronounced for the sample aged with the dummy in front; the NO conversion at this temperature is only 60% for this sample, while it is 82 and 92% for the sample with the DOC upstream during the aging, and the fresh catalyst, respectively. This indicates that the DOC protects the SCR catalysts by capturing part of the phosphorus before it reaches the SCR catalysts. The formation of N_2O is also almost totally suppressed at all temperatures for both P-aged Cu-SSZ-13 samples.

Similar to the VWTi, large effects of the aging configuration, i.e. DOC or dummy upstream of the SCR catalyst during the aging experiment, are observed after the aging with P+S-doped fuel. The sample aged with the dummy upstream has a considerably higher degree of deactivation than the sample that had a DOC in front. As opposed to the aging with only phosphorus doped in the fuel, the conversion at high temperature reaches the same level as the fresh catalyst. For the sample with the DOC a similar conversion level is reached at around 400 °C, while 500 °C is required to reach the same level for the catalyst aged with the dummy.

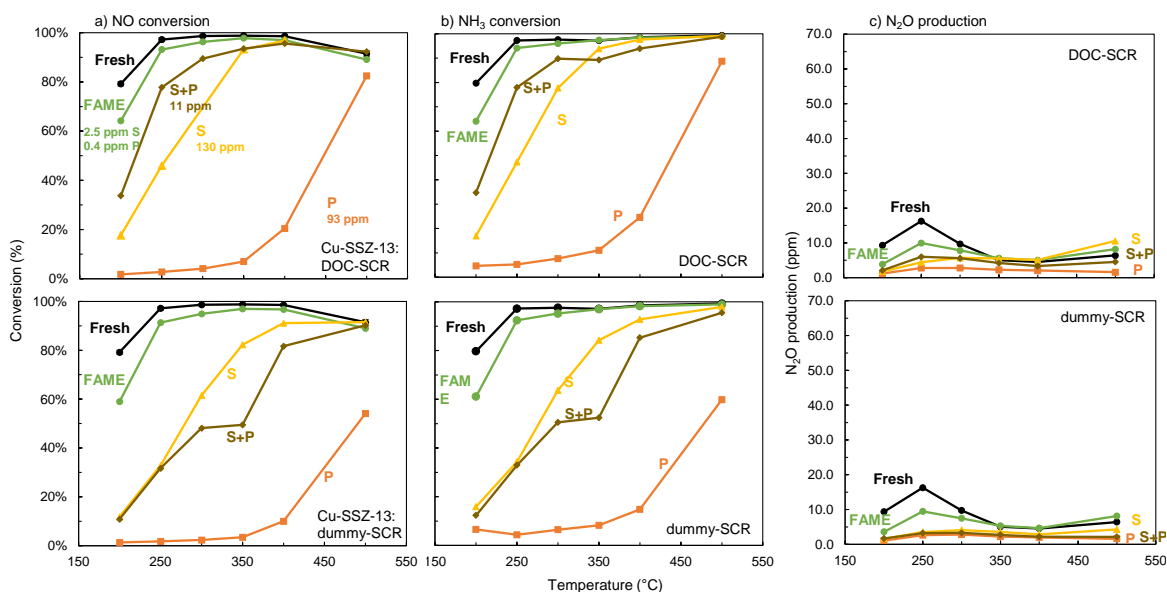


Figure 58: Effect of exposure to (green), P- (orange), S- (yellow), and S+P-doped (brown) biodiesel (FAME) exhaust on NO and NH₃ conversion and N₂O production of Cu-SSZ-13 (Cat A2). DOC-SCR or dummy-SCR configuration during aging. Test conditions: 10% O₂, 1000 ppm NO and NH₃, 5% H₂O, GHSV 120,000 h⁻¹.

A considerable effect is also observed for the aging experiment with high sulfur concentration. Both Cu-SSZ-13 samples from this aging are severely deactivated at temperatures below around 350 °C. Again, a more severe effect is observed for the sample aged with the dummy in front. The N₂O production of the sample aged with the dummy is suppressed at all temperatures, while the sample aged with the DOC instead show an increase in the high-temperature N₂O production. However, at low temperatures the N₂O formation is decreased.

After the aging experiment with pure biodiesel, mainly the low-temperature (200–250 °C) performance of the Cu-SSZ-13 samples is affected. At 200 °C, a decrease in NO conversion from 80 to 64 and 59% was observed for the sample with an upstream DOC and dummy, respectively. A similar effect was seen for the NH₃ conversion for both samples. This was accompanied with a decrease in the low-temperature N₂O production. However, at 500 °C, the N₂O production was slightly higher for the aged samples.

3.5.3 Effect of sulfur desorption during SCR test – partial regeneration of Cu-SSZ-13

During the activity test, I noted significant SO₂ desorption peaks from several of the Cu-SSZ-13 samples, while not observed for the aged vanadium-based catalyst samples. This desorption was especially pronounced for the performance test at 500 °C, and in the step when ammonia was first introduced, varied depending on the aging experiment and configuration (see **Figure 59**). Consequently, most of the Cu-SSZ-13 samples were subjected to a second performance test to investigate

the effect of this removed SO₂ on the NO_x reduction performance. In these second tests, no, or very low amounts of, SO₂ were detected, and an improved SCR performance was observed. This improvement was observed over the whole temperature range where the catalyst was deactivated (see **Paper V**); the effects on the low-temperature are summarized in **Figure 59**, in the form of the relative rate constant ($k_{\text{aged}}/k_{\text{fresh}}$) for the standard SCR reaction at 200 °C, with 10% O₂.

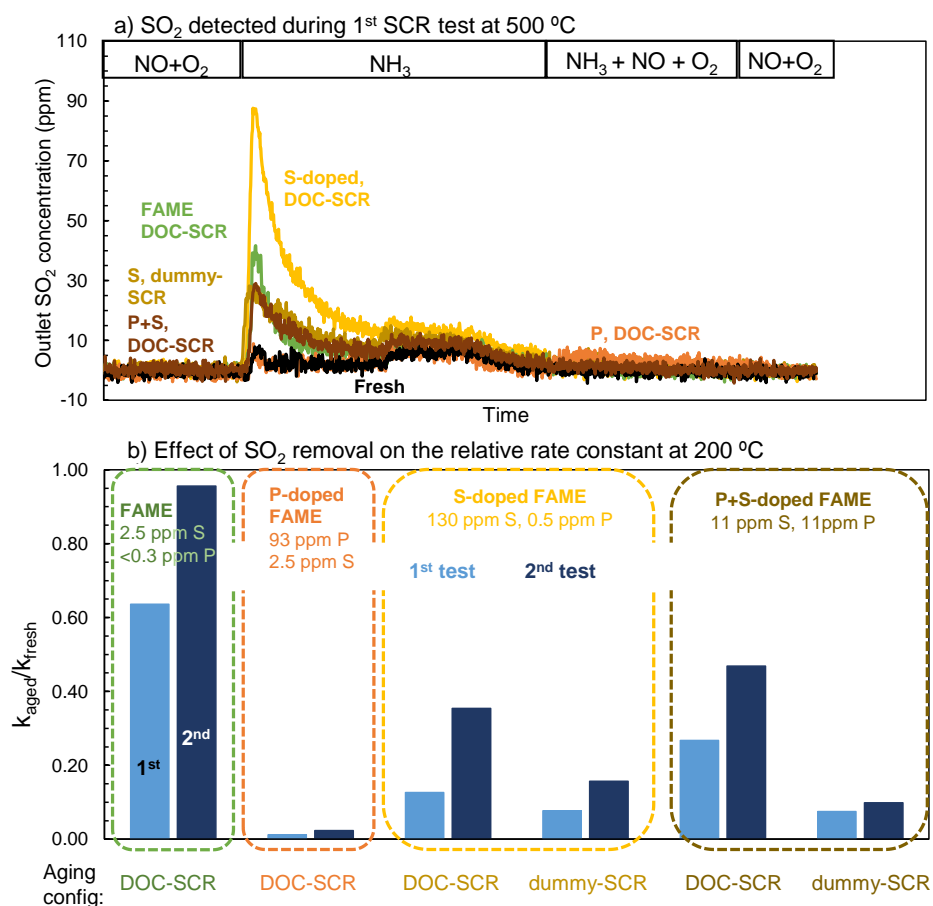


Figure 59: Effect of SO₂ desorbed during the 1st SCR test on the relative rate constant at 200 °C – partial regeneration due to this sulfur removal from the catalyst, as seen when comparing the relative rate constant for the 1st and 2nd SCR tests. Test conditions: 10% O₂, 1000 ppm NO, 1000 ppm NH₃, 5% H₂O, GHSV 120,000 h⁻¹. The total time at 500 °C was around 26 min.

Smaller amounts were detected also at lower temperatures; however, the FTIR detected “SO₂” even for fresh samples, although these samples contained no sulfur. In my approximate quantification of the amount of desorbed SO₂ from the samples during the first SCR test, the values obtained for fresh samples were therefore subtracted from those obtained for the aged samples. It was later found that the FTIR had a cross-sensitivity for ammonia and SO₂, which was dependent on the NH₃ concentration.

3.5.4 Capture of phosphorus and sulfur in the SCR catalysts

Bulk elemental analysis (XRF) of the aged samples shows that both the V_2O_5 - WO_3/TiO_2 and the Cu-SSZ-13 capture phosphorus, while significant amounts of sulfur are only captured by the Cu-zeolite. This agrees well with the results in the SO_2 -aging from **Chapter 3.3**. However, as a promotive effect was observed for the VWTi catalyst upon sulfur-exposure, it is likely that it contains some small amount of surface sulfur species not detectable by the bulk elemental analysis.

Alternatively, the SO_2 induces changes in the catalyst material without self being strongly adsorbed to it.

No other fuel- or lube-oil related contaminants (Na, K, Mg, Ca, or Zn) could be detected at any increased levels compared to the fresh material in any of the VWTi and Cu-SSZ-13 samples.

The V_2O_5 - WO_3/TiO_2 samples exposed to P-doped FAME exhausts (93 ppm P in the fuel) had the highest concentration of phosphorus. The bulk concentration of P in these samples was around 2 wt%, with no difference in concentration between the inlet and the outlet part of the samples. This concentration notably corresponds to a molar P/V ratio of almost 3, i.e. almost three times as much phosphorus as vanadium. This indicates that the phosphorus in the exhaust interacts not only with the vanadium in this catalyst, but also with other parts of the catalyst material e.g. the WO_3 and/or the TiO_2 . Alternatively, more than one phosphorus can be associated with one vanadium.

In the samples from the aging with S-doped FAME, increased concentration of phosphorus was only detected for the sample that had a dummy upstream during the aging. For this sample, a gradient was observed between the inlet and the outlet of the catalyst, with highest concentration in the inlet.

Both samples from the aging experiment with P+S-doped FAME (around 10 ppm P in the fuel) contain increased amounts of phosphorus.

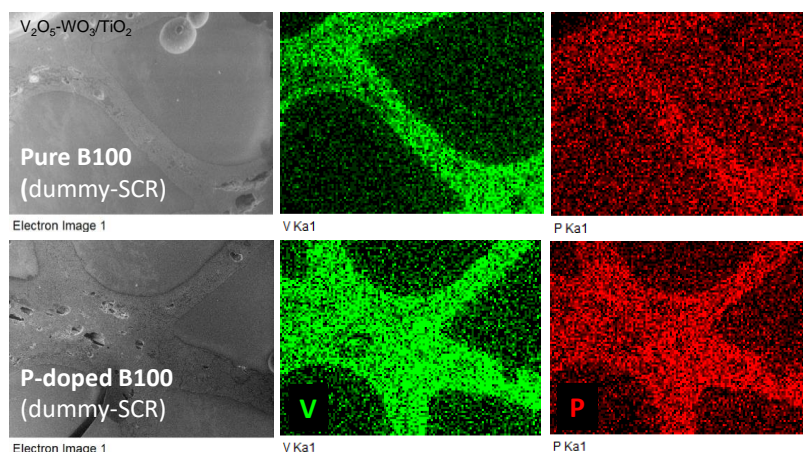


Figure 60: SEM-EDX mapping of $V_2O_5-WO_3/TiO_2$ aged with pure FAME (top) and P-doped FAME (bottom) with a dummy upstream during the aging. The sample exposed to P-doped biodiesel exhausts shows high concentration of P all over the catalyst substrate, similar in inlet as in outlet. The sample exposed to pure FAME-exhaust had a slightly increased P-concentration compared to the fresh catalyst. Magnification: 151x.

The concentration of P is considerably higher in the sample aged with the dummy in front, compared to that with the upstream DOC. However, both samples display an axial concentration gradient with higher concentration of P in the inlet part of the catalyst.

According to SEM-EDX mapping of a cross-section of the pure biodiesel-aged and the P-aged catalysts (**Figure 60**), the phosphorus appears to be evenly distributed throughout the whole substrate thickness in both catalyst samples. The P in the biodiesel-aged catalyst is mainly related to what is present already in a fresh catalyst, as the bulk elemental analysis did not detect increased concentrations of phosphorus in this sample. The P-aged sample contains significantly higher concentrations of P as indicated by the stronger signal for phosphorus (**Figure 60**, lower panels). No accumulation of P on the surface of the catalyst wall was observed.

The Cu-SSZ-13 samples from the aging with the P-doped FAME also contained high concentrations of phosphorus, although significantly lower than in the vanadium catalyst. One reason for the lower total concentration of phosphorus in the Cu-zeolite is probably because this sample is washcoated on a cordierite substrate, while the entire VWTi substrate contains porous and active material. The concentration of phosphorus in the Cu-zeolite was around 0.3-0.4 wt%, with a rather uniform concentration throughout the length of the catalyst core. This concentration corresponds to molar P/Cu ratios of around 1.09 and 0.82 for the sample with an upstream DOC and an upstream dummy, respectively. As opposed to the VWTi samples, the P/Cu ratio for these Cu-zeolite samples is thus close to one, even though the total amount of phosphorus exposed to the catalyst far

exceeds a theoretical 1:1 saturation. This suggests that phosphorus interacts mainly with the copper in this type of catalyst, in a 1:1 relationship.

For the aging experiments with S- and P+S-doped FAME, phosphorus was only detected (>0.1 wt% P) the samples with a dummy in front during the aging. The sample from the P+S-aging had an axially uniform concentration of P of around 0.2 wt%, while the concentration of phosphorus in the S-aged sample was lower. In addition, this sample had a small concentration gradient between the inlet and the outlet, 0.14 and 0.12 wt%, respectively.

A phosphorus concentration in the same range as observed here, 0.3-0.4 wt%, has previously been reported for a deactivated Cu-zeolite after engine-aging in a dynamometer corresponding to 120,000 km [211]. Different from our results though, is that this engine-aged catalyst had an axial gradient, with higher concentration of phosphorus in the inlet part. It also had a concentration gradient within the washcoat thickness, with most of phosphorus being present at the surface of the washcoat [211]. As another example, the P concentration of the engine-aged Cu-SSZ-13 catalyst that was investigated in **Chapter 3.3** (and **Paper III**), was around 0.15 wt% in the inlet and around 0.8 in the outlet part.

Capture efficiencies for phosphorus for the different aging experiments and catalyst samples are presented in **Paper V**, as well as more details about concentrations of P and S in the samples.

Sulfur analysis of all the performance-tested aged Cu-SSZ-13 samples showed an S concentration in the range of 0.02 to 0.11 (<0.01 in fresh), with the highest concentration of sulfur found in the samples from the aging with S-doped FAME. However, remember that a significant amount of SO_2 desorbed from some of the samples during the SCR performance test. Based on the concentration of SO_2 in the effluent gases during the test at 500 °C, and the mass of the catalyst core, it was estimated that roughly 0.02-0.2 wt% of S, i.e. molar S/Cu of around 0-0.6 to 0.5, was lost during this test.

The SEM-images indicate that the phosphorus is evenly distributed in the washcoat thickness, see **Figure 61**. This observation, together with the rather uniform concentration of P axially, indicates that catalyst samples are saturated, or almost saturated, with phosphorus.

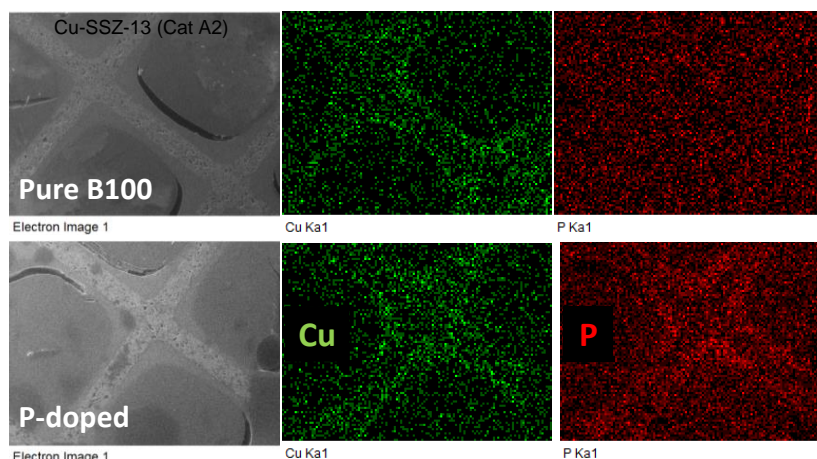


Figure 60: SEM-EDX mapping of Cu-SSZ-13 samples exposed to pure biodiesel exhaust (top) and P-doped biodiesel exhaust (bottom), with a dummy upstream during the aging. The sample exposed to P-doped FAME exhaust contains P in the whole washcoat thickness, while no P is shown in the mapping for the pure FAME exposed sample. Magnification: 151x

3.5.5 SCR performance in relation to captured contaminants

During the different aging experiments, different amounts of S and P were captured in the different catalysts. Furthermore, variations between the two tested configurations, DOC or dummy upstream of the SCR catalyst during the aging, were observed. It is interesting to relate these differences to the effect on the SCR performance. To display the impact of the contaminant concentration on the low-temperature SCR performance, the relative rate constant was plotted against the molar P/V for the VWTi, and P+S/Cu for the Cu-SSZ-13 catalyst (see **Figure 62**). For the Cu-SSZ samples, data for both as-received (full symbols) and partially regenerated (empty symbols) samples are included. The partially regenerated data originate from the second SCR test performed for most of the Cu-zeolite samples, and the corresponding S/Cu ratios are based on the sulfur analysis results obtained by a Leco sulfur analyzer. The S/Cu for the as-received samples are based on a sum of the S content from the sulfur analysis, and the estimated amount of sulfur released during the first SCR test.

From **Figure 62**, we can see that a rather low contamination level results in a quite high degree of deactivation for the Cu-SSZ-13 catalyst. In **Paper V** it was concluded, by comparing the deactivating effect of sulfur with the deactivating effect of phosphorus, that rather similar molar ratios of S or P per Cu result in quite different degrees of deactivations: a S/Cu ratio of 0.75 leads to a relative rate constant of 0.13 while the corresponding values for the sample with a P/Cu of 0.82 results in a relative rate constant of only 0.01 at both temperatures. Furthermore, the P-poisoned sample (P/Cu=0.82) shows considerably lower NO conversion at 300-400 °C than does the S-poisoned sample (S/Cu=0.75) (see **Paper V**).

In the engine-aged catalyst studied in Chapter 4.3 (and **Paper III**), the combined S+P/Cu is around 0.83, and after regeneration at 500 + 700 °C it decreases to 0.68. The corresponding relative rate constants at 220 °C (no test performed at 200 °C) were 0.31 and 0.41, respectively.

Phosphorus deactivates the vanadium-based catalyst as well. However, the degree of deactivation for all of the V₂O₅-WO₃/TiO₂ samples is lower than for the Cu-SSZ-13 samples, even though these samples contain higher levels of contamination. P/V ratios around 0.5 and below do not appear to cause significant deactivation. For a P/V ratio of around 1.2, a deactivation of around 60% is observed, and for the P/V ratios above 2.5 the deactivation is around 90%.

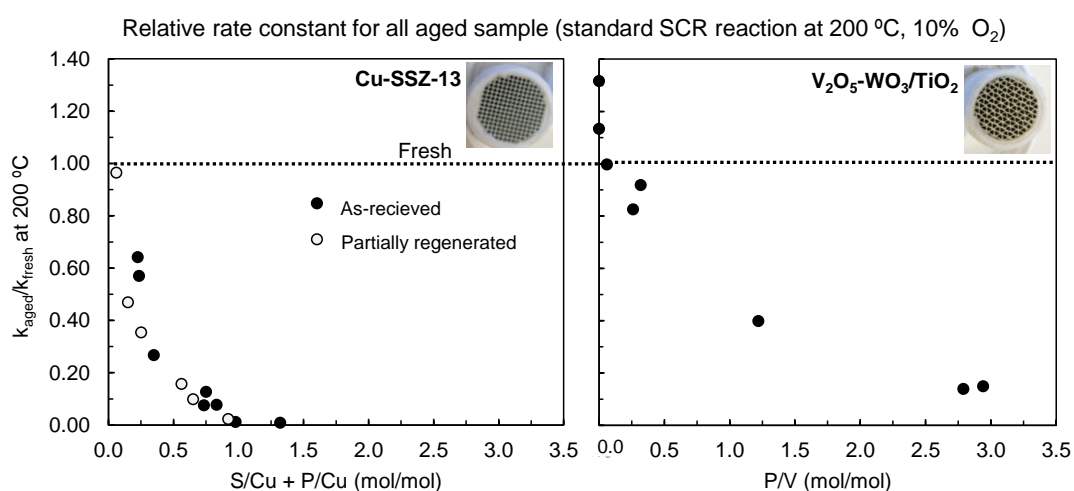


Figure 62: relative rate constant at 200 °C as a function of the molar P/V och S+P/Cu for the investigated Cu-SSZ-13 and VWTi SCR catalysts. Test conditions: 10% O₂, 1000 ppm NO, 1000 ppm NH₃, 5% H₂O, GHSV 120,000 h⁻¹.

In relation to the results from **Paper I**, in which the P/V ratios were 1.1-1.5 for the high concentration level, where phosphorus did not appear to cause any significant deactivation, some differences in the tests performed, and in the contamination procedure, may explain this. First of all, the fast SCR reaction was studied in **Paper I**, and this reaction might not be affected in the same way as the standard SCR reaction (e.g. re-oxidation is easier for fast SCR). Second, the aging methods differ: a wet impregnation in **Paper I**, and a gas-phase aging in this study. In the literature it has earlier been shown that exposing the catalyst to the same P/V, but using either an aerosol or wet impregnation, the aerosol aging resulted in a higher degree of deactivation. [143] The temperature during the aerosol or gas-phase aging might as well have an effect. In our study we have a rather high temperature, 450 °C.

3.5.6 Effect of phosphorus on the DOC

The effects of the different aging experiments on the DOC samples used during those experiments are the subject of an ongoing manuscript. However, a brief discussion of some of the results is included here, as this will improve the understanding about the whole system. The DOC from the aging with the P-doped biodiesel trapped a substantial amount of phosphorus (see **Figure 63**), which also resulted in a severe deactivation of this sample. No NO conversion at all was observed over the whole temperature range tested (80-300 °C, see **Figure 64**), and the highest conversion of C₃H₆ was around 40%. Furthermore, incomplete oxidation of this propylene lead to production of CO at temperatures above around 200 °C and thus an overall negative conversion of CO. The aging with a lower concentration of phosphorus in the exhaust (P+S), resulted only in slight increase of the light-off temperatures for HC and CO, while the NO conversion instead was somewhat improved compared to the fresh catalyst.

The capture efficiency of P in the DOC samples were 7 and 22% for the aging experiments with P- (93 ppm), and P+S-doped (11 ppm P) biodiesel, respectively.

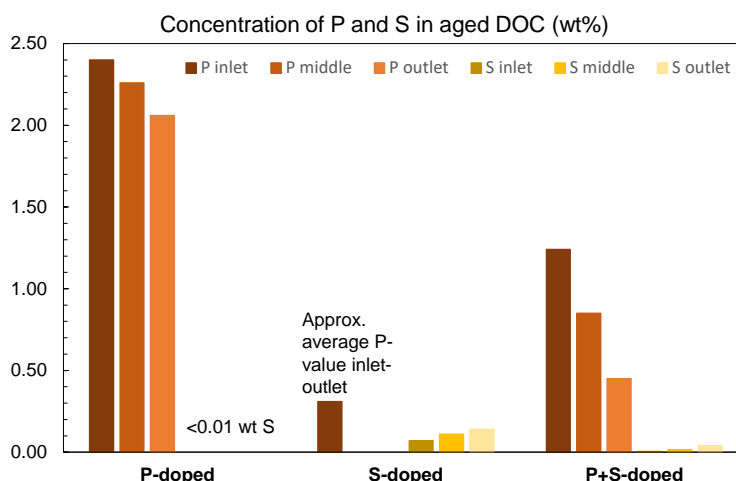


Figure 63: Concentrations of phosphorus and sulfur in the DOC samples exposed to P-, S-, and P+S-doped FAME-exhausts in the diesel burner. Substantial amounts of P are trapped in the DOCs.

For a comparison, the effect of 0.2 wt% P on a DOC from the same batch is shown in **Figure 65**. This phosphorus was added from exposure of a P-containing aerosol using the aging rig constructed during this PhD project. An increase in the CO light-off temperature is observed, as well as a slight decrease in the NO oxidation ability. Note that in this test, the test conditions were not exactly the same as those applied compared to the results in **Figure 64** (e.g. a higher GHSV in the tests for the data in **Figure 65**).

To conclude, a high concentration of phosphorus in the DOC, as for the P-doped aging, is detrimental for all the oxidation reactions; however, for a P-concentration up to around 0.5-1 wt%, the degree of deactivation is rather low.

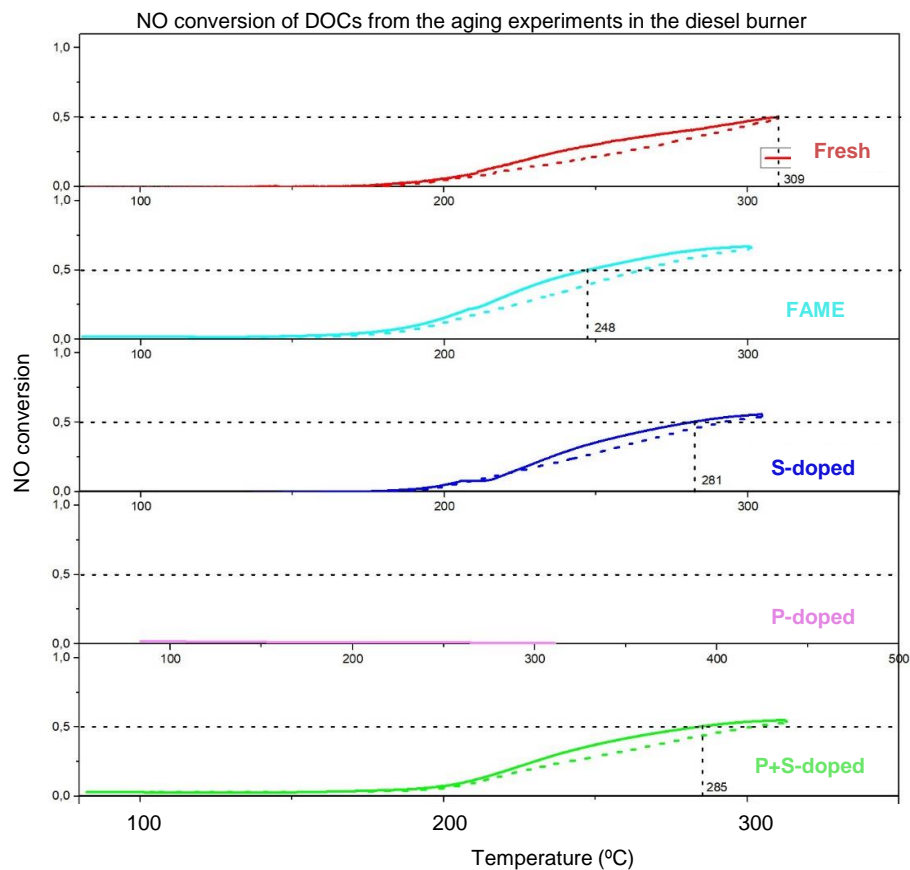


Figure 64: Effects on the NO oxidation abilities of the DOCs from the different aging experiments during heating (and cooling, dotted) at 10 °C/min. GHSV 22,000 h⁻¹, 10% O₂, 5% H₂O, 100 ppm propylene, 100 ppm CO, 1000 ppm NO.

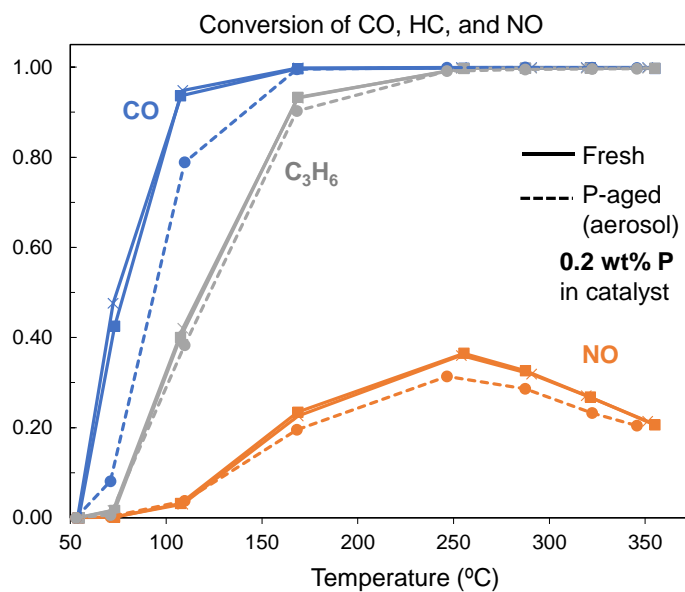


Figure 65: CO, NO, and C₃H₆ conversion for fresh DOCs (2 shown as examples) prior to the aging in the diesel burner, and for a DOC subjected to a preliminary aging experiment with P-doped aerosol in the aging rig constructed during this PhD project. GHSV 80,000 h⁻¹, 10% O₂, 5% H₂O, 100 ppm propylene, 100 ppm CO, 1000 ppm NO.

3.6 The effect of biogas operation on a Pd-Pt oxidation catalyst (Paper VI)

In this study, we investigated how exhaust gases from a biogas-powered Euro VI-engine impact the performance of a bimetallic Pd/Pt oxidation catalyst. The effect of this aging on the ability of the catalyst to oxidize methane, CO and NO is shown in **Figure 66**.

After 900 h of aging, the CH₄ oxidation capability decreased considerably, as can be seen when comparing the aged DOC (DOC in, DOC out) with a fresh reference catalyst. Both the light-off and the maximum conversion are affected, and both the inlet and outlet part of the aged catalyst display only minor CH₄ oxidation activity at temperatures up to 450 °C. A difference between the inlet and outlet is observed, with the inlet being more deactivated than the outlet. Further, it is noted that the CH₄ oxidation ability for all samples is better in presence of the complex gas mixture (CH₄+NO+CO+O₂), compared to when only CH₄ and oxygen is present (**Figure 66a** and **d**, respectively). This effect has also been shown in a previous study [212], and was suggested to be due to a decreased inhibitory effect of water in the presence of NO by forming HNO₂ from H₂O-originating hydroxyl groups.

The activity for CO oxidation is also decreased, as seen by the significantly higher light-off temperature for the aged samples (**Figure 66c, f**). The T₅₀ occurs at 25 and 50 °C higher temperature in the complex and simple reaction mixture, respectively. No change in maximum conversion is observed. For all samples, fresh as well as aged, the CO oxidation activity is higher in absence of NO and CH₄ in the feed, as seen when comparing the light-off curves in **Figure 66c** and **f**. For the fresh catalyst the T₅₀ is almost 50 °C higher in the complex gas mixture, while the differences in light-off temperatures are slightly smaller for the aged samples.

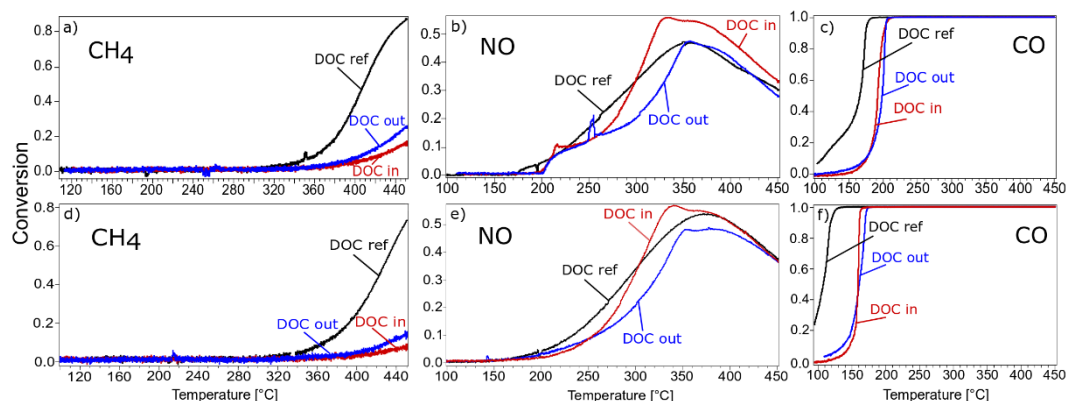


Figure 66: Conversion of CH₄ (a, d), NO (b, e), and CO (e, f) during a heating ramp (5 °C/min) for the inlet and outlet part of the engine-aged catalyst (DOC in and DOC out, respectively) and a fresh reference (DOC ref). The top row consists of a gas mixture including all pollutants simultaneously (1000 ppm CH₄, 1000 ppm NO, 1000 ppm CO); in the bottom row these reactants are introduced separately. In both tests 8% O₂ and 5% H₂O are present with argon as balance, and the GHSV was 45,000 h⁻¹. From Englund et al. Catalysts 9 (2019) 1014 [167].

The NO oxidation ability of the DOC is important for improving the performance of downstream filter and SCR catalyst. At low temperatures, both the inlet and outlet sample show a slightly lower NO conversion than the fresh sample. However, at temperatures above around 300 °C, the NO conversion of the inlet part of the aged catalyst is higher than it is for the reference sample (see **Figure 66b, e**). This is likely due to a growth of the PGM particles during the aging, as NO oxidation is known to be more active on larger Pt particles.

Furthermore, the NO conversion maxima of aged catalyst samples are split in two peaks, which could indicate some separation of PGM particles into monometallic Pt and Pd particles. Pt has significantly higher activity for NO oxidation than does Pd [44, 213]. Thus, it is likely that larger, monometallic Pt particles have formed on the aged catalyst.

The noble metal particle size of the different samples was measured by TEM. The 900 h-aging resulted in an increase in PGM size from around 4 nm to 8-9.5 nm and a broadening of the particle size distribution (see **Table 9**), likely due to hydrothermal effects [214]. Then again, the temperature in the exhaust during the aging did not exceed 550 °C, which means that sintering due to hydrothermal aging should not be severe in this particular aging. However, the presence of S and P in the exhaust could promote sintering of PGM particles [173, 215]. The increase in PGM size is likely responsible for the increased NO conversion above 300 °C.

Table 9: average PGM particle size and distribution, CO uptake, and concentration of contaminants (P, S, and Ca) in fresh and aged catalyst samples (washcoat + cordierite)

	Average PGM particle size (distribution) (nm)	CO uptake (mol CO/mol PGM)	P (wt%) ¹	S (wt%) ¹	Ca ² (wt%)
DOC ref	4.0 (2-9)	0.063	0.00	0.00	0.028
DOC in	9.5 (5-17)	0.001	0.18	0.27	0.047
DOC out	8.0 (2-19)	0.003	0.04	0.25	0.032

¹ ± 0.04 wt%

² ± 0.007 wt%

The CO uptake during CO chemisorption was also shown to be considerably lower on the aged catalyst samples compared to the fresh one. This uptake is related to the PGM size, as smaller more dispersed particles will result in a higher uptake. However, the composition of the PGM particles and chemical impurities on them can also affect the CO uptake.

The XRD results (**Figure 67**) support the conclusions regarding the increase in particle size and the segregation of the noble metals. The peak at 2θ around 39-40°, related to Pt and Pd (39.8, 40.1° for monometallic Pt and Pd, respectively),

shows an increase in intensity as well as a shift towards higher angles for the aged catalyst samples, in particular the inlet sample. The peak at 2θ around 46.5° is related to Pd, and this peak exerts the same behavior as the peak at 40° , especially the inlet sample. The shift is an indication that more monometallic sites are present on this bimetallic catalyst than on the fresh, and the increased intensity is an evidence of larger particles. [216-218] These results agree well with the observations from the TEM and the activity tests, supporting our conclusions about sintering and segregation of PGM due to the biogas aging.

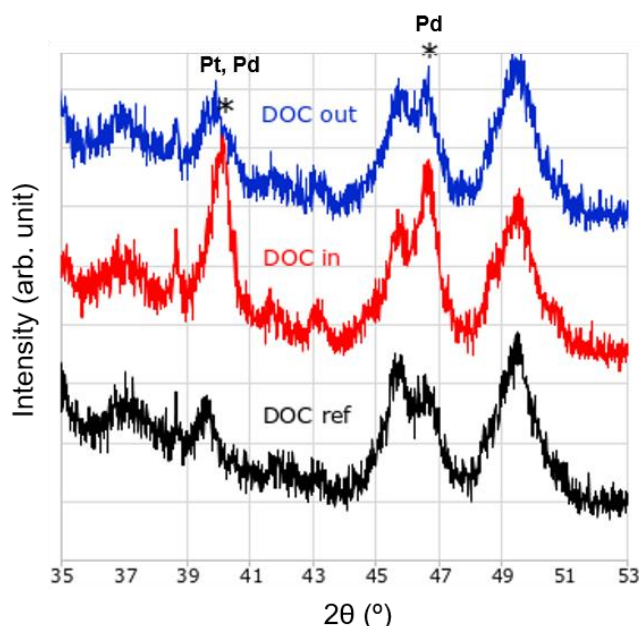


Figure 67: XRD results of fresh and aged Pd-Pt/Al₂O₃ indicating change in PGM size and distribution of Pd and Pt in the particles after aging 900 h with a biogas engine. The peak at 2θ around $39-40^\circ$ is related to Pt and Pd, and the peak at 2θ around 46.5° is related to Pd. Adapted from Englund et al. Catalysts 9 (2019) 1014 [167].

Chemical contamination of the catalyst is confirmed by XRF, XPS, and SEM-EDX mapping of the catalyst washcoat. XRF shows that both P and S have accumulated in the catalyst, with S present in both the inlet and outlet sample while P is mainly present in the inlet sample (see **Table 9**). The aged sample also contained slightly increased concentrations of Ca compared to the fresh catalyst. Significant amounts of S and P are found on the surface of both the inlet and outlet part of the catalyst, detected by XPS (see **Figure 68**). Again, higher concentrations are observed in the inlet compared to the outlet.

The binding energy of phosphorus in the inlet sample indicates that it is present in two different forms, phosphate (PO₄³⁻ (135 eV) and phosphorus pentoxide, P₄O₁₀ (138 eV) [219]. P₄O₁₀ is sticky and covers the surface non-selectively, while phosphates may react with the alumina support [220, 221].

In the outlet sample, mainly phosphate is found, likely due to the sticky phosphate glass being caught in the inlet part. Sulfur is present as a sulfate in both samples,

and is likely related to palladium sulfates rather than platinum sulfates, as the latter normally do not form at ambient pressure [222, 223]. It could also be bound to the alumina in the support, as alumina is a sulfating support [50]. SEM-EDX results show a gradient in phosphorus concentration both axially, both also in the washcoat, with higher concentrations in the inlet part of the catalyst and on the surface of the washcoat. Sulfur on the other hand, is uniformly distributed across both the length and the washcoat layer. Part of the observed decrease in CO uptake as well as deactivation, is likely related to the contaminants present in the aged samples. Thus, both thermal and chemical deactivation are responsible for the change in performance of this Pd-Pt bimetallic oxidation catalyst after 900 h in the engine-bench.

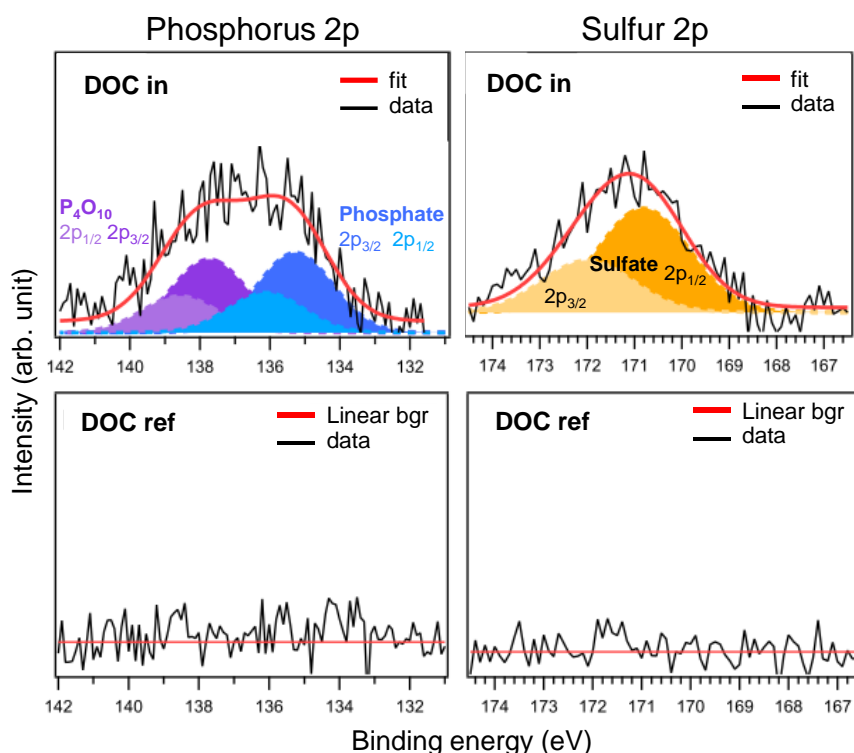


Figure 68: XPS spectra of P 2p and S 2p regions of engine-aged (inlet) and fresh catalyst, showing significant contamination of the engine aged catalyst. Adapted from Englund et al. Catalysts 9 (2019) 1014 [167].

Part IV: Concluding Remarks and Outlook

In this project, the durability of heavy-duty diesel emission control catalysts towards contaminants present in biofuels and lube oil (P, S, Na, K, Mg, Zn) has been investigated. The main focus has been on Cu-SSZ-13 and V_2O_5 - WO_3 /TiO₂ SCR catalysts, but diesel (and biogas) oxidation catalysts have also been included to some extent in the project. For the vanadium-based catalyst, all the above-mentioned contaminants have been investigated, while the effect of sulfur and phosphorus was investigated for the Cu-zeolite. The work was performed by executing different aging experiments, ranging from wet impregnation to gas-phase aging using biodiesel exhausts, with performance tests of the catalysts prior to and after these aging experiments. In addition to the lab-aged catalysts, some vehicle and engine-aged catalysts have been evaluated. To obtain further information about the observed deactivation, characterization of fresh and contaminated catalysts has been conducted as well. This characterization includes, among others, elemental analysis, NH_3 -TPD, and XAS.

The main results and conclusions from this project are summarized below.

Conclusions

Alkali metals are severe poisons for the vanadium-based SCR catalysts, as shown by the results in Paper I as well as by several other research groups. The effect of alkali metals on Cu-SSZ-13 catalysts is less studied, but appears to be significantly less deactivating than for the vanadium-based catalyst.

Phosphorus can be trapped by and deactivate both Cu-SSZ-13 and the V_2O_5 - WO_3 /TiO₂ catalysts. The extent of this deactivation depends on how much P that is trapped by the catalyst, which in turn depends on the concentration of phosphorus in the exhaust, the exposure time, and the presence of other exhaust treatment components present upstream of the SCR catalyst. For the experiments with a high phosphorus concentration, the P-exposure resulted in severe deactivation of both types of SCR catalysts over the entire temperature range 200-500 °C. However, phosphorus has a stronger poisoning effect on the Cu-zeolite than on the vanadium-based catalyst. Although considerably more phosphorus was trapped in the VWTi catalyst, molar P/V ratios of almost 3 were observed, this catalyst was less deactivated than the Cu-SSZ-13 catalyst. The Cu-SSZ-13 catalysts was completely deactivated up to around 350 °C for a P/Cu ratio around 1, which was the highest concentration of P captured in this catalyst. The above observations suggest that phosphorus is not only related to vanadium in the V_2O_5 - WO_3 /TiO₂ catalyst, i.e. it poisons the surface of this catalyst non-selectively. Alternatively, it could be that more than one phosphorus atom can be coordinated to the vanadium.

As opposed to this, the phosphorus in the Cu-SSZ-13 appears to be related mainly to the copper, reaching a 1:1 ratio between phosphorus and copper.

Another observation is that the deactivating effect of phosphorus appears to be dependent on how the aging is performed; exposure to P by wet impregnation methods result in a lower degree of deactivation compared to exposure in gas-phase.

Cu-SSZ-13 catalysts capture significant amounts of sulfur, while the VWTi catalyst does not. This sulfur uptake in the Cu-SSZ-13 catalyst is related to the copper in the catalyst, and results in a considerable deactivation of mainly the low, but also the intermediate, temperature range during standard SCR conditions. Concurrent with the decreased NO_x reduction performance, is a decrease in the low-temperature N₂O formation. Another observation is that phosphorus-poisoned Cu-SSZ-13 samples appear to capture less sulfur than samples without phosphorus. This is probably related to the low ability of P-poisoned Cu-sites to interact with SO₂ and form Cu-S species. Partial removal of sulfur from the Cu-SSZ-13, with concurrent partial recovery of NO_x reduction performance, can be achieved by heating the catalyst to 500 °C in a wet oxidizing atmosphere or using SCR test conditions. Ammonia in the feed appears to facilitate removal of sulfur. The VWTi catalyst can instead be promoted by sulfur.

A DOC can protect the SCR catalysts from phosphorus deactivation as the DOC itself can trap large amounts of phosphorus. However, if too much phosphorus is captured by the DOC, severe deactivation of this catalyst results as well. One of the key roles of the DOC is to provide NO₂ to the SCR catalyst to obtain fast SCR conditions, with NO₂/NO_x around 0.5. For the vanadium-based catalyst, the fast SCR reaction is important to reach high NO_x conversion at low temperatures. It improves both the activity and the selectivity of this catalyst. Cu-SSZ-13 catalysts already have higher NO_x conversion performance at low temperatures and are at fresh conditions not as dependent as VWTi catalyst on having NO₂ in the feed. Moreover, the N₂O production increases significantly with increasing NO₂ content in the feed. It is important not to exceed NO₂ concentrations above 50%, as this results in both excessive N₂O production and a decrease in low-temperature NO_x conversion compared to fast and standard SCR conditions. However, for aged Cu-SSZ-13 catalysts, e.g. SO₂-deactivated, the NO_x reduction performance can be significantly improved by applying fast SCR conditions. Furthermore, this improvement in NO_x reduction, is not accompanied by a high amount of N₂O.

Knowledge and insights from this work will be a good guide for the design of robust exhaust treatment systems for various applications, as well as for the development of suitable regeneration strategies. Additionally, it can aid the work of developing emission control catalysts with higher durability.

Suggestions for further work

The SO₂-poisoning mechanism is still not completely understood. The sulfur uptake/deactivation appears to depend on catalyst specification, atmosphere and maybe the state of the catalyst prior to sulfation. In addition, Cu-SSZ-13 catalysts can be quite different from one another, even with similar Cu/Al and Si/Al ratios, depending on the synthesis route. Well-designed experiments on defined materials, both simple and with a higher degree of complexity, would aid in this understanding. For example, the effect of different pretreatment methods on SO₂-uptake/species and subsequent effect on the SCR performance.

Further characterization of the burner-aged catalysts is recommended to obtain a better understanding of the deactivation mechanisms in the different types of catalysts from the various aging experiments. Additional aging tests in the diesel-burner aging rig would also be useful, for example studying how the capturing of contaminants and deactivation develops as a function of time for a certain contaminant concentration.

For the engine-aged Cu-SSZ-13 catalyst investigated in this project, thermal aging might, in addition to chemical deactivation, have contributed to the observed deactivation. It would thus be interesting to perform some additional tests on this catalyst, to determine if this is the case. For example, an NH₃ oxidation test and NH₃-TPD could be executed.

In another PhD project, my colleague Jonas Granstrand, has investigated the thermal and chemical aging effects of diesel oxidation catalysts by consecutive regeneration steps, including thermal regeneration and washing of the catalyst with water, with performance tests and material characterization in between. This approach could be interesting to perform on engine- or burner-aged SCR catalysts as well.

A collaboration with a research group at Yale-NUS, led by Steven L. Bernasek, was established during my PhD project. In this collaboration, characterization techniques such as in-situ XAS and NAP-XPS, have been utilized to gain additional knowledge about the interaction of contaminants, e.g. sulfur from SO₂-exposure, with the copper in Cu-SSZ-13. The first data from this collaboration was presented in Paper IV. Evaluation of data from additional tests performed during my PhD project, as well as from further planned experiments will be executed. MCR-ALS analysis of the XANES data was found to be a good way of analyzing the XANES data. Furthermore, wavelet-transformation of EXAFS data was shown to be useful for obtaining information from features that are overlapping, and thus difficult to separate, in the fourier-transform of the data. In-situ sulfur regeneration during XAS, studying both sulfur and copper edges at different conditions, is an example

of something that would be interesting to perform in a future study. Moreover, X-ray emission spectroscopy (XES) would be a nice complimentary technique to use, since this technique is more sensitive towards distinguishing the ligand type. Investigating phosphorus poisoning, for example using the catalysts from the diesel-burner aging study, would be another interesting subject.

Regarding the use of diesel-like biofuels, HVO appears to be considerably better to use than biodiesel (FAME), due the lower amounts of contaminants present in HVO. It is important to keep these contaminants at a low level in the fuel, as they can otherwise significantly deactivate the emission control catalysts. The quality of FAME appears to vary, sometimes being very clean with contaminants far below the maximum limits in the standard; however, if the fuel has concentrations of contaminants close to the maximum limits, significant deactivation can occur. Moreover, in favor of the HVO is that it is chemically very similar to conventional diesel, although cleaner. This means that this fuel has the comparable material compatibility as conventional diesel, and consequently, it can be directly used in conventional diesel engines and fuel systems. In addition, HVO has a much better storage stability than does FAME. Note that the hydrogen for HVO production, as well as the methanol for biodiesel, should be sustainably produced.

One part in reaching targeted greenhouse gas emission limits is to increase the fuel efficiency of internal combustion engines. Concurrent with this increase, is a decrease in the exhaust gas temperature. This temperature-decrease puts high demands on the activity of the emission control catalysts, which need to efficiently convert pollutants also at low temperatures. Thus, further research focus needs to be put on emission control that can reach high conversions of pollutants at low temperatures. For example, in the US, the 150 °C-challenge is implemented. In this challenge, the target is to reach 90% conversion of pollutants at a temperature of 150 °C.

Electrification of vehicles using batteries is another important part of the solution to reduce greenhouse-gas emissions and reach global warming targets. However, it is important to remember that both the production of batteries as well as the production of the electricity need to be sustainable. While some heavy-duty vehicles, such as distribution trucks in the cities, currently can be suitable for electric operation, it will take a long time before other types of heavy-duty trucks can be efficiently operated on electricity. In the meantime, a viable solution could be hybrid operation, in which the use of a small battery could result in significant reductions in greenhouse gas emissions. Consequently, the effect of hybrid operation on the components in the emission control system would be motivated to study.

Acknowledgements

First of all, I would like to thank the Swedish Energy Agency, as well as all industrial partners, Scania CV AB, Volvo Group Trucks Technology, and Umicore (former Haldor Topsøe), for the funding of this project (3SAM), which made the project possible. A big thanks to all the participants in the 3SAM-project for an inspiring and fruitful collaboration! Including Lennart, Kunpeng, Soran, and Behrooz at Volvo, Ton and Pär at Umicore Denmark ApS, Johanna, Magnus, and PA at Chalmers, Francesco and Martina at Scania, Lasse at KTH. Thanks to all of you for your interest, good input, discussions and nice company during project meetings as well as conferences.

I want to thank the former and current employees in the group YTMC (formerly UTMC) at Materials Technology, Scania CV AB. Especially Jenny Kylefors, Hanna Lind and Marita Nilsson for encouraging me to do a PhD and giving me the possibility to perform it by taking initiative to and forming this project together with me, while I was working in the group. Current group manager Martina Levin for letting me keep my office-desk although I wasn't there a lot, especially not during the later parts of my PhD studies. Francesco Regali for leading the project and coming with good, critical questions now and then, as well as for reading through part of my thesis and coming with good input. A big thanks to Björn Westerberg (NXPK, Catalyst and filter performance) for helping me with SCR test protocols, teaching me how to operate the SCAT-rig, solving problems appearing with it, as well as providing me with valuable input regarding my results. Thanks to Daniel Bäckström for the collaboration in Paper I. And all other persons at Scania that in some way have been included in the project.

My supervisor Lasse (prof. Lars J. Pettersson, eller Språkpolisen) – you have always been very supportive and encouraging, ever so happy to help out in the lab anytime I needed your help. You always took the time for me when I asked for it, coming with valuable input and wisdom. In addition, I especially enjoy your music advices and music quizzes, as well as our nice food discussions. Och din öldrickarmin såklart!

My smart and fun colleague Johanna Englund at Chalmers, and now also close friend. Johanna, without you this project would have been so much less fun, I'm so glad that Chalmers hired you as "the other" PhD student. Thanks for fun times at Umicore, contaminating the lab with rotten-onion smelling DPDS and Disney princesses, eating a lot of tasty food, and letting me "torturing" you at the gym. For your super-najs company during conferences (e.g. the epic room crawl). For always being happy about running any experiments, for contributing with your smart thoughts when I have been confused about any result. You are awesome Johanna! We have been a great team, and I will miss this a lot! Elise ser för övrigt fram emot att hälsa på Sigrid och Rut i ert hus! ☺

Magnus Skoglundh for always being happy to discussing results with me and coming with valuable input, and for always being encouraging.

All my collaborators at Yale-NUS in Singapore for a great collaboration and exciting research together. Steve (prof. Steven L Bernasek) and Susanna Liljegren Bergman (aka Super-Sulbi, or simply, Princess), thanks for opening up new, stimulating possibilities for

advanced in-situ catalyst characterization. Super-Sulbi, thanks for the nice time we had when I visited you in Princeton, thanks for always believing in me (calling me super-Sandra ☺) and making me believe in me too. Princess and Steve, you made my trip to Singapore highly enjoyable, with the amazing food and nice hikes. In addition, I want to thank you Steve for being my co-supervisor during the last part of my project. Vitaly, and Xiao, thanks for the great job with the XAS data, DFT and modelling, and all your literature search. Also, thanks to Shibo Xi, at the Singapore Synchrotron Light Source for executing the XAS experiments. I´m looking forward to continue the work with you all, and I´m excited about working more with our data and further experiments!

Ton, Peter H, and Henrik M at Umicore. Peter and Ton, thanks for your interests in discussing results and coming with valuable input, thanks for providing samples for further XAS analyses, for help with arranging the elemental analyses, etc. Henrik, thanks for all the help with the diesel burner rig (and other things related to these aging experiments) and for making it run all these hours, solving every problem arising. Det var väldigt trevligt att jobba med dig! Thanks also to all the other nice people at Umicore, which made our stays in Lyngby highly enjoyable. I will miss those.

Thanks to all my colleagues (former and present) and friends at the chemical engineering department, including Jacob, Jonas, Zari, Saiman, Efthymios, Steven, Lina, Moa, Alagar, Fatima, Jerry, Barri, Francesco, Angelica, Elise, Lea, Henrik, Dan and others. For nice lunch breaks and fikas, fun Christmas, crayfish and PhD parties, nice company at conferences, and extremely very good table tennis in the basement... I will miss you all!

Jonas, thanks for building your activity test rig, so I could use it for testing my DOCs, thanks for sometimes frustrating but also nice times in the lab (although the activation energy for starting them could be quite high), modifying your rig to prepare it for SCR tests, thanks for performing XAS and NAP-XPS in Singapore before me so we could learn from your experiences, also thanks for providing me information about what happens in the world, since I´m really bad at taking time for this myself... And thanks for fun table tennis games (in which you sometimes even beat me, which is annoying of course, yet a bit refreshing).

Jacob, tack för en massa trevligt skitsnack om styrketräning, käk, musik och annat. För att du bjudit med mig på en massa bra spelningar, för trevlig öl-drickning. För roliga styrketräningsutmaningar. För schyssta spellistor (använts flitigt). For fun times at conferences, for nice days walking around with you and Albin in Kyoto. We have had a lot of fun together since we got to know each other in Florence. Thanks for always being happy to listen to me talking about my research, look at my pretty graphs and data, coming with good input. And a special thanks for reading through my whole heavy thesis and coming with valuable feedback! I will do the same for you, when your time has come. Om sisådär 10 år eller nåt..? ☺.

Zari, my very nice and social roommate, thanks for inviting me to various social events, coming with nice input on anything from CV to posters, for saffron, pistachio nuts and other Persian specialties. It has been a pleasure sharing the office with you. Good luck with your new work at Northvolt! Lina – special thanks for your inspiring thesis and presentation at your dissertation. I particularly liked your story in the introductory part

and, of course, the acknowledgment - a great place to look if I want to listen to any new music. Richard Nowak Delgado, always being happy to help me in the lab, finding tools and others, and for those super-tasty food-banana things we made one Christmas party. I must try making those myself sometime! Moa – always fun to listen your determined opinions on various subjects, and thanks for taking care of me on my first conferences.

Ann Ekqvist at our HR department, always positive and happy to help! Raimund von der Emden– for always being able to help me with any computer-related issues.

I would also like to thank current and former staff at Chalmers, including Simone, Hanna, Christopher, Felix, Peter, Carl-Robert and others, for a lot of good, fun, crazy times during conferences and for always being very nice and welcoming when I have been at Chalmers for e.g. experiments. Hanna (Prof. Härelind) – you are a true role model, very inspiring, supportive and positive. Thanks for all the nice times we have had during different conferences.

My former internship students Leonhard Schmalhorst and Matthias Feigel from TUM. It was a great pleasure to have you here. Leonhard, thanks for your work, e.g. on my aging rig. Matthias, thanks for your nice Excel scripts, those have been a great aid for my data evaluation. For our Swedish-German lessons in the lab during washcoat scraping, much more pleasant than doing it all alone. And your sharp eyes. (And btw, Elise wants to visit you in Germany 😊). Cornelia Lantto and Noufou Kafando, former master thesis students. Your work on sulfur-poisoning of Cu-SSZ-13 catalysts, using the SCAT-rig and the TGA, respectively, has been very valuable to me. It was very nice to get to know and supervise you all, although not much supervision needed. All of you have contributed significantly to my PhD project, and I am very grateful for this!

Jocce (Joakim Lindblom, JL Integration AB) for teaching me several useful things when helping me with parts of the aging rig construction. Mats Ullberg at CiAB, for always being able to solve problems with e.g. the TPD-TPO-TPR and chemisorption instruments, as well as showing me how to solve things myself, and also always being very nice to meet!

Kunpeng (Volvo), Louise, Aiyong, and the master thesis students Jihao and Sahil (Chalmers) – thanks for a nice collaboration with the burner-aged DOCs. Perfect suggestion from you Kunpeng, otherwise the aged DOCs probably had been left un-analyzed as I didn't have time to do anymore tests. And that would have been annoying!

Romans Stiftelse for providing me with traveling scholarships, enabling me to go to plenty conferences around the world, as well as perform a research exchange at Yale-NUS in Singapore. All of this have given me a lot of inspiration, updates in latest research in my field as well as other, ideas for future experiments, and socializing with other PhD students, post-docs, professors, and other people. Both for the fun of it and for establishing connections.

I would also like to acknowledge Prof. Tapio Salmi at Åbo Akademi who initiated the POKE program - Sustainable chemistry and process technology in the Northern Baltic Sea region. POKE gave me the opportunity to interact and share research experience with other PhD

students and researchers in the Baltic countries in a number of meetings around the Baltic Sea.

Thanks to Svenska Katalyssällskapet for providing me a scholarship at the end of my project.

Matthäus Bäbler, thanks for giving me the opportunity to give lectures in the Transport Phenomena course (a bit scary... but also fun and a good experience). For being an inspiring and devoted teacher in this course. For coming with wise input when discussing my future plans, and also, for reviewing this not-so-very-thin thesis, coming with good input.

Thanks to all my other friends (many of which are beachvolley-related). Thanks for all super-fun time in the sand; playing beachvolley is probably one of the best stress-relieving things to do. Tack för trevliga (drink-) och spelkvällar.

Last, but not least (!), I would like to thank my husband Tauno, and my daughter Elise. Elise, min älskade dotter! Min lilla (eller stora) klätterapa, som ger så mycket glädje. Du kom till oss så passande när jag verkligen behövde en paus från doktorerandet. Ända sen jag kom tillbaka från min föräldraledighet (en väldigt härlig tid) har jag verkligen tyckt om att doktorera (med normala ups and downs såklart). Nya perspektiv på tillvaron, och med en annan effektivitet än tidigare. Tauno, tack för att du uppmuntrade mig att doktorera, för att du stöttat mig, varit hemma och tagit hand om Elise under alla mina konferenser och andra resor. För att du under våra bilresor alltid (typ) kört så jag kunnat jobba samtidigt. För att du läst igenom delar av min avhandling, och annat doktoreringsrelaterat, och kommit med bra input. Tack för att ni finns och har varit här för mig hela tiden, annars hade det nog lätt kunnat bli alldeles för mycket jobb, läsa artiklar, leka runt med data... Och framför allt stort tack för ert stöd och tålamod den här sista tiden av väääldigt mycket och intensivt avhandlingsskrivande. Älskar er! Jag vill också tacka resten av min och Taunos familj, inklusive mamma, pappa, min syster (och beachvolleypartner) Amanda, mina bröder Alex och Simon, svärmor Liisa, svärfar Erik, Taunos bröder Eero, Jussi och Tintti. Tack för all hjälp med bl.a. barnpassning, trevliga middagar och annat! Tack för de grymma brusreducerande hörlurarna, de har underlättat min jobbkoncentrationsförmåga många gånger, särskilt nyttigt nu i slutspurt! Ett speciellt tack för er extra hjälp nu den senaste tiden med att hämta/passa Elise så att jag klarade av att bli klar med avhandlingen i tid (mamma, Liisa och pappa kan känna sig särskilt träffade).

Sandra Dahlin

Stockholm, January 2020

References

- [1] Eurostat, Road freight transport statistics, https://ec.europa.eu/eurostat/statistics-explained/index.php?title=Road_freight_transport_statistics&oldid=213022, (accessed 19 December 2019).
- [2] US Department of Transportation, Status of the Nation's Highways, Bridges, and Transit Conditions and Performance: 23rd Edition: Part III: Highway Freight Transportation - Report to Congress, https://ops.fhwa.dot.gov/freight/infrastructure/nfn/rptc/cp23hwyfreight/iii_ch11.htm#fn1, (accessed 10 December 2019).
- [3] Eurostat, Road transport by distance class in EU 2013-2017, https://ec.europa.eu/eurostat/statistics-explained/images/c/c0/Road_freight_transport_by_distance_class%2C_EU-28%2C_2013-2017_%28based_on_tonne-kilometres%2C_2013%3D100%29.png, (accessed 19 December 2019).
- [4] IPCC, V.P. Masson-Delmotte *et al.*, Global warming of 1.5°C (IPCC), 2019
- [5] R.O. McClellan, T.W. Hesterberg, J.C. Wall, Evaluation of carcinogenic hazard of diesel engine exhaust needs to consider revolutionary changes in diesel technology, *Regul. Toxicol. Pharm.* 63 (2012) 225.
- [6] İ.A. Reşitoğlu, K. Altinişik, A. Keskin, The pollutant emissions from diesel-engine vehicles and exhaust aftertreatment systems, *Clean Technol. Envir.* 17 (2015) 15.
- [7] DieselNet Technology Guide, Diesel exhausts, https://dieselnet.com/tech/diesel_exh.php, (accessed 10 December 2019).
- [8] Air contamination in Ningbo, created by 显. 龙, 2013, Wiki creative commons (CC BY-SA 2.0).
- [9] DieselNet Technology Guide, Emission standards, <https://www.dieselnet.com/standards/>, (accessed 11th Dec 2019).
- [10] EPA, Timeline of Major Accomplishments in Transportation, Air Pollution, and Climate Change, <https://www.epa.gov/transportation-air-pollution-and-climate-change/timeline-major-accomplishments-transportation-air>, (accessed 11th Dec 2019).
- [11] S. Shwan, Metal-exchanged zeolites for NH₃-SCR applications - activity and deactivation studies, PhD thesis, Department of Chemical and Biological Engineering, Chalmers University of Technology, Gothenburg, Sweden, 2014
- [12] European Commission, Reducing CO₂ emissions from heavy-duty vehicles, https://ec.europa.eu/clima/policies/transport/vehicles/heavy_en, (accessed 24 January 2020).
- [13] IPCC, O. Edenhofer *et al.*, Climate Change 2014: Mitigation of Climate Change. Contribution of Working Group III to the Fifth Assessment Report of the Intergovernmental Panel on Climate Change, 2014
- [14] EPA, Renewable fuel standard Program: Overview for Renewable Fuel Standard <https://www.epa.gov/renewable-fuel-standard-program/overview-renewable-fuel-standard>, (accessed 11 December 2019).
- [15] TransportPolicy.net, EU: Fuels: Biofuel Policy, <https://www.transportpolicy.net/standard/eu-fuels-biofuel-policy/>, (accessed 11 December 2019).
- [16] J. Englund, Deactivation of SCR catalysts -Impact of sulfur and the use of biofuels, Lic. thesis, Department of Chemistry and Chemical Engineering, Division of Applied Surface Chemistry, Competence Centre of Catalysis, Chalmers University of Technology, Gothenburg, Sweden, 2018
- [17] Regulation (EU) 2019.1242 of the European Parliament and of the council of 20 June 2019, setting CO₂ emission standards, *Official Journal of the European Union* 25.7.2019 (2019).
- [18] EPA

- DOT Federal-Register, Rules-and-regulations, Final Rule for Greenhouse Gas Emissions and Fuel Efficiency Standards for Medium- and Heavy-Duty Engines and Vehicles - Phase 2, 2016
- [19] California Air Resources Board, CARB, Staff White Paper Current Assessment of the Technical Feasibility of Lower NOx Standards and Associated Test Procedures for 2022 and Subsequent Model Year Medium-Duty and Heavy-Duty Diesel Engines, 2019
- [20] M. Oskarsson, Sveriges riksdag, Katalysatorer på äldre bilar, motion, https://www.riksdagen.se/sv/dokument-lagar/dokument/motion/katalysatorer-pa-aldre-bilar_GM02MJ793, (accessed 11 December 2019).
- [21] DieselNet Technology Guide, Emission standards, EU: Heavy-Duty Truck and Bus Engines, <https://www.dieselnet.com/standards/eu/hd.php> (accessed 11 December 2019).
- [22] DieselNet Technology guide, Emission standards EU: Cars and Light Trucks, <https://www.dieselnet.com/standards/eu/ld.php>, (accessed 11 December 2019).
- [23] R.M. Heck, R.J. Farrauto, S.T. Gulati, Diesel Engine Emissions, in: Catalytic Air Pollution Control: Commercial Technology, Wiley, New Jersey, 2009 pp. 238-294.
- [24] T.V. Johnson, Review of Selective Catalytic Reduction (SCR) and Related Technologies for Mobile Applications, in: I. Nova, E. Tronconi (Eds.) Urea-SCR technology for deNOx after treatment of diesel exhaust - Springer, New York, 2014, pp. pp 3-31.
- [25] ICCT, M. Williams, R. Minjares, A technical summary of Euro 6/VI emission standards, 2016
- [26] IEA, (2019) Tracking Transport, IEA, Paris, <https://www.iea.org/reports/tracking-transport-2019>, (accessed 24 January 2020).
- [27] T. Pauly, Umicore, Catalyst directions for low NOx emissions, CLEERS, 20 September 2018
- [28] W.A. Majewski, H. Jääskeläinen, DieselNet Technology Guide, What is Diesel Fuel, https://www.dieselnet.com/tech/fuel_diesel.php, (accessed 12 December 2019).
- [29] S.C. Gad, Diesel Fuel, in: P. Wexler (Ed.) Encyclopedia of Toxicology (3rd edition), Academic Press, Oxford, 2014, pp. 115-118.
- [30] DieselNet Technology Guide, EU: Fuels: Automotive Diesel Fuel, https://www.dieselnet.com/standards/eu/fuel_automotive.php, (accessed 11 December 2019).
- [31] DieselNet Technology Guide, United States: Diesel Fuel, <https://www.dieselnet.com/standards/us/fuel.php>, (accessed 15 December 2019).
- [32] DieselNet Technology Guide, Brazil: Diesel Fuel: Automotive Diesel Fuel, https://www.dieselnet.com/standards/br/fuel_automotive.php, (accessed 12 December 2019).
- [33] Y. Xi, N.A. Ottinger, Z.G. Liu, New insights into sulfur poisoning on a vanadia SCR catalyst under simulated diesel engine operating conditions, Appl. Catal. B 160-161 (2014) 1.
- [34] IMO, International Maritime Organization, Sulphur 2020 – cutting sulphur oxide emissions, <http://www.imo.org/en/MediaCentre/HotTopics/Pages/Sulphur-2020.aspx>, (accessed 23 January 2020).
- [35] J. Granstrand, S. Dahlin, O. Immele, L. Schmalhorst, C. Lantto, M. Nilsson, R.S. París, F. Regali, L.J. Pettersson, Catalytic aftertreatment systems for trucks fueled by biofuels – aspects on the impact of fuel quality on catalyst deactivation, RSC Catalysis 30 (2018) 64.
- [36] Neste Oil, Hydrotreated vegetable oil (HVO) - premium renewable biofuel for diesel engines, <http://artfuelsforum.eu/wp-content/uploads/2018/05/Acrobat-Document-1.pdf>, (accessed 20 November 2019).
- [37] T. Sarjovaara, Studies on Heavy Duty Engine Fuel Alternatives, PhD thesis, School of Engineering, Department of Energy Technology, Aalto University, Helsinki, Finland, 2015
- [38] CEN, European Committee for Standardization, A change of air with new European Standard for cleaner-burning diesel fuel <https://www.cen.eu/news/brief-news/Pages/NEWS-2016-010.aspx>, (accessed 24 January 2020).
- [39] B. Kampman, R. Verbeek, A. van Grinsven, P. van Mensch, H. Croezen, A. Patuleia, Bringing biofuels on the market Options to increase EU biofuel volumes beyond the current blending limits, CE Delft, TNO, 2013

- [40] P. Stålhammar, Scania, SCANIA – ED95 development, Alcohol CI combustion, <http://www.lth.se/fileadmin/mot2030/filer/11. Stalhammar - Scania ED95 development.pdf>, (accessed 16 December 2019).
- [41] S. Winternell, SEKAB, ED95 The biofuel of the future, <https://www.sekab.com/en/products-services/product/ed95/>, (accessed 12th Dec 2019).
- [42] NEOT, Ethanol Fuel E85, product data sheet, 25.11.2014
- [43] International Renewable Energy Agency, IRENA, Biogas for road vehicles, technology brief, 2018, Abu Dhabi
- [44] R.M. Heck, R.J. Farrauto, S.T. Gulati, Catalytic Air Pollution Control: commercial technology, 3rd ed., Wiley, New Jersey, 2009.
- [45] IEA Bioenergy, M. Persson, O. Jönsson, A. Wellinge, Biogas Upgrading to Vehicle Fuel Standards and Grid Injection, 2006
- [46] CEN, European Committee for Standardization, Project Committee - Biomethane for use in transport and injection in natural gas pipelines, CEN/TC 234/WG 9 Contribution to CEN/TC 408 - Requirements and Recom. for Inject. of N.C.S Gases, 2011
- [47] SGC, SP, K. Arrhenius, B. Magnusson, E. Sahlin, <Impurities in biogas-Validation of methodology of analysis for siloxanes.pdf>, 2011
- [48] H. Jääskeläinen, Dieselnet Technology Guide, Biodiesel Standards & Properties, https://www.dieselnet.com/tech/fuel_biodiesel_std.php, (accessed 11 December 2019).
- [49] J. Jansson, Vanadia-Based Catalysts for Mobile SCR, in: I. Nova, E. Tronconi (Eds.) Urea-SCR technology for deNO_x after treatment of diesel exhaust Springer, New York, 2014, pp. 65-96.
- [50] A. Russell, W.S. Epling, Diesel Oxidation Catalysts, Catal Rev Sci Eng 53 (2011) 337.
- [51] U.P. Kodavanti *et al.*, Diesel exhaust induced pulmonary and cardiovascular impairment: The role of hypertension intervention, Toxicol. Appl. Pharmacol. 268 (2013) 232.
- [52] K. Tsuneyoshi, K. Yamamoto, A study on the cell structure and the performances of wall-flow diesel particulate filter, Energy 48 (2012) 492.
- [53] D.B. Kittelson, W.F. Watts, M. Arnold, Review of diesel particulate matter sampling methods, Supplemental Report #2 Aerosol dynamics, laboratory and on-road studies, 1998
- [54] A. Majewski, W. , H. Jääskeläinen, DieselNet, Exhaust Particulate Matter, https://www.dieselnet.com/tech/images/emi/dpm/pm_filters.jpg, (accessed 19th Jan 2020).
- [55] D. Peitz, A. Bernhard, O. Kröcher, Ammonia Storage and Release in SCR Systems for Mobile Applications, in: I. Nova, E. Tronconi (Eds.) Urea-SCR technology for deNO_x After Treatment of Diesel Exhausts, Fundamental and Applied Catalysis, Springer, New York, 2014.
- [56] A. Kato, S. Matsuda, T. Kamo, F. Nakajima, H. Kuroda, T. Narita, Reaction between nitrogen oxide (NO_x) and ammonia on iron oxide-titanium oxide catalyst, J Phys Chem 85 (1981) 4099.
- [57] C. Ciardelli, I. Nova, E. Tronconi, D. Chatterjee, B. Bandl-Konrad, M. Weibel, B. Krutzsch, Reactivity of NO/NO₂-NH₃ SCR system for diesel exhaust aftertreatment: Identification of the reaction network as a function of temperature and NO₂ feed content, Appl. Catal. B 70 (2007) 80.
- [58] M. Colombo, I. Nova, E. Tronconi, A comparative study of the NH₃-SCR reactions over a Cu-zeolite and a Fe-zeolite catalyst, Catal. Today 151 (2010) 223.
- [59] I. Nova, C. Ciardelli, E. Tronconi, D. Chatterjee, B. Bandl-Konrad, NH₃-NO/NO₂ chemistry over V-based catalysts and its role in the mechanism of the Fast SCR reaction, Catal. Today 114 (2006) 3.
- [60] T.J. Toops, J.A. Pihl, W.P. Partridge, Fe-Zeolite Functionality, Durability, and Deactivation Mechanisms in the Selective Catalytic Reduction (SCR) of NO_x with Ammonia, in: I. Nova, E. Tronconi (Eds.) Urea-SCR technology for deNO_x AfterTreatment of Diesel Exhausts New York, 2014, pp. pp 97-121.
- [61] G. Madia, M. Koebel, M. Elsener, A. Wokaun, Side Reactions in the Selective Catalytic Reduction of NO_x with Various NO₂ Fractions, Ind Eng Chem Res. 41 (2002) 4008.

- [62] T.J. Toops, J.A. Pihl, W.P. Partridge, Fe-Zeolite Functionality, Durability, and Deactivation Mechanisms in the Selective Catalytic Reduction (SCR) of NO_x with Ammonia, in: I. Nova, E. Tronconi (Eds.) Urea-SCR Technology for deNO_x After Treatment of Diesel Exhausts, Fundamental and Applied Catalysis, Springer, New York, NY, 2014, pp. 97–121.
- [63] M. Iwasaki, Mechanistic Aspect of NO–NH₃–O₂ Reacting System, in: I. Nova, E. Tronconi (Eds.) Urea-SCR Technology for deNO_x After Treatment of Diesel Exhausts, Fundamental and Applied Catalysis, Springer, New York, NY, 2014, pp. 221–246.
- [64] A. Vressner, P. Gabrielsson, I. Gekas, E. Senar-Serra, Meeting the EURO VI NO_x Emission Legislation using a EURO IV Base Engine and a SCR/ASC/DOC/DPF Configuration in the World Harmonized Transient Cycle, SAE International 2010-01-1216, 2010.
- [65] I. Nova, M. Colombo, E. Tronconi, V. Schmeißer, B. Bandl-Konrad, L. Zimmermann, Dual-Layer Ammonia Slip Catalysts for Automotive SCR Exhaust Gas Aftertreatment: An Experimental and Modeling Study, in: I. Nova, E. Tronconi (Eds.) Urea-SCR technology for deNO_x after treatments of diesel exhausts, Springer, New York, 2014, pp. 553-586.
- [66] A. Scheuer, W. Hauptmann, A. Drochner, J. Gieshoff, H. Vogel, M. Votsmeier, Dual layer automotive ammonia oxidation catalysts: Experiments and computer simulation, Appl. Catal. B 111-112 (2012) 445.
- [67] M. Colombo, I. Nova, E. Tronconi, A simplified approach to modeling of dual-layer ammonia slip catalysts, Chem. Eng. Sci. 75 (2012) 75.
- [68] P. Wikholm, The Effects of Hydrothermal Aging and Sulfur Poisoning on Dual-Layer Ammonia Slip Catalysts, MSc thesis Chem. Eng., School of Chemical Science and Engineering (CHE), Royal Institute of Technology, KTH, Stockholm, Sweden, 2014
- [69] A. Sagar, A. Trovarelli, M. Casanova, K. Scherz, A New Class of Environmental Friendly Vanadate Based NH₃ SCR Catalysts Exhibiting Good Low Temperature Activity and High Temperature Stability, SAE Int. J. Engines 4 (2011) 1839.
- [70] M.D. Chapman, G. Fu, S. Augustine, M. Watson, J. Crouse, L. Zavalij, D. Perkins-Banks, New Titania Materials with Improved Stability and Activity for Vanadia-Based Selective Catalytic Reduction of NO_x, SAE Int. J. Fuels Lubr. 3 (2010) 643.
- [71] J. Muench, R. Leppelt, R. Dotzel, Extruded Zeolite Based Honeycomb Catalyst for NO_x Removal from Diesel Exhaust, SAE Technical Paper 2008-01-1024 (2008).
- [72] R.M. Heck, R.J. Farrauto, S.T. Gulati, Reduction of NO_x, in: Catalytic Air Pollution Control: commercial technology, Wiley, New Jersey, 2009, pp. 403-439.
- [73] G. Madia, M. Elsener, M. Koebel, F. Raimondi, A. Wokaun, Thermal stability of vanadia-tungsta-titania catalysts in the SCR process, Appl. Catal. B 39 (2002) 181.
- [74] G. He, Z. Lian, Y. Yu, Y. Yang, K. Liu, X. Shi, Z. Yan, W. Shan, H. He, Polymeric vanadyl species determine the low-temperature activity of V-based catalysts for the SCR of NO_x with NH₃, Sci. Adv. 4 (2018) 1.
- [75] N.-Y. Topsøe, Mechanism of the Selective Catalytic Reduction of Nitric Oxide by Ammonia Elucidated by in Situ On-Line Fourier Transform Infrared Spectroscopy, Science 265 (1994) 1217.
- [76] M.A.L. Vargas, M. Casanova, A. Trovarelli, G. Busca, An IR study of thermally stable V₂O₅-WO₃-TiO₂ SCR catalysts modified with silica and rare-earths (Ce, Tb, Er), Appl. Catal. B 75 (2007) 303.
- [77] E. Tronconi, I. Nova, C. Ciardelli, D. Chatterjee, M. Weibel, Redox features in the catalytic mechanism of the “standard” and “fast” NH₃-SCR of NO_x over a V-based catalyst investigated by dynamic methods, J. Catal. 245 (2007) 1.
- [78] M. Iwasaki, Mechanistic Aspect of NO–NH₃–O₂ Reacting System, in: I. Nova, E. Tronconi (Eds.) Urea-SCR technology for deNO_x after treatment of diesel exhausts, Springer, New York, 2014, pp. 221-244.
- [79] M. Koebel, G. Madia, F. Raimondi, A. Wokaun, Enhanced Reoxidation of Vanadia by NO₂ in the Fast SCR Reaction, J. Catal. 209 (2002) 159.

- [80] M. Koebel, M. Elsener, G. Madia, Reaction Pathways in the Selective Catalytic Reduction Process with NO and NO₂ at Low Temperatures, *Ind Eng Chem Res.* 40 (2001) 52.
- [81] R.Q. Long, R.T. Yang, Superior Fe-ZSM-5 Catalyst for Selective Catalytic Reduction of Nitric Oxide by Ammonia, *J. Am. Chem. Soc.* 121 (1999) 5595.
- [82] T. Komatsu, M. Nunokawa, I.S. Moon, T. Takahara, S. Namba, T. Yashima, Kinetic Studies of Reduction of Nitric Oxide with Ammonia on Cu²⁺-Exchanged Zeolites, *J. Catal.* 148 (1994) 427.
- [83] S. Brandenberger, O. Kröcher, A. Tissler, R. Althoff, The State of the Art in Selective Catalytic Reduction of NO_x by Ammonia Using Metal-Exchanged Zeolite Catalysts, *Catal Rev Sci Eng* 50 (2008) 492.
- [84] I. Bull *et al.*, Copper CHA zeolite catalysts United States Patent US 7,601,662 B2
- [85] K. Leistner, L. Olsson, Deactivation of Cu/SAPO-34 during low-temperature NH₃-SCR, *Appl. Catal. B* 165 (2015) 192.
- [86] A. Wang *et al.*, Unraveling the mysterious failure of Cu/SAPO-34 selective catalytic reduction catalysts, *Nat. Commun.* 10 (2019) 1137.
- [87] J. Woo, K. Leistner, D. Bernin, H. Ahari, M. Shost, M. Zammit, L. Olsson, Effect of various structure directing agents (SDAs) on low-temperature deactivation of Cu/SAPO-34 during NH₃-SCR reaction, *Catal. Sci. Technol.* 8 (2018) 3090.
- [88] S.I. Zones, Zeolite SSZ-13 and Its Method of Preparation, US patent 4,544,538, 1985
- [89] J. Song *et al.*, Toward Rational Design of Cu/SSZ-13 Selective Catalytic Reduction Catalysts: Implications from Atomic-Level Understanding of Hydrothermal Stability, *ACS Catal* 7 (2017) 8214.
- [90] C. Paolucci, J.R. Di Iorio, F.H. Ribeiro, R. Gounder, W.F. Schneider, Chapter One - Catalysis Science of NO_x Selective Catalytic Reduction With Ammonia Over Cu-SSZ-13 and Cu-SAPO-34, in: C. Song (Ed.) *Advances in Catalysis*, Academic Press 2016, pp. 1-107.
- [91] E. Borfecchia, P. Beato, S. Svelle, U. Olsbye, C. Lamberti, S. Bordiga, Cu-CHA – a model system for applied selective redox catalysis, *Chem. Soc. Rev.* 47 (2018) 8097.
- [92] F. Gao, C. Peden, Recent Progress in Atomic-Level Understanding of Cu/SSZ-13 Selective Catalytic Reduction Catalysts, *Catalysts* 8 (2018) 140.
- [93] J. Szanyi, J.H. Kwak, H. Zhu, C.H.F. Peden, Characterization of Cu-SSZ-13 NH₃ SCR catalysts: an in situ FTIR study, *PCCP* 15 (2013) 2368.
- [94] T.V.W. Janssens *et al.*, A Consistent Reaction Scheme for the Selective Catalytic Reduction of Nitrogen Oxides with Ammonia, *ACS Catal* 5 (2015) 2832.
- [95] F. Gao, D. Mei, Y. Wang, J. Szanyi, C.H.F. Peden, Selective Catalytic Reduction over Cu/SSZ-13: Linking Homo- and Heterogeneous Catalysis, *J. Am. Chem. Soc.* 139 (2017) 4935.
- [96] C. Paolucci *et al.*, Dynamic multinuclear sites formed by mobilized copper ions in NO_x selective catalytic reduction, *Science* 357 (2017) 898.
- [97] L. Chen, H. Falsig, T.V.W. Janssens, H. Grönbeck, Activation of oxygen on (NH₃CuNH₃)⁺ in NH₃-SCR over Cu-CHA, *J. Catal.* 358 (2018) 179.
- [98] J.S. McEwen, T. Anggara, W.F. Schneider, V.F. Kispersky, J.T. Miller, W.N. Delgass, F.H. Ribeiro, Integrated operando X-ray absorption and DFT characterization of Cu-SSZ-13 exchange sites during the selective catalytic reduction of NO_x with NH₃, *Catal. Today* 184 (2012) 129.
- [99] T. Hao, J. Wang, T. Yu, J.-Q. Wang, M.-Q. Shen, Effect of NO₂ on the Selective Catalytic Reduction of NO with NH₃ over Cu/SAPO-34 Molecular Sieve Catalyst, *Acta Phys-Chim Sin.* 30 (2014) 1567.
- [100] H.-Y. Chen, Z. Wei, M. Kollar, F. Gao, Y. Wang, J. Szanyi, C.H.F. Peden, A comparative study of N₂O formation during the selective catalytic reduction of NO_x with NH₃ on zeolite supported Cu catalysts, *J. Catal.* 329 (2015) 490.
- [101] M. Bendrich, A. Scheuer, R.E. Hayes, M. Votsmeier, Unified mechanistic model for Standard SCR, Fast SCR, and NO₂ SCR over a copper chabazite catalyst, *Appl. Catal. B* 222 (2018) 76.

- [102] P. Velin, Spectroscopic characterisation of surface hydroxyls during catalytic methane oxidation, Lic. thesis, Department of Chemistry and Chemical Engineering, Chalmers University of Technology, Gothenburg, Sweden, 2018
- [103] C.H. Bartholomew, Mechanisms of catalyst deactivation, *Appl. Catal. A* 212 (2001) 17.
- [104] D.W. Brookshear, J.-g. Nam, K. Nguyen, T.J. Toops, A. Binder, Impact of sulfation and desulfation on NO_x reduction using Cu-chabazite SCR catalysts, *Catal. Today* 258, Part 2 (2015) 359.
- [105] H. Jääskeläinen, DieselNet Technology Guide, Impact of Engine Oil on Emissions and Fuel Economy, https://www.dieselnet.com/tech/lube_emissions.php, (accessed 15 December 2019).
- [106] H. Jääskeläinen, K. Froelund, DieselNet Technology Guide, Lubricating oil consumption, https://www.dieselnet.com/tech/lube_cons.php, (accessed 15 December 2019).
- [107] P. Blakeman, K. Arnby, P. Marsh, C. Newman, G. Smedler, Optimization of an SCR Catalyst System to Meet EU IV Heavy Duty Diesel Legislation, SAE Technical Paper 2008-01-1542, 2008.
- [108] P.S. Hammershøi, A.D. Jensen, T.V.W. Janssens, Impact of SO₂-poisoning over the lifetime of a Cu-CHA catalyst for NH₃-SCR, *Appl. Catal. B* 238 (2018) 104.
- [109] P.S. Hammershøi, Y. Jangjou, W.S. Epling, A.D. Jensen, T.V.W. Janssens, Reversible and irreversible deactivation of Cu-CHA NH₃-SCR catalysts by SO₂ and SO₃, *Appl. Catal. B* 226 (2018) 38.
- [110] P.S. Hammershøi, A.L. Godiksen, S. Mossin, P.N.R. Vennestrøm, A.D. Jensen, T.V.W. Janssens, Site selective adsorption and relocation of SO_x in deactivation of Cu-CHA catalysts for NH₃-SCR, *React. Chem. Eng.* 4 (2019) 1081.
- [111] Y. Jangjou *et al.*, Nature of Cu Active Centers in Cu-SSZ-13 and Their Responses to SO₂ Exposure, *ACS Catal* 8 (2018) 1325.
- [112] Y. Jangjou, C.S. Sampara, Y. Gu, D. Wang, A. Kumar, J. Li, W.S. Epling, Mechanism-based kinetic modeling of Cu-SSZ-13 sulfation and desulfation for NH₃-SCR applications, *React. Chem. Eng.* 4 (2019) 1038.
- [113] S. Dahlin, C. Lantto, J. Englund, B. Westerberg, F. Regali, M. Skoglundh, L.J. Pettersson, Chemical aging of Cu-SSZ-13 SCR catalysts for heavy-duty vehicles – Influence of sulfur dioxide, *Catal. Today* 320 (2019) 72.
- [114] K. Wijayanti, K. Leistner, S. Chand, A. Kumar, K. Kamasamudram, N.W. Currier, A. Yezerets, L. Olsson, Deactivation of Cu-SSZ-13 by SO₂ exposure under SCR conditions, *Catal. Sci. Technol.* 6 (2016) 2565.
- [115] L. Olsson, K. Wijayanti, K. Leistner, A. Kumar, S.Y. Joshi, K. Kamasamudram, N.W. Currier, A. Yezerets, A kinetic model for sulfur poisoning and regeneration of Cu/SSZ-13 used for NH₃-SCR, *Appl. Catal. B* 183 (2016) 394.
- [116] Y. Cheng, C. Lambert, D.H. Kim, J.H. Kwak, S.J. Cho, C.H.F. Peden, The different impacts of SO₂ and SO₃ on Cu/zeolite SCR catalysts, *Catal. Today* 151 (2010) 266.
- [117] Y. Wang, Z. Li, R. Fan, X. Guo, C. Zhang, Y. Wang, Z. Ding, R. Wang, W. Liu, Deactivation and Regeneration for the SO₂-Poisoning of a Cu-SSZ-13 Catalyst in the NH₃-SCR Reaction, *Catalysts* 9 (2019) 797.
- [118] Z. Chen, C. Fan, L. Pang, S. Ming, P. Liu, T. Li, The influence of phosphorus on the catalytic properties, durability, sulfur resistance and kinetics of Cu-SSZ-13 for NO_x reduction by NH₃-SCR, *Appl. Catal. B* 237 (2018) 116.
- [119] A. Kumar, M.A. Smith, K. Kamasamudram, N.W. Currier, A. Yezerets, Chemical deSO_x: An effective way to recover Cu-zeolite SCR catalysts from sulfur poisoning, *Catal. Today* 267 (2016) 10.
- [120] A. Kumar, M.A. Smith, K. Kamasamudram, N.W. Currier, H. An, A. Yezerets, Impact of different forms of feed sulfur on small-pore Cu-zeolite SCR catalyst, *Catal. Today* 231 (2014) 75.
- [121] J. Luo, D. Wang, A. Kumar, J. Li, K. Kamasamudram, N. Currier, A. Yezerets, Identification of two types of Cu sites in Cu/SSZ-13 and their unique responses to hydrothermal aging and sulfur poisoning, *Catal. Today* 267 (2016) 3.

- [122] A.J. Shih *et al.*, Spectroscopic and kinetic responses of Cu-SSZ-13 to SO₂ exposure and implications for NO_x selective catalytic reduction, *Appl. Catal. A* 574 (2019) 122.
- [123] Y. Shan, X. Shi, Z. Yan, J. Liu, Y. Yu, H. He, Deactivation of Cu-SSZ-13 in the presence of SO₂ during hydrothermal aging, *Catal. Today* (2017).
- [124] R. Ando, T. Hihara, Y. Banno, M. Nagata, T. Ishitsuka, N. Matsubayashi, T. Tomie, Detailed Mechanism of S Poisoning and De-Sulfation Treatment of Cu-SCR Catalyst, SAE Technical Paper 2017-01-0944 (2017).
- [125] W. Su, Z. Li, Y. Zhang, C. Meng, J. Li, Identification of sulfate species and their influence on SCR performance of Cu/CHA catalyst, *Catal. Sci. Technol.* 7 (2017) 1523.
- [126] P.S. Hammershøi, P.N.R. Vennestrøm, H. Falsig, A.D. Jensen, T.V.W. Janssens, Importance of the Cu oxidation state for the SO₂-poisoning of a Cu-SAPO-34 catalyst in the NH₃-SCR reaction, *Appl. Catal. B* 236 (2018) 377.
- [127] L. Zhang, D. Wang, Y. Liu, K. Kamasamudram, J. Li, W. Epling, SO₂ poisoning impact on the NH₃-SCR reaction over a commercial Cu-SAPO-34 SCR catalyst, *Appl. Catal. B* 156–157 (2014) 371.
- [128] G. Yang, X. Du, J. Ran, X. Wang, Y. Chen, L. Zhang, Understanding SO₂ Poisoning over Different Copper Species of Cu-SAPO-34 Catalyst: A Periodic DFT Study, *J. Phys. Chem. C* 122 (2018) 21468.
- [129] H. Kamata, K. Takahashi, C.U.I. Odenbrand, Surface acid property and its relation to SCR activity of phosphorus added to commercial V₂O₅(WO₃)/TiO₂ catalyst, *Catal. Lett.* 53 (1998) 65.
- [130] M. Klimczak, P. Kern, T. Heinzelmann, M. Lucas, P. Claus, High-throughput study of the effects of inorganic additives and poisons on NH₃-SCR catalysts—Part I: V₂O₅–WO₃/TiO₂ catalysts, *Appl. Catal. B* 95 (2010) 39.
- [131] O. Kröcher, M. Elsener, Chemical deactivation of V₂O₅/WO₃–TiO₂ SCR catalysts by additives and impurities from fuels, lubrication oils, and urea solution: I. Catalytic studies, *Appl. Catal. B* 77 (2008) 215.
- [132] D. Nicosia, M. Elsener, O. Kröcher, P. Jansohn, Basic investigation of the chemical deactivation of V₂O₅/WO₃–TiO₂ SCR catalysts by potassium, calcium, and phosphate, *Top. Catal.* 42–43 (2007) 333.
- [133] F. Castellino, S.B. Rasmussen, A.D. Jensen, J.E. Johnsson, R. Fehrmann, Deactivation of vanadia-based commercial SCR catalysts by polyphosphoric acids, *Appl. Catal. B* 83 (2008) 110.
- [134] R. Eschrich, J. Schröder, F. Hartmann, R. Gläser, Aging of Diesel Exhaust Catalysts in Use with Biofuels, *MTZ worldwide* 76 (2014) 44.
- [135] J. Blanco, P. Avila, C. Barthelemy, A. Bahamonde, J.A. Odriozola, J.F.G. De La Banda, H. Heinemann, Influence of phosphorus in vanadium-containing catalysts for NO_x removal, *Appl. Catal.* 55 (1989) 151.
- [136] K. Xie, K. Leistner, K. Wijayanti, A. Kumar, K. Kamasamudram, L. Olsson, Influence of phosphorus on Cu-SSZ-13 for selective catalytic reduction of NO_x by ammonia, *Catal. Today* 297 (2017) 46.
- [137] I. Lezcano-Gonzalez, U. Deka, H.E. van der Bij, P. Paalanen, B. Arstad, B.M. Weckhuysen, A.M. Beale, Chemical deactivation of Cu-SSZ-13 ammonia selective catalytic reduction (NH₃-SCR) systems, *Appl. Catal. B* 154–155 (2014) 339.
- [138] K. Xie, A. Wang, J. Woo, A. Kumar, K. Kamasamudram, L. Olsson, Deactivation of Cu-SSZ-13 SCR catalysts by vapor-phase phosphorus exposure, *Appl. Catal. B* 256 (2019) 117815.
- [139] J.P. Chen, M.A. Buzanowski, R.T. Yang, J.E. Cichanowicz, Deactivation of the Vanadia Catalyst in the Selective Catalytic Reduction Process, *J. Air Waste Manage* 40 (1990) 1403.
- [140] L. Chen, J. Li, M. Ge, The poisoning effect of alkali metals doping over nano V₂O₅–WO₃/TiO₂ catalysts on selective catalytic reduction of NO_x by NH₃, *Chem. Eng. J.* 170 (2011) 531.
- [141] X. Guo, Poisoning and sulfation on vanadia SCR catalyst, Department of Chemical Engineering, Brigham Young University, 2006

- [142] S. Putluru, A. Jensen, A. Riisager, R. Fehrmann, Alkali Resistant Fe-Zeolite Catalysts for SCR of NO with NH₃ in Flue Gases, *Top. Catal.* 54 (2011) 1286.
- [143] F. Castellino, Deactivation of SCR Catalysts by additives, PhD thesis, Department of Chemical and Biochemical Engineering, Technical University of Denmark, Copenhagen, Denmark, 2008
- [144] G. Cavataio, H.-W. Jen, D.A. Dobson, J.R. Warner, Laboratory Study to Determine Impact of Na and K Exposure on the Durability of DOC and SCR Catalyst Formulations, (2009).
- [145] H. Kamata, K. Takahashi, C.U.I. Odenbrand, The role of K₂O in the selective reduction of NO with NH₃ over a V₂O₅(WO₃)/TiO₂ commercial selective catalytic reduction catalyst, *J. Mol. Catal. A: Chem.* 139 (1999) 189.
- [146] A. Kling, C. Andersson, A. Myringer, D. Eskilsson, S. Järås, Alkali deactivation of high-dust SCR catalysts used for NO_x reduction exposed to flue gas from 100 MW-scale biofuel and peat fired boilers: Influence of flue gas composition, *Appl. Catal. B* 69 (2007) 240.
- [147] D. Nicosia, I. Czekaj, O. Kröcher, Chemical deactivation of V₂O₅/WO₃–TiO₂ SCR catalysts by additives and impurities from fuels, lubrication oils and urea solution: Part II. Characterization study of the effect of alkali and alkaline earth metals, *Appl. Catal. B* 77 (2008) 228.
- [148] Y. Peng, J. Li, W. Si, J. Luo, Y. Wang, J. Fu, X. Li, J. Crittenden, J. Hao, Deactivation and regeneration of a commercial SCR catalyst: Comparison with alkali metals and arsenic, *Appl. Catal. B* 168–169 (2015) 195.
- [149] C. Fan *et al.*, Steam and alkali resistant Cu-SSZ-13 catalyst for the selective catalytic reduction of NO_x in diesel exhaust, *Chem. Eng. J.* 334 (2018) 344.
- [150] C. Wang, W. Yan, Z. Wang, Z. Chen, J. Wang, J. Wang, J. Wang, M. Shen, X. Kang, The role of alkali metal ions on hydrothermal stability of Cu/SSZ-13 NH₃-SCR catalysts, *Catal. Today* (2019).
- [151] L. Liu, X. Wu, Y. Ma, X. Zhang, R. Ran, Z. Si, D. Weng, Potassium deactivation of Cu-SSZ-13 catalyst for NH₃-SCR: Evolution of salts, zeolite and copper species, *Chem. Eng. J.* 383 (2020) 123080.
- [152] C. Wang, C. Wang, J. Wang, J. Wang, M. Shen, W. Li, Effects of Na⁺ on Cu/SAPO-34 for ammonia selective catalytic reduction, *J. Environ. Sci.* 70 (2018) 20.
- [153] K.B. Albert, C. Fan, L. Pang, Z. Chen, S. Ming, T. Albert, T. Li, The influence of chemical poisoning, hydrothermal aging and their co-effects on Cu-SAPO-34 catalyst for NO_x reduction by NH₃-SCR, *Appl. Surf. Sci.* 479 (2019) 1200.
- [154] X. Liu, X. Wu, D. Weng, Z. Si, Durability of Cu/SAPO-34 catalyst for NO_x reduction by ammonia: Potassium and sulfur poisoning, *Catal. Commun.* 59 (2015) 35.
- [155] J. Ma, Z. Si, D. Weng, X. Wu, Y. Ma, Potassium poisoning on Cu-SAPO-34 catalyst for selective catalytic reduction of NO_x with ammonia, *Chem. Eng. J.* 267 (2015) 191.
- [156] S.S.R. Putluru, A. Riisager, R. Fehrmann, Alkali resistant Cu/zeolite deNO_x catalysts for flue gas cleaning in biomass fired applications, *Appl. Catal. B* 101 (2011) 183.
- [157] P. Kern, M. Klimczak, M. Lucas, A. Döring, P. Claus, Development of a technology platform for the study of the chemical poisoning of ammonia selective catalytic reduction (SCR) and NO oxidation catalysts with combinatorial and rational means, *Chemie-Ingenieur-Technik* 81 (2009) 289.
- [158] P. Kern, M. Klimczak, T. Heinzelmann, M. Lucas, P. Claus, High-throughput study of the effects of inorganic additives and poisons on NH₃-SCR catalysts. Part II: Fe–zeolite catalysts, *Appl. Catal. B* 95 (2010) 48.
- [159] F. Gao, Y. Wang, N.M. Washton, M. Kollár, J. Szanyi, C.H.F. Peden, Effects of Alkali and Alkaline Earth Cocations on the Activity and Hydrothermal Stability of Cu/SSZ-13 NH₃-SCR Catalysts, *ACS Catal* 5 (2015) 6780.
- [160] D.W. Brookshear, K. Nguyen, T.J. Toops, B.G. Bunting, W.F. Rohr, J. Howe, Investigation of the effects of biodiesel-based Na on emissions control components, *Catal. Today* 184 (2012) 205.
- [161] A.-C. Larsson, J. Einvall, M. Sanati, Deactivation of SCR Catalysts by Exposure to Aerosol Particles of Potassium and Zinc Salts, *Aerosol Sci. Technol.* 41 (2007) 369.

- [162] A.-C. Larsson, J. Einvall, A. Andersson, M. Sanati, Targeting by Comparison with Laboratory Experiments the SCR Catalyst Deactivation Process by Potassium and Zinc Salts in a Large-Scale Biomass Combustion Boiler, *Energy & Fuels* 20 (2006) 1398.
- [163] X. Auvray, O. Mihai, B. Lundberg, L. Olsson, Deactivation of Cu/SSZ-13 NH₃-SCR Catalyst by Exposure to CO, H₂, and C₃H₆, *Catalysts* 9 (2019).
- [164] J. Luo, K. Kamasamudram, N. Currier, A. Yezerets, NH₃-TPD methodology for quantifying hydrothermal aging of Cu/SSZ-13 SCR catalysts, *Chem. Eng. Sci.* 190 (2018) 60.
- [165] J. Woo, D. Bernin, H. Ahari, M. Shost, M. Zammit, L. Olsson, Understanding the mechanism of low temperature deactivation of Cu/SAPO-34 exposed to various amounts of water vapor in the NH₃-SCR reaction, *Catal. Sci. Technol.* 9 (2019) 3623.
- [166] H. Kannisto, H.H. Ingelsten, M. Skoglundh, Ag–Al₂O₃ catalysts for lean NO_x reduction—Influence of preparation method and reductant, *J. Mol. Catal. A: Chem.* 302 (2009) 86.
- [167] J. Englund *et al.*, Deactivation of a Pd/Pt Bimetallic Oxidation Catalyst Used in a Biogas-Powered Euro VI Heavy-Duty Engine Installation, *Catalysts* 9 (2019).
- [168] A.S. Hoffman, L.M. Debeve, A. Bendjeriou-Sedjerari, S. Ouldchikh, S.R. Bare, J.-M. Basset, B.C. Gates, Transmission and fluorescence X-ray absorption spectroscopy cell/flow reactor for powder samples under vacuum or in reactive atmospheres, *Rev. Sci. Instrum.* 87 (2016) 073108.
- [169] S. Calvin, XAFS for everyone, CRC Press, Boca Raton, FL, 2013.
- [170] F.J. Timmermans, C. Otto, Contributed Review: Review of integrated correlative light and electron microscopy, *Rev. Sci. Instrum.* 86 (2015) 011501.
- [171] J.C. Yang, M.W. Small, R.V. Grieshaber, R.G. Nuzzo, Recent developments and applications of electron microscopy to heterogeneous catalysis, *Chem. Soc. Rev.* 41 (2012) 8179.
- [172] M. Mazumder, R. Ahmed, A. Wajahat Ali, S.-J. Lee, SEM and ESEM techniques used for analysis of asphalt binder and mixture: A state of the art review, *Construction and Building Materials* 186 (2018) 313.
- [173] A. Winkler, D. Ferri, M. Aguirre, The influence of chemical and thermal aging on the catalytic activity of a monolithic diesel oxidation catalyst, *Appl. Catal. B* 93 (2009) 177.
- [174] J.H. Kwak, H. Zhu, J.H. Lee, C.H.F. Peden, J. Szanyi, Two different cationic positions in Cu-SSZ-13?, *Chem. Commun.* 48 (2012) 4758.
- [175] M. Naderi, Surface Area: Brunauer–Emmett–Teller (BET), in: S. Tarleton (Ed.) *Progress in Filtration and Separation*, Academic Press, Oxford, 2015, pp. 585-608.
- [176] N.R. Draper, H. Smith, *Applied Regression Analysis*, Wiley, New York, 1998.
- [177] H. Kamata, K. Takahashi, C.U. Ingemar Odenbrand, Kinetics of the Selective Reduction of NO with NH₃ over a V₂O₅(WO₃)/TiO₂ Commercial SCR Catalyst, *J. Catal.* 185 (1999) 106.
- [178] A. Martini *et al.*, Composition-driven Cu-speciation and reducibility in Cu-CHA zeolite catalysts: a multivariate XAS/FTIR approach to complexity, *Chem. Sci.* 8 (2017) 6836.
- [179] L.S. Kau, D.J. Spira-Solomon, J.E. Penner-Hahn, K.O. Hodgson, E.I. Solomon, X-ray absorption edge determination of the oxidation state and coordination number of copper. Application to the type 3 site in *Rhus vernicifera* laccase and its reaction with oxygen, *J. Am. Chem. Soc.* 109 (1987) 6433.
- [180] J. Felten, H. Hall, J. Jaumot, R. Tauler, A. de Juan, A. Gorzsás, Vibrational spectroscopic image analysis of biological material using multivariate curve resolution–alternating least squares (MCR-ALS), *Nature Protocols* 10 (2015) 217.
- [181] D. Bazin, J.J. Rehr, Limits and Advantages of X-ray Absorption Near Edge Structure for Nanometer Scale Metallic Clusters, *J. Phys. Chem. B* 107 (2003) 12398.
- [182] P. Giannozzi *et al.*, Advanced capabilities for materials modelling with Quantum ESPRESSO, *J. Phys.: Condens. Matter* 29 (2017) 465901.
- [183] O.D. Frutos, G. Quijano, A. Aizpuru, R. Muñoz, A state-of-the-art review on nitrous oxide control from waste treatment and industrial sources, *Biotechnol. Adv.* 36 (2018) 1025.

- [184] M. Devadas, O. Kröcher, M. Elsener, A. Wokaun, N. Söger, M. Pfeifer, Y. Demel, L. Mussmann, Influence of NO₂ on the selective catalytic reduction of NO with ammonia over Fe-ZSM5, *Appl. Catal. B* 67 (2006) 187.
- [185] Z. Wang, Y. Zhu, S. Zhou, Y. Feng, Reaction mechanism and chemical kinetics of NH₃-NO/NO₂-SCR system with vanadium-based catalyst under marine diesel exhaust conditions, *J. Power and Energy* (2019) 1.
- [186] F. Mafuné, K. Miyajima, K. Morita, Release of Oxygen from Copper Oxide Cluster Ions by Heat and by Reaction with NO, *J. Phys. Chem. C* 119 (2015) 11106.
- [187] X. Liu, X. Wu, D. Weng, Z. Si, R. Ran, Migration, reactivity, and sulfur tolerance of copper species in SAPO-34 zeolite toward NO_x reduction with ammonia, *RSC Advances* 7 (2017) 37787.
- [188] B. Pereda-Ayo, U. De La Torre, M.J. Illán-Gómez, A. Bueno-López, J.R. González-Velasco, Role of the different copper species on the activity of Cu/zeolite catalysts for SCR of NO_x with NH₃, *Appl. Catal. B* 147 (2014) 420.
- [189] K. Leistner, O. Mihai, K. Wijayanti, A. Kumar, K. Kamasamudram, N.W. Currier, A. Yezerets, L. Olsson, Comparison of Cu/BEA, Cu/SSZ-13 and Cu/SAPO-34 for ammonia-SCR reactions, *Catal. Today* 258 (2015) 49.
- [190] A.R. Fahami *et al.*, The dynamic nature of Cu sites in Cu-SSZ-13 and the origin of the seagull NO_x conversion profile during NH₃-SCR, *React. Chem. Eng.* 4 (2019) 1000.
- [191] S. Dahlin, M. Nilsson, D. Bäckström, S.L. Bergman, E. Bengtsson, S.L. Bernasek, L.J. Pettersson, Multivariate analysis of the effect of biodiesel-derived contaminants on V₂O₅-WO₃/TiO₂ SCR catalysts, *Appl. Catal. B* 183 (2016) 377.
- [192] S. Shwan, J. Jansson, L. Olsson, M. Skoglundh, Chemical deactivation of Fe-BEA as NH₃-SCR catalyst—Effect of phosphorous, *Appl. Catal. B* 147 (2014) 111.
- [193] S. Andonova, E. Vovk, J. Sjöblom, E. Ozensoy, L. Olsson, Chemical deactivation by phosphorous under lean hydrothermal conditions over Cu/BEA NH₃-SCR catalysts, *Appl. Catal. B* 147 (2014) 251.
- [194] X. Wu, W. Yu, Z. Si, D. Weng, Chemical deactivation of V₂O₅-WO₃/TiO₂ SCR catalyst by combined effect of potassium and chloride, *Front. Env. Sci. Eng.* 7 (2013) 420.
- [195] L. Lietti, P. Forzatti, G. Ramis, G. Busca, F. Bregani, Potassium doping of vanadia/titania de-NO_xing catalysts: Surface characterisation and reactivity study, *Appl. Catal. B* 3 (1993) 13.
- [196] H. Jensen-Holm, N.-Y. Topsøe, J.J. Cui, Implementation of SCR DeNO_x Technology on Coal-Fired Boilers in P.R. China, 2006 Lyngby, Denmark
- [197] R. Khodayari, I.C.U. Odenbrand, Regeneration of commercial SCR catalysts by washing and sulphation: effect of sulphate groups on the activity, *Appl. Catal. B* 33 (2001) 277.
- [198] A. Kumar *et al.*, Catalyst Sulfur Poisoning and Recovery Behaviors: Key for Designing Advanced Emission Control Systems, SAE Technical Paper 2017-26-0133, 2017.
- [199] I.A. Pankin, A. Martini, K.A. Lomachenko, A.V. Soldatov, S. Bordiga, E. Borfecchia, Identifying Cu-oxo species in Cu-zeolites by XAS: A theoretical survey by DFT-assisted XANES simulation and EXAFS wavelet transform, *Catal. Today* (2019).
- [200] T. Zhang, F. Qiu, H. Chang, X. Li, J. Li, Identification of active sites and reaction mechanism on low-temperature SCR activity over Cu-SSZ-13 catalysts prepared by different methods, *Catal. Sci. Technol.* 6 (2016) 6294.
- [201] M. Urrutxua, B. Pereda-Ayo, U. De-La-Torre, J.R. González-Velasco, Evaluation of Cu/SAPO-34 Catalysts Prepared by Solid-State and Liquid Ion-Exchange Methods for NO_x Removal by NH₃-SCR, *ACS Omega* 4 (2019) 14699.
- [202] F. Gao, N.M. Washton, Y. Wang, M. Kollár, J. Szanyi, C.H.F. Peden, Effects of Si/Al ratio on Cu/SSZ-13 NH₃-SCR catalysts: Implications for the active Cu species and the roles of Brønsted acidity, *J. Catal.* 331 (2015) 25.
- [203] M. Shen, Z. Wang, X. Li, J. Wang, J. Wang, C. Wang, J. Wang, Effects of regeneration conditions on sulfated CuSSZ-13 catalyst for NH₃-SCR, *Korean J. Chem. Eng.* 36 (2019) 1249.

- [204] B. Chen, R. Xu, R. Zhang, N. Liu, Economical Way to Synthesize SSZ-13 with Abundant Ion-Exchanged Cu⁺ for an Extraordinary Performance in Selective Catalytic Reduction (SCR) of NO_x by Ammonia, *Environ Sci Technol* 48 (2014) 13909.
- [205] J.H. Kwak, T. Varga, C.H.F. Peden, F. Gao, J.C. Hanson, J. Szanyi, Following the movement of Cu ions in a SSZ-13 zeolite during dehydration, reduction and adsorption: A combined in situ TP-XRD, XANES/DRIFTS study, *J. Catal.* 314 (2014) 83.
- [206] Y. Liu *et al.*, Mapping XANES spectra on structural descriptors of copper oxide clusters using supervised machine learning, *J. Chem. Phys.* 151 (2019) 164201.
- [207] V. Gombac, L. Sordelli, T. Montini, J.J. Delgado, A. Adamski, G. Adami, M. Cargnello, S. Bernal, P. Fornasiero, CuO_x-TiO₂ Photocatalysts for H₂ Production from Ethanol and Glycerol Solutions, *J. Phys. Chem. A* 114 (2010) 3916.
- [208] M.G. Méndez-Medrano *et al.*, Surface Modification of TiO₂ with Ag Nanoparticles and CuO Nanoclusters for Application in Photocatalysis, *J. Phys. Chem. C* 120 (2016) 5143.
- [209] B.E. Etschmann, W. Liu, D. Testemale, H. Müller, N.A. Rae, O. Proux, J.L. Hazemann, J. Brugger, An in situ XAS study of copper(I) transport as hydrosulfide complexes in hydrothermal solutions (25–592°C, 180–600bar): Speciation and solubility in vapor and liquid phases, *Geochim. Cosmochim. Acta* 74 (2010) 4723.
- [210] Wang, Hou, Yan, Zhang, Wang, Wang, Shen, Kang, The Role of SO₃ Poisoning in CU/SSZ-13 NH₃-SCR Catalysts, *Catalysts* 9 (2019).
- [211] Y. Cheng, L. Xu, J. Hangas, M. Jagner, C. Lambert, Laboratory Postmortem Analysis of 120k mi engine aged urea SCR catalyst, *SAE Technical Paper* 2007-01-1579, 2007.
- [212] N. Sadokhina, G. Smedler, U. Nylén, M. Olofsson, L. Olsson, The influence of gas composition on Pd-based catalyst activity in methane oxidation – inhibition and promotion by NO, *Appl. Catal. B* 200 (2017) 351.
- [213] H. Dubbe, F. Bühner, G. Eigenberger, U. Nieken, Hysteresis Phenomena on Platinum and Palladium-based Diesel Oxidation Catalysts (DOCs), *Emiss. Control Sci. Technol.* 2 (2016) 137.
- [214] J. Andersson, M. Antonsson, L. Eurenus, E. Olsson, M. Skoglundh, Deactivation of diesel oxidation catalysts: Vehicle- and synthetic aging correlations, *Appl. Catal. B* 72 (2007) 71.
- [215] E. Fridell, A. Amberntsson, L. Olsson, A.W. Grant, M. Skoglundh, Platinum oxidation and sulphur deactivation in NO_x storage catalysts, *Top. Catal.* 30 (2004) 143.
- [216] K. Persson, A. Ersson, S. Colussi, A. Trovarelli, S.G. Järås, Catalytic combustion of methane over bimetallic Pd–Pt catalysts: The influence of support materials, *Appl. Catal. B* 66 (2006) 175.
- [217] M. Martin-Martinez, L.M. Gómez-Sainero, J. Bedia, A. Arevalo-Bastante, J.J. Rodriguez, Enhanced activity of carbon-supported Pd–Pt catalysts in the hydrodechlorination of dichloromethane, *Appl. Catal. B* 184 (2016) 55.
- [218] R. Esparza, A. Santoveña, A. Ruíz-Baltazar, A. Angeles-Pascual, D. Bahena, J. Maya-Cornejo, J. Ledesma-García, R. Pérez, Study of PtPd Bimetallic Nanoparticles for Fuel Cell Applications, *Mat Res.* 20 (2017) 1193.
- [219] P.M.A. Sherwood, Introduction to Studies of Phosphorus-Oxygen Compounds by XPS, *Surf. Sci. Spectra* 9 (2002) 62.
- [220] M. Kärkkäinen *et al.*, The Influence of Phosphorus Exposure on a Natural-Gas-Oxidation Catalyst, *Top. Catal.* 59 (2016) 1044.
- [221] S. Eaton, K. Nguyen, B. Bunting, Deactivation of Diesel Oxidation Catalysts by Oil-Derived Phosphorus SAE International, 2006.
- [222] H.N. Sharma, V. Sharma, A.B. Mhadeshwar, R. Ramprasad, Why Pt Survives but Pd Suffers From SO_x Poisoning?, *J. Phys. Chem. Lett.* 6 (2015) 1140.
- [223] M.S. Wilburn, W.S. Epling, SO₂ adsorption and desorption characteristics of bimetallic Pd-Pt catalysts: Pd:Pt ratio dependency, *Catal. Today* 320 (2019) 11.